Electrochemical Performances of Ni-based Cermet Anodes for Direct Methane Solid Oxide Fuel Cells

You Hongxin

GRADUATE SCHOOL OF SCIENCE AND TECHNOLOGY

HIROSAKI UNIVERSITY

2017

Electrochemical Performances of Ni-based Cermet Anodes for Direct Methane Solid Oxide Fuel Cells

by

You Hongxin

A Dissertation Presented to

the Graduate School of Science and Technology

of the Hirosaki University in partial fulfillment of the requirement

for the degree of Doctor of Philosophy in Energy Engineering

HIROSAKI UNIVERSITY

2017

Abstract

Solid Oxide Fuel Cell (SOFC) operates directly with hydrocarbon fuels is widely expected to be an important objective for power generation in the future. However, when hydrocarbon fuels such as methane is directly used as the fuel in an SOFC system, the performance decreases obviously with the susceptibility of conventional Ni-based anodes to carbon deposition. Therefore, it is necessary to investigate the reaction mechanisms of methane on the anode (Chapter 3, 4). Besides, the optimization of nickel based anodes (Chapter 5, 6 and 7) and the development of alternative materials (Chapter 8) is another approach for the direct utilization of hydrocarbon fuels.

In order to investigate the reactions mechanism of dry methane on the Ni-YSZ (or Ni-ScSZ) anode, different concentration of dry methane was used to as fuels. The anode exhaust gases, measured by on-line chromatography, were summarized to analysis the reactions of concentration of dry methane on anodes. And the reaction pathway mathematical relationships between dry methane flux and current for different anode reaction was obtained by analyzing the activation energy of methane elementary reactions. As the oxygen ion concentration at the anode three-phase boundary increasing continuously, the following reactions with low concentration methane occurs in sequence $CH_4 + O^{2-} \rightarrow CO + 2H_2 + 2e^-$, $CH_4 + 2O^{2-} \rightarrow CO + H_2O + H_2 + 4e^-$, $CH_4 + 3O^{2-} \rightarrow CO + 2H_2O + 6e^-$, $CH_4 + 4O^{2-} \rightarrow CO_2 + 2H_2O + 8e^-$, the first two or three reactions occur with intermediate methane concentration, and the first reaction occurs only with high methane concentration, both on Ni-YSZ and Ni-ScSZ anode. The judgment of methane in low, medium or high concentration depends on $v(CH_4) \leq I/(4F)$, $I/(4F) \leq v(CH_4) \leq I/(2F)$, $v(CH_4) \geq I/(2F)$ respectively, which are based on Faraday's first law and the relationship among reactant species. In addition, the influence of dry methane concentration on the output performance of cell with Ni-ScSZ anode was investigated in Chapter 4. For low concentrations of dry methane, the cell performance degraded rapidly at relative high current density. This phenomenon could be attribute to the production of H_2O in transition of reaction, resulting in the increase of $p(H_2O)/p(CH_4)$ at anode side, as well as the polarization, which caused the anode degradation.

For the direct utilization of hydrocarbon fuels, in Chapter 5, a series of novel Ni_xCu_{1-x} (x = 0.8, 0.5, 0.2) alloy materials were prepared by hard template method using activated carbon fiber (ACF) as template, and a cubic crystal structure were observed. Scanning electron microscope (SEM) showed that Ni_xCu_{1-x} alloy powders with a columnar shape were closely connected with each other to form porous structure. The cells with such Ni_xCu_{1-x} alloy anodes exhibited good performance under methane, and its power density increased with the Ni content in Ni_xCu_{1-x} anode increase, and $Ni_{0.8}Cu_{0.2}$ anode achieved the highest value of 315 $mW \cdot cm^{-2}$ at 1073 K. Also,

compared with the rapid degradation of conventional Ni-based anode when methane used as fuel, the Ni_xCu_{1-x} anodes showed a stable property after 10 h operation, indicating that the Ni-Cu bimetallic material could effectively inhibit carbon deposition in anode.

Impregnated nanoparticles into porous anode framework are very effective in improving the electrochemical performance of SOFC anodes possibly due to the extension of reaction sites and/or the enhancement of catalytic activity. Thus, in Chapter 6, the tubular YSZ with the stereo structure was firstly prepared by hard template method to form a three dimensionally porous anode framework, and then $Ni_{0.5}Cu_{0.5}O_x$ as catalysts was impregnated into YSZ skeleton to fabricate $Ni_{0.5}Cu_{0.5}O_x$-YSZ composite anode. YSZ electrolyte-supported single cell with $Ni_{0.5}Cu_{0.5}O_x$-YSZ anode was fabricated for the power generation performance test and the long-term stability test at 1073 K. The maximum power densities were reached more than 900, 315.52 and 241.77 $mW \cdot cm^{-2}$ when H_2, dry CH_4 and wet CH_4 (3%H_2O) were used as fuel, respectively. The high performance of $Ni_{0.5}Cu_{0.5}O_x$ impregnated tubular YSZ anode demonstrates that the improved performance is mainly attributed to the significantly improved extension of three phase boundary. Moreover, by comparing the results of the 100 h long-term stability tests under dry CH_4 and wet CH_4 (3%H_2O) respectively, the cell with dry CH_4 showed an obvious voltage drop of 5.27% but the one with wet CH_4 showed the more stable property, indicating that the presence of 3%H_2O had an obvious impact on inhibiting carbon deposition on the anode. SEM and EDS results confirmed that the porous anode structure was quite steady, as well as less carbon was formed in the anode using wet CH_4 (3%H_2O) as fuel after 100 h operation. Therefore, the stereo structure design with YSZ micro tube as skeleton and impregnated $Ni_{0.5}Cu_{0.5}O_x$ as catalyst is indeed an alternative and effective technique to enhance cell performance, stability and reliability for SOFCs.

$Ni_{0.5}Cu_{0.5}O_x$-YSZ was verified as a potential anode material. However, to further enhance the anode coking resistance for directly using dry CH_4, $Ce_{0.8}Sm_{0.2}O_{1.9}$ (SDC) was adopted to replace YSZ as anode scaffold and $Ni_{0.5}Cu_{0.5}Ba_{0.05}O_x$ was used as the impregnated catalyst to prepare $Ni_{0.5}Cu_{0.5}Ba_{0.05}O_x$/SDC anode. It is expected to obtain excellent cell performance with high anti-coking property by optimizing the anode composition. In addition, $Ni_{0.5}Cu_{0.5}Ba_{0.05}O_x$ powder was prepared by sol-gel method and then mixed with SDC powder as a comparison anode ($Ni_{0.5}Cu_{0.5}Ba_{0.05}O_x$-SDC), and the single cells with such two contrastive anodes were fabricated to investigate the anode microstructure effect on the cell performance due to the consistence of the cathode and electrolyte fabricating process. The cell with $Ni_{0.5}Cu_{0.5}Ba_{0.05}O_x$/SDC anode generated maximum power density of 384.54 $mW \cdot cm^{-2}$ under dry CH_4 at 1073 K, which was higher than that of the $Ni_{0.5}Cu_{0.5}Ba_{0.05}O_x$-SDC anode of 324.99 $mW \cdot cm^{-2}$. According to the SEM analysis results, it is inferred that the high performance of $Ni_{0.5}Cu_{0.5}Ba_{0.05}O_x$/SDC anode could be mainly attributed to the effective covering from $Ni_{0.5}Cu_{0.5}Ba_{0.05}O_x$ particles on the surface of tubular SDC backbone,

as well as a steady and porous stereoscopic structure was formed for gas diffusion, leading to increase TPB. Besides, the cell with $Ni_{0.5}Cu_{0.5}Ba_{0.05}O_x$/SDC anode showed a good stability for 100 h operation in dry CH_4, while the cell with $Ni_{0.5}Cu_{0.5}Ba_{0.05}O_x$-SDC dropped rapidly after 10 h. SEM results shows $Ni_{0.5}Cu_{0.5}Ba_{0.05}O_x$/SDC anode presented a stable structure, suggesting that the fabrication of anti-carbon catalyst combined with three-dimensional electrode is potential measure to enhance durability for direct utilization of dry methane as fuel in SOFCs.

Besides the optimizations of conventional Ni based anodes, developing new alternative materials such as perovskites is another effective approach to avoid carbon deposition. In Chapter 8, $SrMoO_4$ based materials are preliminarily investigated as good candidates for SOFC anodes. $SrMoO_4$ was synthesized by hard template method, using ACF a template. No observable impurity phases are formed when $SrMoO_4$ mixed and co-fired with YSZ as a potential anode. However, the cell with $SrMoO_4$-YSZ showed a lower electrochemical performance due to its limited catalytic activity, both in H_2 and CH_4. $Gd_{0.2}Ce_{0.8}O_{1.9}$ (GDC) was introduced into $SrMoO_4$ by wet impregnation to further improving its potential as SOFC anode materials. The introduction of GDC showed excellent effects of enhancing catalytic activity, resulting in a higher cell performance. In addition, the effects of different composition within YSZ and $SrMoO_4$ and GDC impregnation on the cell performance were further investigated, respectively. When the mass ratio of $SrMoO_4$ to YSZ was 5:5, and the GDC impregnation loading reached an optimal value, 50wt% (relative to $SrMoO_4$ and YSZ), the cell exhibited a high performance, with a maximum power density of 361.01 mW·cm^{-2} in dry CH_4 at 1073 K.

Table of Contents

List of Tables

List of Figures

Figure8.5 SEM images of anode after test (a) anode surface microstructure of single cell; (b) cross-sectional microstructure of single cell

Chapter 1

Introduction

1.1 Solid oxide fuel cell

1.1.1 Introduction

Fuel cell is a power device that can convert chemical energy into electric power through direct electric catalytic oxidation of a fuel with an oxidant. Compared with the conventional battery device, it can utilize the continuous fuel supplied from external to generate electricity within the fuel cell, and it is not limited by Carnot cycle. Its invention is attributing to Grove knight and named by Mond and Langer. The common fuel cells include five types as follows: Alkaline Fuel Cell (AFC), Phosphorous Acid Fuel Cell (PAFC), Molten Carbonate Fuel Cell (MCFC), Proton Exchange Membrane (PEMFC), and Solid Oxide Fuel Cell (SOFC). Among them, SOFC as a solid state power device have attracted more and more attention due to its high electrical efficiency, low emissions, wide fuel flexibility and low manufacture cost. According to the configuration structure, cells are being fabricated in many different configurations, such as planar cells [1], tubular cells [2] or flat-plates cells [3].

1.1.2 Principle of operation

Similar to the conventional fuel cell, a SOFC is constructed with a sandwich structure mainly consisted of three parts: anode, electrolyte and cathode [4-5]. Fig. 1.1 shows the typical schematic diagram of SOFC.

At cathode side, the oxidant (oxygen or ambient air) is supplied and the oxygen is absorbed on the cathode. Then, oxygen was reduced and obtained two electrons from an external circuit to form oxygen ions. Meanwhile, fuel is oxidized at the anode. The overall reaction of oxygen at cathode is as follows.

$$1/2O_2 + 2e^- \rightarrow O^{2-} \tag{1.1}$$

The generated oxide ions, driven by the difference in oxygen activity of the two gases at the electrodes, transported to the anode side through the ceramic electrolyte. At the anode side, the oxygen ions combined with fuel such as hydrogen at the three phase boundary composed of electrolyte, catalyst and reaction gas to complete oxidation reaction to form water liberating electrons

1

through external connections and back to the cathode. As such, the total circuit was completed and electrical energy was generated. The overall reaction of H_2 at anode is as follows.
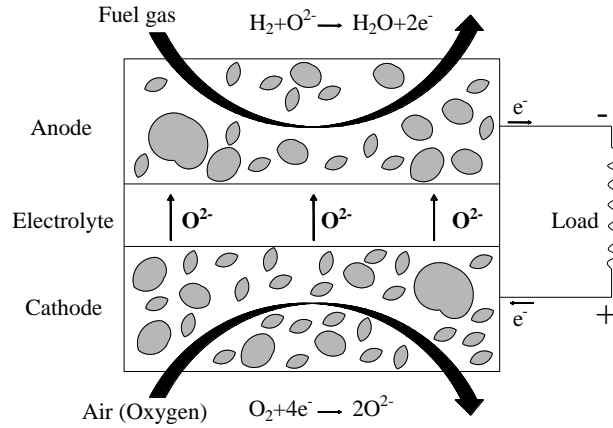
Fig 1.1 Principle of SOFC [4-5]

$$O^{2-}+H_2 \rightarrow H_2O+2e^- \tag{1.2}$$

However, for CH_4 used as fuel, the reaction mechanism at anode is significantly different from H_2 as fuel. Abuliti [6] fabricated the single cell consisting of Ni-YSZ anode and used different concentrations (flux) dry CH_4 as fuel research to investigate the reactions at anode by measuring the anode exhausted gases combined with comparing the electron number of anode exhaust gas and the need of generated current. Following reactions occur at anode.

$$CH_4 \rightarrow 2H_2+C \tag{1.3}$$

$$C + O^{2-} \rightarrow CO+2e^- \tag{1.4}$$

$$CH_4 + 4O^{2-} \rightarrow CO_2+ 2H_2O + 8e^- \tag{1.5}$$
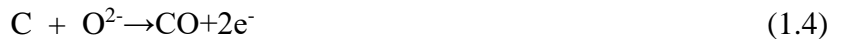
That is CH_4 was firstly decomposed C at anode; At low current density, the generated C in three phase boundary was reacted with the oxygen ions to form CO, and the partial oxidation reaction of CH_4 was happened; At high current density, CH_4 was reacted and formed CO_2 and H_2O, and the complete oxidation reaction of CH_4 was occurred.

1.2 Thermodynamics of SOFC

SOFC provides a reaction zone in which the chemical energy can convert electrical energy. In a SOFC system, thermodynamics is not only related to the output, but also determine the occurrence of a chemical reaction. The system energy state function is enthalpy in thermodynamics [5, 7-8], commonly represented with symbol H.

$$H = U + p \cdot V \tag{1.6}$$

where, U is the system internal energy, p is system pressure and V is system volume.

Entropy is another thermodynamic state function, which represents the uncertainty of a system. A chemical reaction whether occur or not is judged in two possible conditions. One is that system enthalpy H decreases, i.e. $\Delta H < 0$. Another is that entropy S increases, i.e. $\Delta S > 0$.

Besides, another state function, the Gibbs energy, represents the chemical reaction driving force, is given by the expressions:

$$G = H\text{-}T\text{·}S \tag{1.7}$$

where, T is the temperature.

ΔG is defined as the Gibbs free energy change of a reaction in Equation [1.8].

$$\Delta G = \Delta H\text{-}T\text{·}\Delta S \tag{1.8}$$

It can be inferred that Gibbs free energy change ΔG couples the system enthalpy and entropy change.

Therefore, the positive and negative of ΔG can be used to judge whether a reaction occur spontaneously or not.

The reaction can occur spontaneously when $\Delta G < 0$. Electric power can be extracted from the reaction.

The reaction can not occur spontaneously when $\Delta G > 0$. Reverse reaction occur spontaneously.

When $\Delta G = 0$, the positive reaction is equilibrated with the reverse reaction, and the electric power can not be extracted from the reaction.

The Gibbs free energy change of a reaction will be fully converted into electrical power in a fuel cell system with redox reaction. The intrinsic relationship between the Gibbs energy change $\triangle G$ and the electromotive force E is

$$\Delta G = -nFE \tag{1.9}$$

where, n is the unleashed number of free electrons when the fuel with oxygen-ion take place electrochemical catalytic reaction at the anode; F is the Faraday constant. $\triangle G$ and E can be replaced by $\triangle G^{0}$ and E_0 respectively under standard conditions.

$$\Delta G^{0} = -nFE_{0} \tag{1.10}$$

The electromotive force is affected by temperature, pressure, and material activity.

The chemical potential of v_i is introduced for i components involved in a reaction. Chemical potential reflects the change in Gibbs free energy as the chemical properties of the system varies. Each chemical reaction system has a chemical potential. Each substance in reaction system has a chemical potential, defined as

$$v_i = \left(\frac{\partial G}{\partial m_i}\right)_{T, P, n\ j \neq i} \tag{1.11}$$

where, m_i is the number of moles of i component. $(\partial G/\partial n_i)_{T, P, nj\neq i}$ represents the change of Gibbs free energy when i substance has an infinitely small increase. When changing the amount of chemical substances in the fuel cell, the free energy of the system will be changed, thus affecting the electromotive force.

The i substance chemical potential is associated with the concentration of i substance by activity of a_i.

$$v_i = v_i^0 + RT \ln \alpha_i \tag{1.12}$$

where, v_i^0 is the chemical potential of i substance in standard state.

Material activity is determined by its chemical properties. If all the gases are ideal gases in electrode chamber, then the activity of i gas a_i is related to pressure p_i and p^0, which is given by expression

$$a_i = p_i / p^0 \tag{1.13}$$

where, p_i is the partial pressure of i gas, p^0 is the standard state pressure (atmospheric pressure at 298K, which is 101.325kPa).

A chemical reaction，such as

$$aA + bB \leftrightarrow cC + dD \tag{1.14}$$

where, A and B is reactant, C and D is reaction product. a, b, c, d is the number moles of A, B, C, D respectively. Equation (1.15) shows that $\triangle G$ can be calculated by the chemical potential of reactants and products

$$\Delta G = \left(c v_C^0 + d v_D^0\right) - \left(a v_A^0 + b v_B^0\right) + RT \ln \frac{\alpha_C^c \alpha_D^d}{\alpha_A^1 \alpha_B^b} \tag{1.15}$$

Chemical potential at standard state is represented by the free energy change in the standard state $\triangle G^0$. So it can be inferred that

$$\Delta G = \Delta G^0 + RT \ln \frac{\alpha_C^c \alpha_D^d}{\alpha_A^a \alpha_B^b} \tag{1.16}$$

Using the relationship between Gibbs free energy change and the electromotive force, the Nernst equation for reaction is obtained.

$$E = E^0 - \frac{RT}{nF} \ln \frac{\alpha_C^c \alpha_D^d}{\alpha_A^1 \alpha_B^b} \tag{1.17}$$

This equation is one of the cores for fuel cell thermodynamics, which represents the relationship of electromotive force with materials in the fuel cell reaction at a certain temperature.

Equation (1.17) is substituted into equation (1.10) and (1.13) to give the reaction electromotive force at any temperature and pressure for calculation equation (1.18).

$$E = -\frac{\Delta G^0}{nF} - \frac{RT}{nF} \ln\left[\frac{(p_C/p^0)^c(p_D/p^0)^d}{(p_A/p^0)^a(p_B/p^0)^b}\right] \tag{1.18}$$

1.3 Reaction dynamics of SOFC

Thermodynamics in SOFC can be viewed as an extreme case of chemical kinetics while time approximating to an infinite equilibrium state. Thermodynamics of a cell is a case where a cell is in equilibrium. Electrodynamic potential obtained for a cell is maximum electrodynamic potential from a theoretic perspective, also an extreme case where no current exists.

Without presence of current, SOFC as a generating device is meaningless. When a current exists, the electrochemical reaction occurs inside a cell, which leads to transmission of electrons in circuits. As the transmission is driven by power, thus polarization happens.

1.3.1 Polarization

When current passes through electrode, the electrode potential of a cell deviates from equilibrium potential, thus polarization is generated. Resistance during electrochemical reaction is the main reason for polarization, and energy consumption is needed to overcome the resistance, leading to loss of voltage.

Dependent on different reasons for polarization, types of polarization to be defined vary, mainly including activation polarization, ohmic polarization and concentration polarization.

i) Activation Polarization

In essence, electrochemical reaction is a process of reactant receiving or losing electrons, during which corresponding resistance must be overcome. This resistance is called activation energy, and the polarization resulting from activation energy is called activation polarization. Different activation energies lead to different electrochemical reactions.

ii) Ohmic Polarization

Ohmic polarization is resulted from such internal resistance as ionic conduction resistance of electrolyte and resistance of electron conduction on anode.

iii) Concentration Polarization

Transportation of reactants and reaction products on the electrode-electrolyte interface is an

unavoidable process for polarization. If there is current passing by the substance flow surrounding electrode changes when compared with its original flow, which leads to deviation of electrode potential. The concentration polarization is resulted from hindrance of material migration and transformation of chemical reaction.

Concentration polarization relates double electrode layers inside the cell, which is divided into compact layer and dispersion layer. When both electrode surface charge density and reaction medium concentration are small, the electrostatic energy inside the double electrode layer is far less than ionic energy of thermal motion; when both electrode surface charge density and reaction medium concentration are large, the electrostatic energy inside the double electrode layer is far more than ionic energy of thermal motion. The ratio of potential difference in dispersion layer in total potential difference is increasingly smaller.

I-V curve representing different polarization during power generation of single cell is shown in Fig.1.2 [8].
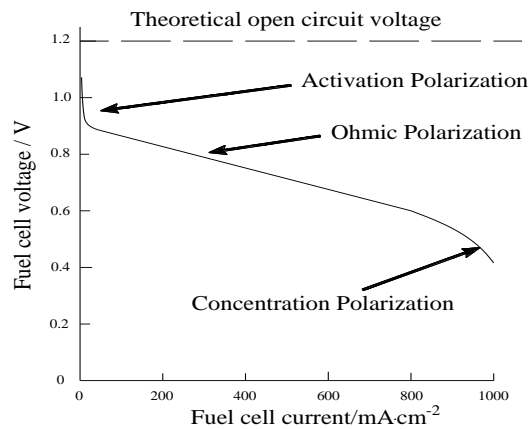
Fig.1.2 I-V curve representing different polarization during power generation of single cell [8]

1.3.2 Activation energy

Chemical Reaction Kinetics discusses chemical reaction rate and reaction mechanism, with its research object including elementary reaction. In chemical reaction kinetics, reaction mode and activation energy are research hotspots.

Judgment on whether reactions are spontaneous is from the ΔG perspective of thermodynamics, while dynamic hindrance must be overcome in many reactions of thermodynamic energy. Therefore, Ryan [9] considered it is necessary to consider thermodynamics and dynamics of reactions as a whole. Under the condition that what sorts of reaction of methane happening on SOFC anode are unknown, it is difficult to carry out thermodynamic analysis.

According to the collision of reaction theory, in order to enable reaction, reaction particles or free radicals must collide with each other, and reaction occurs only when collision takes place [10]. Aside from collision, no reaction takes place unless reaction particles or free radicals are provided with an energy called activation energy. Out of two comparable reactions, the one with less activation energy is liable to take place [11]. According to the transition state theory of reaction kinetics, when activated molecules of reactants collide with each other, it is necessary to generate an activated complex that has a state potential energy higher than primary and final state potential energies, followed by a transition state that is to be decomposed into intermediates or products.

Zhang [12] believed that the basic law of energy change has to be abided by in every procedure of organic reaction accompanied with change of energy, although types of organic reaction vary. While determining the direction of chemical reaction, the lowest energy principle is a compulsory condition of energy to be followed. As for complicated reaction processes, analyzing the activation energy in every step of reaction is a key to clarification of reaction pathway.

The decomposition process of methane on catalyst Ni is [13]:

$$CH_4 \rightarrow CH_3(ads) + H\ (ads) \tag{1.19a}$$

$$CH_3\ (ads) \rightarrow CH_2\ (ads) + H\ (ads) \tag{1.19b}$$

$$CH_2\ (ads) \rightarrow CH\ (ads) + H\ (ads) \tag{1.19c}$$

$$CH\ (ads) \rightarrow C\ (ads) + H\ (ads) \tag{1.19d}$$
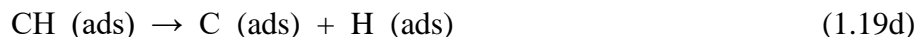
Main paths to generate CO and CO_2 through the reaction of CH_4/O_2 on catalyst Ni are shown in Fig.1.3 [14], where the subscript s represents solid phase and g represents gas phase.

$$CH_{4,g} \rightarrow CH_{x,s} \xrightarrow{\ O_s\ } CO_s \rightarrow CO_g$$
$$\downarrow O_s$$
$$CO_{2,s} \rightarrow CO_{2,g}$$
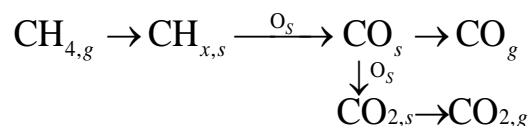
Fig. 1.3 Oxidation process of CH_4 on Ni catalyst [14]

Wu [14] studied the mechanism of partial oxidation reaction of methane on catalyst Ni using the bond-order conservation method. In the partial oxidation reaction of methane, CH oxidizing reaction is a main path to generate CO, while deep oxidation of CO will generate CO_2. Thermodynamic comparison of the activation energy of $148 KJ \cdot mol^{-1}$ for CO generated from C + O and the activation energy of 47 $KJ \cdot mol^{-1}$ for CO generated from CH + O shows CH is easier than C to be oxidized for generation of CO.

The reaction mechanism of hydrocarbon on Ni-YSZ is shown in Tab. 1.1 [15]. The mechanism initially developed and used for verification of the steam assisted oxidation of methane. Out of 42 irreplaceable reactions, there are 6 gas phase reactions and 12 surface adsorption reactions, most of

which reaction rate goes by equation Arrhenius and viscosity coefficient. Activation energies of reactions 12, 20, 21 & 23 shown in Tab. 1.1 are to be calculated with CO(s) coverage rate $\theta_{\text{co(s)}}$ based on the following formula:

$$k = AT^b \exp\left(-\frac{E}{RT}\right)\exp\left(-\frac{\varepsilon_{CO(s)}\theta_{CO(s)}}{RT}\right) \tag{1.20}$$

Wherein, k stands for reaction rate constant, A for prefactor, also the constant (frequency factor) of collision with reactant molecule, T for temperature, E for activation energy, R for gas constant, b for times exponents, $\varepsilon_{CO\,(s)}$ for mole internal energy of CO molecule.

Thermodynamic analysis helps determine whether a reaction takes place, polarization analysis of reaction kinetics states that it is inevitable for output voltage drops with the increase of current density during cell operation, and the activation energy in reaction kinetics is a key to understand anode reaction mechanism. Reactions in SOFC are different from conventional chemical reactions where no formation and transmission of oxygen anion is involved, while reactions on anode in SOFC relates to not only quantity of methane but also quantity delivered of O^{2-}, resulting in difficulties to identify anodic reaction mechanisms.

1.4 Utilization mode of methane in SOFC

H_2 is an optimal fuel for SOFC. However, about 96% of hydrogen is produced from such hydrocarbon fuels as natural gas by steam-reforming reaction. Therefore, extensive researches were conducted on substituting hydrocarbon gas (such as methane) for hydrogen as a SOFC fuel, which can significantly reduce system complexity, energy costs and increase cell efficiency.

Dependent on types of anodic reaction, the utilization modes of methane in SOFC mainly include Steam Reforming, Dry Reforming of Methane, Partial Oxidation Reforming, and Direct Electrochemical Oxidation.

1.4.1 Reforming of internal methane steam in SOFCs

The mixture of methane and water steam can take place the reaction of reforming of methane, which is given by the expressions.

$$CH_4 + H_2O \rightarrow CO + 3H_2. \tag{1.21}$$

After being simultaneously introduced into cell anode, methane and water steam are reformed. This utilization mode of methane is called internal reforming of methane. If surplus water steam is exposed to the internal reforming reaction, the shift reaction,

$$CO+H_2O \rightarrow CO_2+H_2 \tag{1.22}$$

may happen.

Tab1.1 Oxidation reaction mechanism of CH_4 over Ni- YSZ [15]

	Reaction	A	B	E/ KJ·mol^{-1}
1	$H_2 + Ni(s) + Ni(s) \rightarrow H(s) + H(s)$	1.000×10^{-02}	0.0	0.00
2	$H(s) + H(s) \rightarrow Ni(s) + Ni(s) + H_2$	$5.593 \times 10^{+19}$	0.0	88.12
3	$O_2 + Ni(s) + Ni(s) \rightarrow O(s) + O(s)$	1.000×10^{-02}	0.0	0.00
4	$O(s) + O(s) \rightarrow Ni(s) + Ni(s) + O_2$	$2.508 \times 10^{+23}$	0.0	470.39
5	$CH_4 + Ni(s) \rightarrow CH_4(s)$	8.000×10^{-03}	0.0	0.00
6	$CH_4(s) \rightarrow Ni(s) + CH_4$	$5.302 \times 10^{+15}$	0.0	33.15
7	$H_2O + Ni(s) \rightarrow H_2O(s)$	1.000×10^{-01}	0.0	0.00
8	$H_2O(s) \rightarrow Ni(s) + H_2O$	$4.579 \times 10^{+12}$	0.0	62.68
9	$CO_2 + Ni(s) \rightarrow CO_2(s)$	1.000×10^{-05}	0.0	0.00
10	$CO_2(s) \rightarrow Ni(s) + CO_2$	$9.334 \times 10^{+07}$	0.0	28.80
11	$CO + Ni(s) \rightarrow CO(s)$	5.000×10^{-01}	0.0	0.00
12	$CO(s) \rightarrow Ni(s) + CO$	$4.041 \times 10^{+11}$	0.0	112.85
		$\xi CO(S)$		-50.0
13	$O(s) + H(s) \rightarrow OH(s) + Ni(s)$	$5.000 \times 10^{+22}$	0.0	97.90
14	$OH(s) + Ni(s) \rightarrow O(s) + H(s)$	$2.005 \times 10^{+21}$	0.0	37.19
15	$OH(s) + H(s) \rightarrow H_2O(s) + Ni(s)$	$3.000 \times 10^{+20}$	0.0	42.70
16	$H_2O(s) + Ni(s) \rightarrow OH(s) + H(s)$	$2.175 \times 10^{+21}$	0.0	91.36
17	$OH(s) + OH(s) \rightarrow O(s) + H_2O(s)$	$3.000 \times 10^{+21}$	0.0	100.00
18	$O(s) + H_2O(s) \rightarrow OH(s) + OH(s)$	$5.423 \times 10^{+23}$	0.0	209.37
19	$O(s) + C(s) \rightarrow CO(s) + Ni(s)$	$5.200 \times 10^{+23}$	0.0	148.10
20	$CO(s) + Ni(s) \rightarrow O(s) + C(s)$	$1.418 \times 10^{+22}$	-3.0	115.97
		$\xi CO(S)$		-50.0
21	$O(s) + CO(s) \rightarrow CO_2(s) + Ni(s)$	$2.000 \times 10^{+19}$	0.0	123.60
		$\xi CO(S)$		-50.0
22	$CO_2(s) + Ni(s) \rightarrow O(s) + CO(s)$	$3.214 \times 10^{+23}$	-1.0	86.50
23	$HCO(s) + Ni(s) \rightarrow CO(s) + H(s)$	$3.700 \times 10^{+21}$	0.0	0.00
		$\xi CO(S)$		-50.0
24	$CO(s) + H(s) \rightarrow HCO(s) + Ni(s)$	$2.338 \times 10^{+20}$	-1.0	127.98
25	$HCO(s) + Ni(s) \rightarrow O(s) + CH(s)$	$3.700 \times 10^{+24}$	-3.0	95.80
26	$O(s) + CH(s) \rightarrow HCO(s) + Ni(s)$	$7.914 \times 10^{+20}$	0.0	114.22
27	$CH_4(s) + Ni(s) \rightarrow CH_3(s) + H(s)$	$3.700 \times 10^{+21}$	0.0	57.70
28	$CH_3(s) + H(s) \rightarrow CH_4(s) + Ni(s)$	$4.438 \times 10^{+21}$	0.0	58.83
29	$CH_3(s) + Ni(s) \rightarrow CH_2(s) + H(s)$	$3.700 \times 10^{+24}$	0.0	100.00
30	$CH_2(s) + H(s) \rightarrow CH_3(s) + Ni(s)$	$9.513 \times 10^{+22}$	0.0	52.58
31	$CH_2(s) + Ni(s) \rightarrow CH(s) + H(s)$	$3.700 \times 10^{+24}$	0.0	97.10
32	$CH(s) + H(s) \rightarrow CH_2(s) + Ni(s)$	$3.008 \times 10^{+24}$	0.0	76.43
33	$CH(s) + Ni(s) \rightarrow C(s) + H(s)$	$3.700 \times 10^{+21}$	0.0	18.80
34	$C(s) + H(s) \rightarrow CH(s) + Ni(s)$	$4.400 \times 10^{+22}$	0.0	160.49
35	$O(s) + CH_4(s) \rightarrow CH_3(s) + OH(s)$	$1.700 \times 10^{+24}$	0.0	88.30
36	$CH_3(s) + OH(s) \rightarrow O(s) + CH_4(s)$	$8.178 \times 10^{+22}$	0.0	28.72
37	$O(s) + CH_3(s) \rightarrow CH_2(s) + OH(s)$	$3.700 \times 10^{+24}$	0.0	130.10
38	$CH_2(s) + OH(s) \rightarrow O(s) + CH_3(s)$	$3.815 \times 10^{+21}$	0.0	21.97
39	$O(s) + CH_2(s) \rightarrow CH(s) + OH(s)$	$3.700 \times 10^{+24}$	0.0	126.80
40	$CH(s) + OH(s) \rightarrow O(s) + CH_2(s)$	$1.206 \times 10^{+23}$	0.0	45.42
41	$O(s) + CH(s) \rightarrow C(s) + OH(s)$	$3.700 \times 10^{+21}$	0.0	48.10
42	$C(s) + OH(s) \rightarrow O(s) + CH(s)$	$1.764 \times 10^{+21}$	0.0	129.08

H$_2$ and CO was electrochemical oxidized generated from on anode, as well as power generation occurs. Among the reactions on anode, water steam reforming reaction (1.21) and reaction (1.22) are chemical reactions, in which fuel gases convert.

Electrochemical oxidation of methane is an ideal choice, but carbon deposition may undermine cell performance by reducing anode activity. A gas mixture such as H$_2$ and CO resulted from methane reforming is an effective measure to restrain carbon deposition. Here below are two major modes of methane reforming:

i) External reforming refers to the process that the gas mixture of CO and H$_2$ resulted from methane reacting with water steam outside the cell enters the SOFC for power generation. This may prevent anode carbon deposition from happening, but needs investment in external reforming device with complicated process.

ii) Internal reforming refers to that two processes such as reforming conversion and electrochemical oxidation are simultaneously completed on anode surface after methane and water steam are directly input into SOFC in high-temperature running so as to remove external reformer and simplify the system. This is an important topic for current SOFC research. Some researchers adopted the anodic gas circulation method [16] and the progressive methane steam reforming method [17] to add a certain amount of water steam into methane as a fuel gas.

Fig.1.4 and Fig.1.5 show possible paths in the methane reforming process in SOFC [7]. In a direct reforming process, anode functions in catalyzing conversion of hydrocarbon fuel into H$_2$ and CO, H$_2$ and CO oxidized into H$_2$O and CO$_2$ by electro-catalyzing and electric and ion conduction.
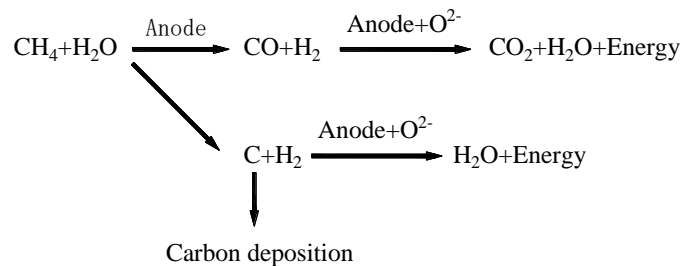
Fig.1.4 The possible paths of methane internal reforming process in SOFC [7]
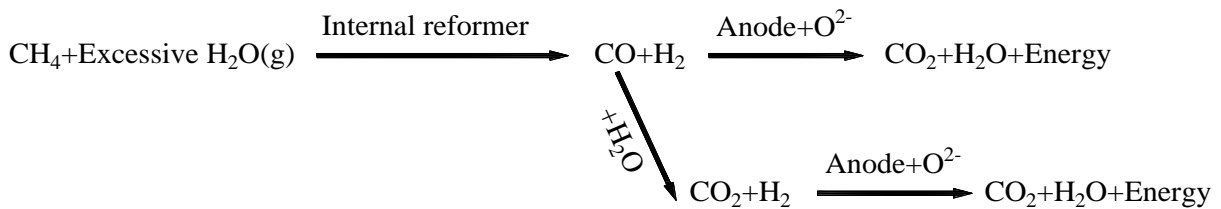
Fig.1.5 The possible paths of methane indirectly internal reforming process in SOFC [7]

Reforming of methane steam inside the cell has the following advantages:

i) Good cooling effect on cell is brought about by endothermal reaction of reform;

ii) High thermodynamic efficiency of steam reform approximates to that of direct oxidation of methane;

iii) No need of external reformer reduces investment and simplifies the system.

Methane steam reforming reaction and its kinetic behavior is another topic of SOFC research. Methane steam reforming is an extremely complicated process, which not only involves mass transfer of reactants and resultants on catalyst surface and inside catalyst, but also involves many parallel reactions, particular electrochemical reactions.

General studies focus on the internal reforming process in SOFC under the condition of methane added with small amount of water steam. An earlier study on internal reforming in SOFC was carried out by Murray [18], who concluded that the performance of cell is basically similar with that of dry methane by conducting a test with 3%H_2O+97% CH_4 on composite anode Ni-YSZ/YDC; following steady cell running at earlier 100h, cell performance is unsteady at lower voltage due to anode deactivation. In a relevant study conducted by Kawano [19], the cell performance of 97%CH_4+ 3%H_2O as a fuel for SOFC was tested on different anodes.

Anode is provided with two reaction functions, namely methane steam reforming and electrochemical oxidation of hydrogen in sequence. Theoretically, different anode materials (catalysts) may be selected based on different anodic functions so that selection scope of anode materials could be widened. While selecting anode materials, it is required to follow the principle that under the condition that the fuel mixture contains no water, carbon deposition on anode shall not undermine its catalytic activity. Research shows that anode Ru/$LaCrO_3$ [20] has a good catalytic performance, methane is almost completely converted and no carbon deposited even after 100 h operation under the condition of 973k and the ratio of n(Steam): n(CH_4) less than 1.

Electrochemical oxidation of CO may be disregarded [21-22], as compared with it, electrochemical oxidation of hydrogen is faster, and most CO can be converted into CO_2 and H_2 through the water gas shift reaction $CO+ H_2O \rightarrow CO_2+ H_2$. In practice, a small amount of steam and methane are required to mix them up at beginning to push forward subsequent reactions. That is the reason why a small amount of water is added into the methane fuel for SOFC [16, 23], and the reason why circulation of anodic gas and progressive methane steam reforming are adopted [17].

Carbon deposits cannot be completely removed by adding a small amount of water steam into methane as a fuel gas, the practice of which is helpful for steam reforming reaction. Kawano [19] and Gunji [24] discovered that a small amount of water steam added into methane may lead to few carbon

deposits on cell anode, because of O^{2-} reacting with C and CH_4, or H_2O generated electrochemically on anode reacts with C or CH_4.

1.4.2 CO2 reforming of methane

CO_2 Reforming of methane is also called dry reforming of methane. The process of preparation of mixture gas through CH_4-CO_2 reforming is an effective path to utilization of CH_4 and CO_2. In this process, the ratio of H_2/CO is about 1 in mixture gas, and H_2/CO can be directly used as raw materials for carbonyl synthesis and the Fischer-Tropsch reaction. The CO_2 reforming reaction is

$$CH_4 + CO_2 \rightarrow 2CO + 2H_2 \tag{1.23}$$
$$CH_4 + 2CO_2 \rightarrow 3CO + H_2 + H_2O \tag{1.24}$$

Internal methane reforming and dry reforming of methane with reaction time of several seconds is a slower reaction relative to electrochemical reaction [25].

Belyaev [26] investigated CO_2 reforming of CH_4 on the Pt|$0.9ZrO_2$+ $0.1Y_2O_3$|Pt+PrO_{2-X} cell by using CH_4 and CO_2 as fuels to generate mixture gas. Taking effect of current into account, the experiment concluded that under the condition of CO_2/$CH_4 \approx 6.7$ at 1073K, the percentage of CO and H_2 reduces as current rises.

The heat of CO_2 reforming reaction of methane reaches 247kJ·mol^{-1} at 1073K and internal thermal equilibrium also exists in this strongly endothermic reaction similar with internal reforming of methane. Carbon deposition is a major disadvantage existing during CO_2 reforming. Although CO_2 functions in removing carbon deposits and moderate amount of CO_2 may relieve inactivation of carbon deposit on anode, sustaining steady operation of cells, the cell performance will, after every carbon deposition-carbon removal process, not restore to the status prior to carbon deposition; and carbon deposition will, after every carbon deposition-carbon removal process, be easier than ever before [27].

1.4.3 Autothermal reforming of methane

Combining advantages of both processes of conventional steam reforming reaction and partial oxidation, autothermal reforming is a process synchronizing partial oxidation of methane and its electrochemical reaction and performing integrated energy matching.

Hibino[28] is an earlier researcher putting forward the concept of single-chamber solid oxide fuel cells (SC-SOFC), the Ni-YSZ/YSZ/Au cell is introduced with a mixture gas of methane and oxygen at the mole ratio of 2:1 at 1223k, and open-circuit voltage of 350mV and the maximum power density of 2.3 mW·cm^{-2} are obtained.

Singhal [7] believed that three reaction paths may exist for methane and oxygen in SOFC during autothermal reforming, as shown in Fig.1.6.
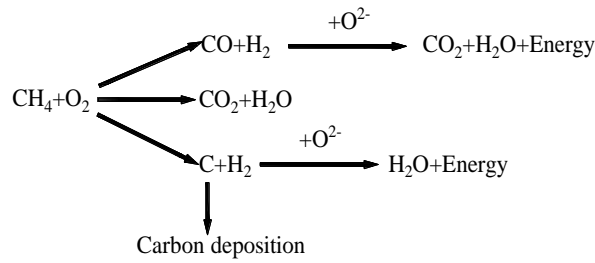
Fig. 1.6 The possible paths of methane partial oxidation reforming process in SOFC [7]

Yano [29] summarized the advance of single-cell autothermal reforming and the geometry of single cell subject to three autothermal reforming processes is shown in Fig.1.7. When methane is used as fuel gas, H_2 and CO are generated from exothermal partial oxidation of methane occurred on anode of single cell, O^{2-} that is transmitted via electrolyte reacts with H_2 and CO to generate H_2O and CO_2.
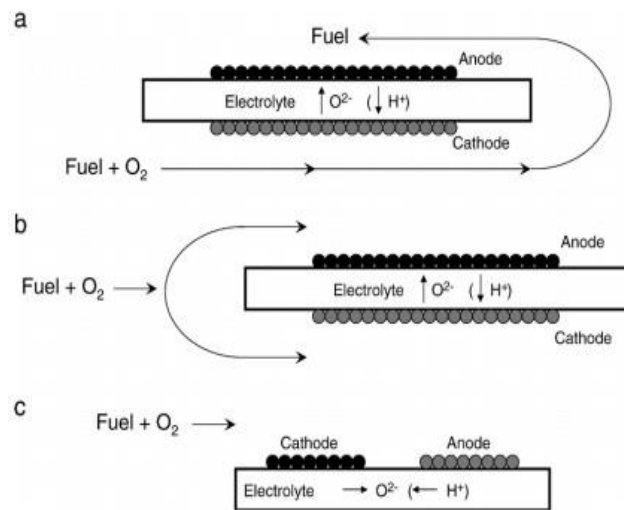
Fig. 1.7 Three types of geometries for SC-SOFCs [29]

Heinzel [30] conducted a research on the autothermal reforming of methane process, and performed a comparative analysis on steam reforming and autothermal reforming. Based on experiment and calculation of thermodynamic equilibrium, Heinzel found that under the experimental condition of 1atm and 973K, the outlet gas composition during steam reforming and autothermal reforming approximates to thermodynamic equilibrium, and maximum H_2 and CO flow is achieved. 80% H_2 flow is for the steam reforming process and 30% H_2 flow for the autothermal reforming process.

Making a single cell by combining 4 conventional NiO-YSZ/YSZ/LSM/ cells and taking CH_4 as fuel at 1023K, Wei [31] measured the cell power of 421 mW.

Although the autothermal reforming single cell has advantages of simple structure, fast start speed and no need of sealing material, its power generation performance is affected by many factors, including inlet flow, proportion of inlet mixture in addition to electrode and electrolyte materials.

Difference between the partial oxidation and reforming process and direct electrochemical oxidation of methane is detailed as follows:

i)　　In the partial oxidation and reforming process, O_2 reacts with methane, the process of which is a chemical reaction; while in the direct electrochemical oxidation of methane process, O^{2-} (from cathodic O_2) reacts with methane, the process of which is an electrochemical reaction.

ii)　　No electric energy is generated from the partial oxidation and reforming process, but its reactants such as H_2 and CO can further react with O^{2-} electrochemically, with current generated; while in the direct electrochemical oxidation of methane process, methane directly reacts with O^{2-} electrochemically, with current generated.

With oxygen and methane that undergo the autothermal reforming process entering into the cell, the lower explosion limit of methane in air is 5.3% and its upper limit is 14% [32], the above limits of which must be avoided, and higher requirements on leak proofness of cells and cell stacks in real applications and tests. Moreover, proper matching of methane and oxygen is very important for the partial oxidation and reforming process. According to analysis as shown in Fig.1.6, existence of some oxygen after partial oxidation and reforming of methane is necessary for the reformed gas to continue its electrochemical oxidation.

1.4.4 Direct electrochemical oxidation of dry methane in SOFC

As for direct electrochemical catalysis and oxidation of dry methane, different researchers found multiple reactions occurring on anode. Aside from the electrochemical reaction in which dry methane reacts with O^{2-} on the cell anode, dry methane could also react with coexist gases. Tab. 1.2 is electrochemical and chemical reactions for methane in the cell anode, in which methane reacts with O^{2-} on anode: partial oxidation reaction in which methane reacts with O^{2-} to generate CO and H_2 and release electrons [6,33], complete oxidation reaction in which methane reacts with O^{2-} to generate CO_2 and H_2O and release electrons [6,33-34], carbon deposition reactions [35], including the reaction (1.3), the reaction (1.25) and the reaction (1.26).

$$2CO \rightarrow C + CO_2 \tag{1.25}$$

$$CO + H_2 \rightarrow C + H_2O \tag{1.26}$$

The reaction of methane on the cell anode is closely related with such factors as methane flow, transfer rate of O^{2-} and reaction temperature.

i) Reaction

Taking the Pt/YSZ/Pt cell as the research object, Ma [36] conducted a research on direct electrochemical oxidation of methane in SOFC. Dependent on operating temperature and reaction airspeed of the cell, multiple reaction mechanisms exist in the oxidation process of methane on anode. The reaction of methane in SOFC is a partial oxidation instead of complete oxidation. With the increase of reaction airspeed, the conversion quantity of methane and production of H_2 and CO tend to drop down and go steady. Gas composition analysis shows that carbon imbalance exists before and after the reaction and carbon deposition occurs on anode.

Tab.1.2 Reactions of methane on the anode

The anode reactions	
Electrochemical reactions	$CH_4 + O^{2-} \rightarrow CO + 2H_2 + 2e^-$
	$CH_4 + 2O^{2-} \rightarrow CO + H_2O + H_2 + 4e^-$ [33]
	$CH_4 + 3O^{2-} \rightarrow CO + 2H_2O + 6e^-$ [37-39]
	$CH_4 + 4O^{2-} \rightarrow CO_2 + 2H_2O + 8e^-$ [6,33-34]
	$H_2 + O^{2-} \rightarrow H_2O + 2e^-$ [34,40]
	$CO + O^{2-} \rightarrow CO_2 + 2e^-$ [40-41]
	$C + O^{2-} \rightarrow CO + 2e^-$ [40-41]
Chemical reactions	$CH_4 \rightarrow C + 2H_2$ [6,42]
	$CH_4 + H_2O \rightarrow CO + 3H_2$ [34,40]
	$CO + H_2O \rightarrow CO_2 + H_2$ [43]
	$CH_4 + CO_2 \rightarrow 2CO + 2H_2$ [18]
	$2CO \rightarrow C + CO$ [44]
	$C + H_2O \rightarrow CO + H_2$ [45]

Possibility of reactions should be taken into account for direct oxidation of methane. According to thermodynamic data of relevant reactions shown in Tab. 1.3, which is calculated by the software of Hsc and the Nernst equation, Gibbs energy changes of 4 oxidation reactions of methane are negative, and these 4 reactions are spontaneous.

With the increase of the proportion of O^{2-} in reaction, electromotive force E^0 gradually reduces. In a power-generating test, with the gradual increase of current, the number of O^{2-} increases and the initial electromotive force of the cell decreases; and the test voltage suddenly drops down as abrupt transition of reaction happens. As shown in Tab. 1.3, maximum change occurs in electromotive force when the reaction $CH_4 + 1/2O_2 \rightarrow CO + 2H_2$ transits toward the reaction $CH_4 + O_2 \rightarrow CO + H_2O + H_2$; while smaller change occurs in electromotive force when transition occurs between other reactions; furthermore, the decline amplitude of electromotive force, which is caused during transition

15

from the reaction $CH_4 + 1/2O_2 \rightarrow CO + 2H_2$ to the reaction $CH_4 + O_2 \rightarrow CO + H_2O + H_2$ at high temperature, is higher than that at low temperature.

Above calculations involve the reactions in which methane reacts with oxygen or the gases that react may react with oxygen. However, it is worth mentioning that the reaction in which various sorts of gases react with oxygen on the cell anode is the reaction with O^{2-}.

Tab. 1.3 The ΔH、ΔG and E^0 of different reaction at the anode at 1073K and 1273K

Reactions at anode(1073K)	$\Delta H_{1073}/$ $KJ\cdot mol^{-1}$	$\Delta G_{1073}/$ $KJ\cdot mol^{-1}$	$E_{1073}{}^0$ $/ V$
$CH_4 + 1/2O_2 \rightarrow CO + 2H_2$	-22.02	-234.16	1.2135
$CH_4 + O_2 \rightarrow CO + H_2O + H_2$	-270.44	-422.84	1.1474
$CH_4 + 3/2O_2 \rightarrow CO + 2H_2O$	-519.39	-611.25	1.0557
$CH_4 + 2O_2 \rightarrow CO_2 + 2H_2O$	-801.70	-800.46	1.0369
$H_2 + 1/2O_2 \rightarrow H_2O$	-248.20	-188.69	0.9777
$CO + 1/2 O_2 \rightarrow CO_2$	-282.32	-189.21	0.9804
$C + 1/2O_2 \rightarrow CO$	-112.44	-206.73	1.0711
Reactions at anode (1273K)	ΔH_{1273} $/ KJ\cdot mol^{-1}$	ΔG_{1273} $/ KJ\cdot mol^{-1}$	$E_{1273}{}^0$ $/ V$
$CH_4 + 1/2O_2 \rightarrow CO + 2H_2$	-23.42	-273.15	1.4153
$CH_4 + O_2 \rightarrow CO + H_2O + H_2$	-272.68	-450.66	1.1675
$CH_4 + 3/2O_2 \rightarrow CO + 2H_2O$	-521.94	-628.16	1.0849
$CH_4 + 2O_2 \rightarrow CO_2 + 2H_2O$	-803.40	-800.09	1.0364
$H_2 + 1/2O_2 \rightarrow H_2O$	-249.26	-177.50	0.9197
$CO + 1/2O_2 \rightarrow CO_2$	-281.46	-171.93	0.8908
$C + 1/2O_2 \rightarrow CO$	-113.71	-224.20	1.1617

Suppose that quantity of O^{2-} transferred to the anode is rising up with the steady increase of the current in a test. Partial oxidation of 1mol methane consumes $1molO^{2-}$, while complete oxidation of 1mol methane consumes $4molO^{2-}$. Under the condition of the changing of the flux of methane and current, the following questions may be raised: whether the reactions of methane are affect by the flux of methane? what is relation between the flux of methane and current?

ii) Research methods

Laosiripojana [46] studied the direct oxidation process of methane in the catalyst 5% Ni/Al_2O_3 impured with CeO_2 made by an impregnation method, the reaction process of methane on catalyst at room temperature at 1273K with different content of CeO_2 added. 8% CeO_2 impured as an excellent catalyst to direct oxidation of dry methane may effectively suppress carbon deposits. With S standing for absorbable solid phase, the decomposition course of methane is

$$CH_4 + 2S \rightarrow CH_3 -S + H-S \tag{1.27a}$$

$$CH_3 -S + S \rightarrow CH_2 -S \tag{1.27b}$$

$$CH_2\text{-}S + S \rightarrow CH\text{-}S + H\text{-}S \quad\quad\quad (1.27c)$$

$$CH\text{-}S + S \rightarrow C\text{-}S + H\text{-}S \quad\quad\quad (1.27d)$$

$$C\text{-}S + O_x \rightarrow CO + O_{x\text{-}1} + S \quad\quad\quad (1.27e)$$

$$2H\text{-}S \rightarrow H_2 + 2S \quad\quad\quad (1.27f)$$

Possible carbon deposition reactions include methane pyrolysis reactions (1.3), the reaction (1.22) and the reaction (1.23). The research of Laosiripojana showed that the anodic reactions are associated with elementary reactions.

Kendall [47] concluded the reaction of pure methane happening under the open-circuit condition is partial oxidation of methane by analyzing open-circuit voltage based on the cell test done with hydrogen plus steam and dry methane on nickel anode containing 5% cerium, and dependent on electromotive force at different temperatures according to Nernst quotation. Fig.1.8 shows theoretical electromotive force and open-circuit voltage obtained from experiment.

(a)   (b)
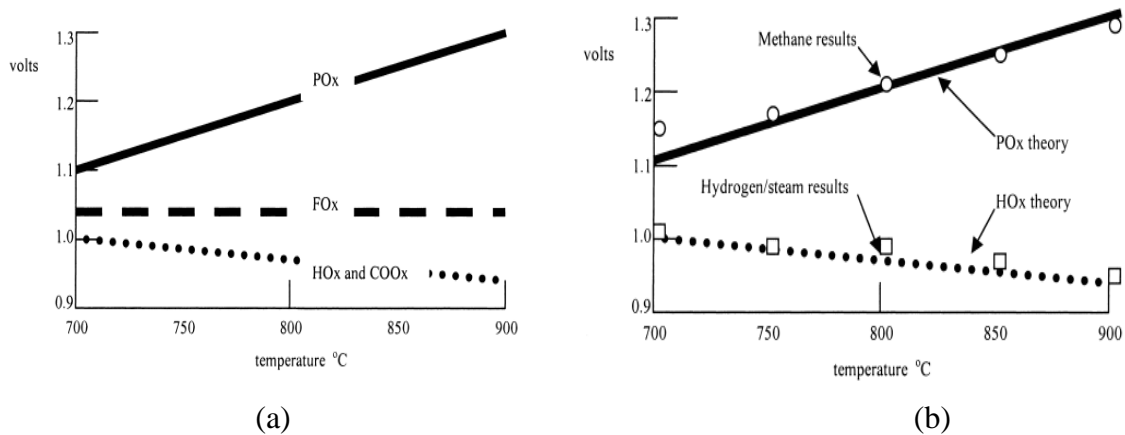
Fig. 1.8 Results of K. Kendall's work
(a) Theoretical OCV for methane, hydrogen and CO oxidation as a function of temperature
(b)Comparison of Nernst theory and results for methane and hydrogen with steam [47].

On this basis, Kendall concluded that changes occurred in reaction mechanism of diluted methane, transiting to complete oxidation from partial oxidation. The research conducted by Kendall provided a way to judge on reaction attribute of SOFC under the open-circuit condition. However, there were no clear explanations about changes in reaction mechanism for the test with diluted methane, and the reasons why the measured open-circuit voltages are sometimes higher or lower than the theoretical value.

Bruce [48] studied the direct oxidation of methane on the anode of $La_{0.75}Sr_{0.25}Cr_{0.5}Mn_{0.5}O_{3\text{-}\delta}$ –Cu–YSZ, and determined whether the relevant reaction happened by making comparison between

the open-circuit voltage measured through H_2 mixed fuel containing CO_2 and H_2O at different flow and the theoretical open-circuit voltage anticipated on the basis of Nernst equation.

Based on the following two reactions,

$$C + O^{2-} \rightarrow CO + 2e^- \tag{1.4}$$

$$CH_4 + 4O^{2-} \rightarrow CO_2 + 2H_2O + 8e^- \tag{1.5}$$
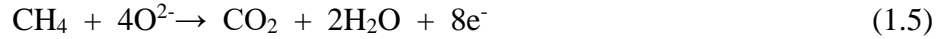
Abuliti [6] studied reaction of dry methane on the anode Ni-YSZ. 1mol C and 1mol CH_4 contribute 2mol and 8mol e^- through the reaction (1.4) and reaction (1.5) respectively. Analysis of electrons contributed through anode exhaust gas composition and electrons carried with current shows that partial oxidation of 4.2% dry methane happens on the anode Ni-YSZ at low current density, complete oxidation happens at high current density.

You [49] researched the reaction mechanisms of low concentration of dry methane at Ni-YSZ and Ni-ScSZ anodes by the quantitative analysis of elements at different current densities as well as the analysis of the activation energy of elementary reactions of CH_4 were investigated to identify the types of methane reactions. It was found that electrochemical oxidation reactions of methane occurred according to the following sequence with increasing current density:

$CH_4 + O^{2-} \rightarrow CO + 2H_2 + 2e^-$

$CH_4 + 2O^{2-} \rightarrow CO + H_2O + H_2 + 4e^-$

$CH_4 + 3O^{2-} \rightarrow CO + 2H_2O + 6e^-$

$CH_4 + 4O^{2-} \rightarrow CO_2 + 2H_2O + 8e^-$
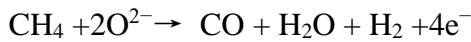
When the latter reactions that consume much more O^{2-} take place, the former reactions that consume relatively less O^{2-} are still ongoing.

With the increase of O^{2-} involved in reaction, electromotive force E^0 gradually reduces. In a power-generating test, with the gradual increase of current, the number of O^{2-} increase and the initial electromotive force of the cell drops; when abrupt shift of reaction happens, the measured voltage also suddenly drops . As shown in Tab. 1.3, maximum change occurs in electromotive force when the reaction $CH_4 + 1/2O_2 \rightarrow CO + 2H_2$ transits toward the reaction $CH_4 + O_2 \rightarrow CO + H_2O + H_2$; while smaller change occurs in electromotive force when transition occurs between other reactions; furthermore, the decline amplitude of electromotive force, which is caused during transition from the reaction $CH_4 + 1/2O_2 \rightarrow CO + 2H_2$ to the reaction $CH_4 + O_2 \rightarrow CO + H_2O + H_2$ at high temperature, is higher than that at low temperature. But less test and research show and explain the phenomenon of the rapid drop of voltage when different reactions take place.

Partial oxidation of 1mol methane consumes 1mol O^{2-}, while complete oxidation of 1mol methane consumes 4mol O^{2-}. In a SOFC, the operation may be conducted at current and flux of dry methane changed. Under the condition of the changed of current or the flux of dry methane, the following questions may be raised: whether the anode reaction is single reaction？ what is the relation between current and the flux of dry methane? what is condition for partial oxidation dry methane? and what is condition for complete oxidation of dry methane? When the current density varies continuously, the reactions of methane at anode remain to be studied.

1.5 Analysis method of anode exhausts gas

Many types of anode exhaust gas components are generated from electrochemical reaction with dry methane used as fuel gas passing through cell anode. On-line analysis on output anode exhaust gas components shows what sorts of gas are generated and helps determine the conversion rate of fuel entering into anode when components of anode exhaust gas are obtained through quantitative analysis, and learns about change rule and reaction characteristics of exhaust gas components generated and indirectly infers the real trend of electrochemical reaction of dry methane on anode. Therefore, it is necessary to know the analytic method of anode exhaust gas.

As an efficient isolation technology, Gas Chromatography aims to segregate compounds by utilizing the difference of boiling point, polarity and adsorbability [52].

Common quantitative chromatographic methods including external standard method, internal standard method, peak area (peak height) percentage method and normalization method are generally adopted for chromatographic measurement and quantitative analysis. Among them, the external standard method is commonly used in which sample components under the same analytical condition are compared with peak area or peak height shown in chromatographic analysis of samples. As long as working curves are determined from standard samples determining flow, quantitative analysis can be done to unknown samples under the same condition.

When using external standard method, chromatographic peak corresponding to standard gas is used to determine the component name according to peak position, and to determine component concentration according to peak area.

When methane was used as fuel, the exhaust gases of anode side were analyzed on-line using chromatography system to analyze anode reaction characteristics. Huang [53] used CO-NDIR and CO-2NDIR to test CO and CO_2, and two gas chromatographs in series were used to measure other

exhaust gas components. Abuliti [54] used multiple chromatographs specific to different components and inferred anodic reaction from an analysis of anode exhaust gas tested.

In above studies on methane oxidation on anode in SOFC, chromatography is an effective means to measure anode exhaust gas. The basic reaction process of methane on cell anode can be inferred from chromatographic measurement of anode exhaust gas. Out of many reactions of fuel gas occurring on anode, the primary and basic reaction is the top concern of relevant researchers. Chromatograph is not the only means to measure exhaust gas, mass spectrum or other measurement means may be used to analyze anode exhaust gas. Fisher [40] used 4-electrode mass spectrometer to measure components of anode exhaust gas. Zhan [51] measured the outlet gases of the Ni-YSZ anode side by using Transpector 2® Gas Analysis System. Besides, the catalytic reaction occurring on anode can be directly tested by Pulsed-Laser Imaging Atom-Probe (PLLAP) [50]. However, further study is required to determine whether an influence of the heating of the probe exposed to laser irradiation on surface catalysis exists or not.

1.6 Anode materials

The conventional SOFC configuration consists of a dense electrolyte between a porous cathode and a porous anode [4, 5]. Among all of the components in SOFC, the main role of a dense electrolyte is used to prevent gas mixing and two electrodes to come into electronic contact, as well as allows the flow of charged ions from cathode to anode. Generally, there are several ionic conductors including doped-ZrO_2 [55], doped-CeO_2 [56], doped-Bi_2O_3 [57] and perovskite [58] are proven and used as good candidates for SOFC electrolyte. A cathode is used to provide a reactive site to absorb oxygen molecule for reductive reaction and form oxygen ions. Perovskite materials, i.e. $La_{0.8}Sr_{0.2}MnO_{3-\delta}$ (LSM), $La_{0.6}Sr_{0.4}CoO_{3-\delta}$, $(La_{0.6}Sr_{0.4})_{1-s}Fe_{0.8}Co_{0.2}O_{3-\delta}$, $La_{1-\delta}Fe_{0.4}Ni_{0.6}O_{3-\delta}$ are usually used as cathode materials [59-61].

Anode plays a critical role in SOFC, in which the oxidation of fuel and generation of electrons is occurred. An ideal anode is required to provide [62-63]:

(i)   High electronic and ionic conductivity

(ii)   High catalytic activity

(iii)   High permeability for the fuel gas and the reaction products

(iv)   Uniform distribution and percolation of all three phases

(v)   High thermal and chemical stability in reduction atmosphere

(vi)   High compatibility with electrolyte

(vii)   High coking and sulfur resistance for hydrocarbon-fueled SOFCs

To meet these requirements, various materials including noble and non-noble metals, fluorites, and perovskites have been prepared and investigated as potential anodes.

1.6.1 Ni based anode

Ni has several advantages, including low cost, ease of fabrication, high electronic conductivity, high electrochemical activity, and high reforming activity, in comparison to other potential anode materials for SOFC. Therefore, mixtures of Ni and ionic conductor, such as yttria-stabilized zirconia (YSZ) are used as conventional anode due to its chemical stability at high temperature and close compatibility with YSZ electrolyte [64]. In a Ni-YSZ anode, the YSZ play a role in constituting a framework for the uniformly dispersion of Ni grains and prevent the agglomeration of Ni particles at high temperature both in fabrication and SOFC operation. Additionally, the dispersed YSZ in the cermet can provide part of ionic conductivity to expand three-phase boundary. Fig. 1.9 shows the variation curves of the electronic conductivity in the Ni-YSZ anode as a function of Ni content predicated by percolation theory [65].
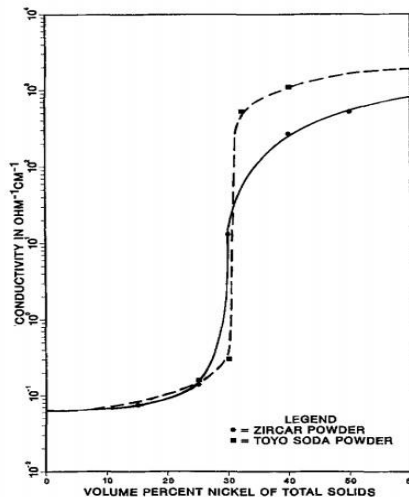
Fig. 1.9 Conductivity of cermets as function of nickel concentration of
Ni-YSZ cermet at 1273K [65]

It can be inferred that the threshold value of Ni-YSZ is at about 30% Ni content. Below this threshold value, Ni-YSZ anode exhibits an ionic conducting behavior and its conductivity is nearly identical to pure YSZ [66]. In practical application, the Ni content is usually controlled between 40% and 60% [67]. Generally, a Ni-YSZ anode is obtained by mixing NiO with YSZ powder and then co-fired with electrolyte and reduced in a reduction atmosphere for characterization.

It is well known that Ni-YSZ anode work satisfactorily with hydrogen because of the high electrochemical catalytic activity of mental Ni. Unfortunately, when hydrocarbons such as methane are directly used as fuel, Ni-YSZ anode has number of disadvantages including Ni coarsening at high temperature, mechanical instability under redox cycling, sulfur poisoning and carbon deposition. Especially, carbon will easily form and deposit on a Ni-YSZ anode, resulting in not only the lower fuel utilization but also anode deactivation [68]. The main reason is metal Ni has high catalytic activity for breaking C-H bond [69]. Therefore, for direct utilization of hydrocarbon, it is vital to solve the carbon coking problem. It is well known that adding H_2O reform hydrocarbons is an effective way to mitigate the coking problem. However, the cell will be damaged and the system complexity will be increased due to high content of H_2O [70].

To date, several efforts are devoted to suppress carbon deposition. Among them, optimizing the conventional Ni based anodes and/or developing new alternative materials are main approaches to direct utilization of hydrocarbon fuels. On the one hand, alloying the poor catalytically active Cu [71], Fe [72], Co [71], and Au [73] with Ni to prepare bimetallic anode are widely confirmed an effective measure for anti-carbon formation. Sin [74] found that Ni-Cu bimetallic anode had the good durability under dry methane for 1300 h at 1023K. Rismanchian [75] developed a Ni-Cu alloy as anode catalyst which could suppress carbon formation for hydrocarbon fuels. Apart from carbon deposition, poor mechanical instability under redox cycling is another drawback for conventional Ni-YSZ anode [76]. Ni is easily oxidized to NiO at high temperature when seal leakage appears and fuel gas stops, resulting in the co-existed Ni and NiO in anode functional layer. The re-oxidization of Ni to NiO can cause the phase change with a volumetric of 69%, resulting in the mechanical expansion of cell. Chen [77] detailedly investigated the degradation mechanisms of nickel-based anode in low concentrations dry methane, and found that the degradation of Ni-based anode could be mainly attributed to the re-oxidation of Ni.

1.6.2 Cu based anode

Ni has high catalytic activity for breaking C-H bond when hydrocarbon was used as fuel. Therefore, in order to avoid the carbon deposition on a Ni-YSZ anode, several alternative materials was developed to replace Ni-YSZ as potential anode. Among these efforts, using Cu to replace Ni is an effective method to suppress coking due to its stability and high electronic conductivity; as well as poor catalytic activity for making and breaking C-C bonds [78-80]. However, the melting points of Cu (1358K) or copper oxide (CuO, 1600K) is significantly lower than the temperature of the fabrication of conventional Ni-based anode SOFC. For example, the sintering temperature of YSZ electrolyte is

reached 1773K, which is not possible to prepare Cu-YSZ anode. Therefore, Grote [68, 81] prepared Cu-YSZ by an effective method in which an YSZ porous framework first and then impregnated Cu into YSZ and followed by sintering at relative temperature. Also, considering the lower catalytic activity of Cu for fuel, CeO_2 as a catalyst is usually impregnated into Cu-YSZ to prepare CeO_2-Cu-YSZ anode.

Ceria-based anodes, with a fluorite structure, have a high resistance to carbon deposition [82]. CeO_2 or doped-CeO_2 shows a special mixed ionic-electronic conductivity in fuel atmosphere due to the reduction of Ce^{4+} to Ce^{3+}, which can be used as a SOFC candidate anode material. It is well known that Ceria-based materials have good catalytic activity for methane. The main reason is maybe that CeO_2 has good storage, release and transport capacity of oxide ions O^{2-}. Recently, it has been reported that the active lattice oxygen in CeO_2 is the essential reason for inhibiting carbon deposition [83-85]. However, the electronic conduction of CeO_2 system is a small activation transition process, suffering from the influence of temperature on electronic conductivity, resulting in the restriction of CeO_2-based anode material for SOFC. For example, the electronic conductivity of $Ce_{0.8}Y_{0.2}O_{1.9}$ is only 0.08~0.1 S cm^{-1} at 1073K. To overcome this problem, CeO_2 and metal (Pd [86], Au [87]) are usually adopted to modify the metal-based anode (Ni-based, Cu-based), which can not only meet the electronic conductivity but also improve catalytic activity and coking resistance [68].

1.6.3 Perovskits anode material

Perovskite-type oxides have been investigated as potential anodes for intermediate temperatures SOFC. The lattice structure of perovskites, abbreviated as ABO_3, consisted of three elements, namely the large cations, A^{n+}, the small cations, $B^{(6-n)+}$, and the oxide ions O^{2-}. In the idealized cubic of a perovskite, the atom A, B, and oxygen occupy the center position (0, 0, 0), the body centered position (1/2, 1/2, 1/2) and the faced centered sites (1/2, 1/2, 0). However, in a perovskite structure, A and B sites can be partially or fully substituted, leading to a wide range of oxygen vacancies and enhancement of electronic conductivity. Generally, substitution of A site cations with a lower valence cations, creating an A-site charge deficiency and oxygen vacancies in the perovskite structure. Also, a reducible transition metallic ion is used as B site cation to change the B site valence, therefore, perovskite exhibits the electronic conductivity [88-90].

Perovskite-type materials [91-92] have several advantages including mixed ionic-electronic conductivity, excellent thermal and mechanical stability, coking resistance and sulfur resistance. It is well known that doped-$LaCrO_3$ [93-96] and doped-$SrTiO_3$ [97-101] are performed as potential materials for the direct utilization of hydrocarbons. Besides, Goodenough [102] reported a double

perovskite-type material $Sr_2Mg_{1-x}Mn_xMoO_{6-\delta}$, which exhibited high electrocatalytic activity and sulfur resistance. Ruiz-Morales [103] also investigated the possibility and applicability of $La_4Srn_{-4}TinO_{3n+2}$ as SOFC anode materials, and found that it show high electrode performance. However perovskite-type materials still have some disadvantages [104,105], i.e. immature manufacturing process, low electronic conductivity, low stability. It is necessary to further develop perovskite-type materials as potential anodes both in microstructure and composition [103,106].

As reviewed above, energy conversion efficiency and flexibility of fuels in SOFC are mainly determined by anode materials. For the direct utilization of hydrocarbon fuels, an anode candidate requires to provide coking resistance, sulfur resistance and thermal stability, as well as high electrochemical activity. Developing new type anode materials and/or optimizing conventional Ni based anode is an important technical objective in the future. Compared with conventional Ni-YSZ anode, perovskite-type anode material has several drawbacks. i.e. low conductivity, low catalytic activity. Therefore, Ni-based anode still attracts wide attention. So the key problem of anode materials is how to realize the organic unity including conductivity, catalytic activity, coking resistance and stability.

1.6.4 Three phase boundary

As indicated above, the electrochemical reactions occur in the anode interface in which is within a distance of less than 10-20 μm from the electrolyte surface [107,108]. This zone is referred to as the functional layer. The reactions of fuel with oxygen ion not only need fuel, oxygen ion and catalyst, but also require the generated electron to be transported out. The place where reactions occur is termed triple phase boundaries (TPBs). At the same time, effective transport pathways of fuel, oxygen ion and electron need to be established to and from each TPB. Fig. 1.10 [109] shows a typical schematic of triple phase boundary interface. It is generally accepted that electrode microstructure plays an important role in determining the length of TPB of SOFCs. Investigations have shown the performance and durability of SOFCs are determined by TPB length. Therefore, the relationships between microstructure and TPB need to be understood in order to develop optimum electrodes.

Zhu [110] proposed the TPB length could be optimized by improving microstructure parameters such as the porosity and the particle size. High electrode porosity is crucial to promote gas flow to the TPB, where reactions occur, but conductivity and mechanical strength are compromised if the porosity is too high. It is well known that adding the pore former into the raw anode materials is one of the most effective methods to improve anode porosity. The pore formers, including flour, graphite, carbon dust，and polymers, are combustible additives [111-112]. They can be burned off during high

temperature-treatment, leaving pores in the anode. Pan [113-114] added paper-fibers and/or polyvinyl alcohol (PVA) fibers into Ni-YSZ to prepare porous anode, which showed a high cell performance. Sarikaya [115] modified the anode microstructure by using Polymethyl methacrylate (PMMA) as pore former, and the cell also exhibited high performance. Sumi [116] investigated the effects of anode microstructures on cell performance and durability in wet methane, and found that graphite as the anode pore former can enhance the cell durability.
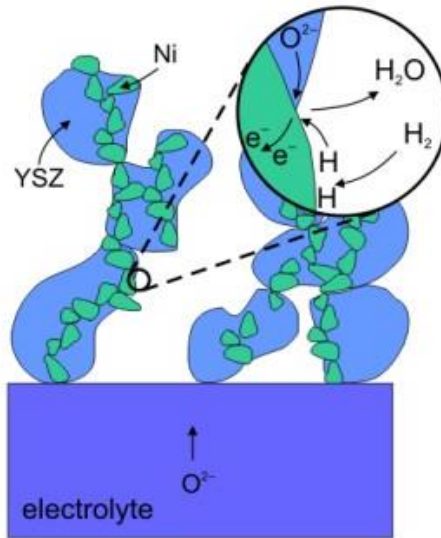
Fig. 1.10 Triple phase boundary structure in the anode [109]

Apart from adding pore former to increase porosity, hard template method has typical advantage in its shape and structure to prepare porous microstructure material with high specific surface; and the prepared material can copy the template structure after the template is burned off. While wet impregnation method can produce anode materials with different metal ions doping; and the prepared materials can enhance the contact between catalyst and electrolyte. You [117] used activated carbon fiber (ACF) as template to prepare tubular YSZ as skeleton first, and then dipped in salt solutions containing various concentrations of Ni and Cu species by wet impregnation method to fabricate $Ni_{0.5}Cu_{0.5}O_x$ coated tubular YSZ powders, which effectively extended the TPB lengths to achieve high performance. Dong [118] has employed the thin film inside the egg shell as template to prepare $Sm_{0.5}Sr_{0.5}CoO_3$ (SSC) electrolyte material, whose microstructure is hollow fiber network structure, and show high performance. Pinedo [119] adopted colloid as a template for preparing porous $Pr_{0.7}Sr_{0.3}Fe_{0.8}Ni_{0.2}O_3$ perovskite-type oxides. Koh [120] used two 3-D graphite template to build the three-dimensional SOFC cell. Besides, Liu [121] significantly increased the TPB lengths by impregnated catalyst into porous anode substrate. Ding et al. [122-123] developed the relationship of

25

modified particle loading and porosity and the length of the TPB both in theory and experiment. Results have shown that the TPB length increased with the coverage of modified particles in the porosity range of 0.30~0.53. In sum, the improvement of TPB should be developed in order to improve performance and durability of SOFCs.

1.7 Motivation and objectives

As reviewed above, SOFC operates directly with hydrocarbon fuels is widely expected to be an important objective for power generation in the future. Therefore, for direct utilization of hydrocarbon, it is vital to understand the reaction mechanism of methane on anode and/or develop alternative materials with high performance as potential SOFC anode.

The objectives of this study are:

(i) Gain a better understands on the reaction mechanisms of dry methane on the anode.

(ii) Gain a better understands on the performance change mechanism of Ni-ScSZ anode in different concentration of dry methane.

(iii) Optimize conventional Ni based anodes for hydrocarbon-fuelled SOFCs, both in the composition and microstructure.

(iv) Develop alternative perovskites materials as potential anode for hydrocarbon-fuelled SOFCs.

1.8 Organization and outline of the thesis

In this study, the reaction mechanisms of dry methane on the anode (Ni-YSZ or Ni-ScSZ) are investigated detailedly, utilizing a combined theoretical and experimental approach. The degradation mechanism of Ni- ScSZ anode in low concentration of dry methane is explored. Besides, the optimization of conventional Ni based anodes and development of alternative materials for direct utilization of hydrocarbon fuels SOFCs are focused.

Chapter 1 presents a brief introduction on basic concepts, the main component materials, thermodynamics, and reaction dynamics of SOFCs, as well as the utilization of methane mode. At the end it also lists the approaches, motivation, objectives and outline of this study.

Chapter 2 gives the flow process of material preparation, fabrication and measurements of single cells, as well as characterization techniques, especially on the Agilent GC 7890A gas chromatography system for analyzing the outlet gases of anode side on-line.

Chapter 3 evaluates the influence of dry methane concentration on reactions mechanism at Ni-YSZ anode in SOFC, and explores the mathematical relationship between the concentration of dry methane and the amount of oxygen ions by a new monitoring method. In order to understand the reactions on

anode supplied by different concentration of dry methane, the exhaust gases of anode side was analyzed on-line and its regular pattern was concluded by using the chromatography. Also, the reaction pathway between dry methane flux and SOFC operated current was developed by using the activation energy of methane elementary reactions for different anode reaction. The mathematical relationships between dry methane flux and operated current was obtained. It was expected to understand clearly the occurred sequence of electrochemical reactions for dry methane in a Ni-YSZ anode.

Chapter 4 clarifies the influence of dry methane concentration on the output performance of cells with Ni-ScSZ anode by a similar monitoring method described in Chapter 3. The main reason for the output performance change was further discussed from electrochemical reaction kinetics. Especially in low concentrations of dry methane, the phenomenon with rapid cell output voltage at high current density was observed and further studied. A better understand on the rapid degradation mechanism of Ni-ScSZ anode in the condition without mechanical damage and seal leakage will be achieved.

Chapter 5 creates a Ni_xCu_{1-x} alloy anode with novel structure for the direct utilization of hydrocarbon fuels. The novel anode prepared directly by alloying the poor catalytically active Cu with Ni was elaborated in this chapter. The as-prepared material with a columnar shape and cubic crystal structure was observed. The possibility of Ni-Cu alloy as a potential anode was investigated in dry CH_4, both in performance test and stability test.

Chapter 6 designs an anode microstructure modification process to obtain a high performance anode for methane direct oxidation. Besides, as indicated in Chapter 5, carbon deposition could be effectively suppressed by using a Ni-Cu alloy anode. Therefore, in this chapter, the tubular YSZ with the stereo structure was firstly prepared by hard template method to form a three dimensionally porous anode framework, and then $Ni_{0.5}Cu_{0.5}O_x$ as catalysts was impregnated into YSZ skeleton to fabricate $Ni_{0.5}Cu_{0.5}O_x$-YSZ composite anode. The performance and stability of $Ni_{0.5}Cu_{0.5}O_x$-YSZ anode was characterized when CH_4 was used as fuel, which will be discussed in detail in this chapter [117].

Chapter 7 demonstrates the optimization of $Ni_{0.5}Cu_{0.5}O_x$-YSZ anode in Chapter 6 for further enhancement of coking resistance. In this chapter, $Ce_{0.8}Sm_{0.2}O_{1.9}$ (SDC) was adopted to replace YSZ as anode scaffold and $Ni_{0.5}Cu_{0.5}Ba_{0.05}O_x$ was used as the impregnated catalyst to prepare three-dimensional $Ni_{0.5}Cu_{0.5}Ba_{0.05}O_x$/SDC anode. In addition, the anode microstructure effect on the cell performance was investigated by using a powdered $Ni_{0.5}Cu_{0.5}Ba_{0.05}O_x$-SDC anode, which was prepared by mixing $Ni_{0.5}Cu_{0.5}Ba_{0.05}O_x$ powder and SDC powder. The single cells with such contrastive anodes were fabricated for the power generation performance test and the long-term stability test. The carbon formation was also detected to reveal the cell degraded phenomenon.

Chapter **8** discusses the possibility and applicability of the $SrMoO_4$ based materials as an alternative candidate for SOFC anodes. Considering the low catalytic activity of $SrMoO_4$-YSZ in preliminarily investigation, $Gd_{0.2}Ce_{0.8}O_{1.9}$ (GDC) was introduced into $SrMoO_4$ by wet impregnation to further improving its potential as SOFC anode materials. In order to further improve cell performance, the composition of this composite anode was further optimized, which will be discussed in detail in this chapter [124].

Finally, a detailed conclusion in **Chapter 9** is presented on the general discussion of the results in the whole report. It emphasizes the most important conclusions in the study and finally comments on how the research of this topic could be continued.

References

[1] K. Lee, J. Yun, K. Ahn, S. Lee, S. Kang, S. Yu, Operational characteristics of a planar steam reformer thermally coupled with a catalytic burner, *Int. J. Hydrogen Energy* **38(11)** (2013) 4767-4775.

[2] D. Cui, B. Tu, M. Cheng, Effects of cell geometries on performance of tubular solid oxide fuel cell, *J. Power Sources* **297** (2015) 419-426.

[3] H. Orui, K. Watanabe, M. Arakawa, Electrochemical characteristics of tubular flat-plate-SOFCs fabricated by co-firing cathode substrate and electrolyte, *J. Power Sources* **112(1)** (2002) 90-97.

[4] D. X. Cao, G. L. Wang, Y. Z. Lv, Fuel cell system, X. Yang(Eds.), Beihang University Press, Beijing, 2009.

[5] Y. Li, L. S. Wang, Fuel Cell, Z. G. Wang(Eds.), Metallurgical Industry Press, Beijing, 2000.

[6] A. Abudula, M. Ihara, H. Komiyama, K. Yamada, Oxidation mechanism and effective anode thickness of SOFC for dry methane fuel, *Solid State Ionics* **86-88(Part 2)** (1996) 1203-1209.

[7] S. C. Singhal, K. Kendall, High Temperature Solid Oxide Fuel Cells, Foundamentals, Design and Application, S. C. Singhal, K. Kendall (Eds), Elsevier Ltd., Amsterdam, 2003.

[8] G. Xiao, Fuel Cell Technology, L.S. Zhao (Eds.), Publishing House of Electronics Industry, Beijing, 2009.

[9] R. O' Hayre, S. W. Cha, W. Colella, F. B. Prinz, Fuel Cell Fundamentals, H. P. Tan, D. H. Dan(Eds.), Publishing House of Electronics Industry, Beijing, 2007.

[10] J. T. Wang, Advanced Organic Chemistry, Higher Education Press, Beijing, 1980.

[11] J. M. Smith, H. C. Van Ness, M. M. Abbott, Introduction to Chemical Engineering Thermodynamics, 7th edition, Z.X. Jiang(Eds.), Chemical Industry Press, Beijing, 2008.

[12] Y. D. zhang, X. L. Gao, W. Li, Z. J. Wang, H. P. Wu, The Lowest Energy Principle and Its Applications in Organic Chemistry Reaction, *J. Zhengzhou Univ. Tech.* **21**(2000) 44-47..

[13] T. Hibino, A. Hashimoto, M. Suzuki, M. Sano, A solid oxide fuel cell with a novel geometry that eliminates the need for preparing a thin electrolyte film, *J. Electrochen. Soc.* **149(2)** (2002) A195-A200.

[14] Y. H. Wu, H. Y. Wang, A study on the bond-order-conservation model of the mechanism of methane partial oxidation to syngas on Ni, *J. Zhejiang Norm. Uni. (Nat.Sci)* **19(1)** (1996) 48-52.

[15] E. S. Hecht, G. K. Gupta, H. Y. Zhu, A. M. Dean, R. J. Kee, L. Maier, O. Deutschmann, Methane reforming kinetics within a Ni-YSZ SOFC anode support, *Appl. Catal., A* **295(1)** (2005) 40-51.

[16] R. Peters, R. Dahl, U. Klüttgen, C. Palm, D. Stolten, Internal reforming of methane in solid oxide fuel cell systems, *J. Power Sources* **106(1-2)** (2002) 238-244.

[17] P. Vernoux, M. Guillodo, J. Fouletier, A. Hammou, Alternative anode material for gradual methane reforming in solid oxide fuel cells, *Solid State Ionics* **135(1-4)** (2000) 425-431.

[18] E. Perry Murray, T. Tsai, S. A. Barnett, A direct-methane fuel cell with a ceria-based anode, *Nat.* **400(6745)** (1999) 649-651.

[19] M. Kawano, T. Matsui, R. Kikuchi, H. Yoshida, T. Inagaki, K. Eguchi, Steam reforming on Ni-samaria-doped ceria cermet anode for practical size solid oxide fuel cell at intermediate temperatures, *J. Power Sources* **182(2)** (2008) 496-502.

[20] T. Ishihara, T. Yamada, T. Akbay, Y. Takita, Partial oxidation of methane over fuel cell type reactor for simultaneous generation of synthesis gas and electric power, *Chem. Eng. Sci.* **54(10)** (1999) 1535-1540.

[21] A. M. Sukeshini, B. Habibzadeh, B. P. Becker, G. S. Jackson, Electrochemical oxidation of H_2, CO, and CO/H_2 mixtures on patterned Ni anodes on YSZ electrolytes, *J. Electrochen. Soc.* **153(4)** (2006) A705-A715.

[22] A. Weber, B. Sauer, A. C. Müller, D. Herbstritt, E. Ivers-Tiffée, Oxidation of H_2, CO and methane in SOFCs with Ni/YSZ-cermet anodes, *Solid State Ionics* **152-153(12)** (2002) 543-550.

[23] R. Peters, E. Riensche, P. Cremer, Pre-reforming of natural gas in solid oxide fuel-cell systems, *J. Power Sources* **86(1-2)** (2002) 432-441.

[24] A. Gunji, C. Wen, J. Otomo, T. Kobayashi, K. Ukai, Y. Mizutani, H. Takahashi, Carbon deposition behaviour on Ni-ScSZ anodes for internal reforming solid oxide fuel cells, *J. Power Sources* **131(1-2)** (2004) 285-288.

[25] B. Qi, The Intrinsic Kinetics of Methane Steam Reforming and Reaction Performance Study in Micro-channel Reactor, Chongqing University, 2009.

[26] V. Belyaev, V. Galvita, V. Sobyanin, Effect of anodic current on carbon dioxide reforming of methane on Pt electrode in a cell with solid oxide electrolyte, *React. Kinet. Catal. Lett.* **63(2)** (1998) 341-348.

[27] N. Lu, Research of SOFC Performance feeded with CH_4 and Experience of Changing Characteristic over Anode, Dalian University of Technology, 2006.

[28] T. Hibino, H. Iwahara, Simplification of solid oxide fuel cell system using partial oxidation of methane, *Chem. Lett.* **7(7)** (1993)1131-1134.

[29] M. Yano, A. Tomita, M. Sano, T. Hibino, Recent advances in single-chamber solid oxide fuel cells: A review, *Solid State Ionics* **177(39-40)** (2007) 3351-3359.

[30] A. Heinzel, B. Vogel, P. Hübner, Reforming of natural gas-hydrogen generation for small scale stationary fuel cell systems, *J. Power Sources* **105(2)** (2002) 202-207.

[31] B. Wei, Z. Lü, X.Q. Huang, M. L. Liu, D. Jia, W. H. Su, A novel design of single-chamber SOFC micro-stack operated in methane-oxygen mixture, *Electrochem. Commun.* **11(2)** (2009) 347-350.

[32] D. T. Wang, W. P. He, Chemical Safety and Environmental Protection, S. J. Zhang(Eds.), Chemical Industry Press, Beijing, 2011.

[33] X. Zhang, S. Ohara, C. Hong, T. Fukui, Conversion of methane to syngas in a solid oxide fuel cell with Ni-SDC anode and lsgm electrolyte *Fuel* **81(8)**(2002) 989-996.

[34] J. H. Koh, Y. S. Yoo, J. W. Park, H. C. Lim, Carbon deposition and cell performance of Ni-YSZ anode support SOFC with methane fuel, *Solid State Ionics* **149(3-4)** (2002) 157-166.

[35] T. H. Wu, Q. G. Yan, J. T. Li, C. R. Luo, W. Z. Wen, L. F. Yang, H. L. Wan, Mechanism study of carbon depoition on a Ni/Al_2O_3 catalyst during partial oxidation of methane to syngas, *J.Nat. Gas Chem.* **9(2)** (2000) 89-89-1002.

[36] Z. F. Ma, B. C. Huang, X. Z. Liao, Y. J. Leng, Investigation of the performance of CH_4 oxidation at SOFC anode, *Chin. J.Power Sources* **23(3)** (1999) 164-166.

[37] P. Zhang, Y. H. Huang, J. G. Cheng, Z. Q. Mao, J. B. Goodenough, Sr_2CoMoO_6 anode for solid oxide fuel cell running on H_2 and CH_4 fuels, *J. Power Sources* **196(4)** (2011) 1738-1743.

[38] A. Sin, E. Kopnin, Y. Dubitsky, A. Zaopo, A. S. AricÒ, L. R. Gullo, D. L. Rosa, V. Antonucci, Stabilisation of composite LSFCO-CGO based anodes for methane oxidation in solid oxide fuel cells, *J. Power Sources* **145(1)** (2005) 68-73.

[39] Y. Nabae, I. Yamanaka. Alloying effects of Pd and Ni on the catalysis of the oxidation of dry CH_4 in solid oxide fuel cells, *Appl. Catal., A* **369(1-2)** (2009) 119-124.

[40] J. C. F. Ii, S. S. C. Chuang, Investigating the CH_4 reaction pathway on a novel LSCF anode catalyst in the SOFC, *Catal. Lett.* **10(6)** (2009) 772-776.

[41] K. Ke, A. Gunji, H. Mori, S. Tsuchida, H. Takahashib, K. Ukaic,Y. Mizutanic, H. Sumic, M. Yokoyamac, K. Wakia, Effect of oxide on carbon deposition behavior of CH_4 fuel on Ni/ScSZ cermet anode in high temperature SOFCs, *Solid State Ionics* **177(5-6)** (2006) 541-547.

[42] N. C. Triantafyllopoulos, S. G. Neophytides. The nature and binding strength of carbon adspecies formed during the equilibrium dissociative adsorption of CH_4 on Ni-YSZ cermet catalysts, *J. Catal.* **217(2)** (2003) 324-333.

[43] N. Laosiripojana, S. Assabumrungrat. Catalytic steam reforming of methane, methanol, and ethanol over Ni/YSZ: The possible use of these fuels in internal reforming SOFC, *J. Power Sources* **163(2)** (2007) 943-951.

[44] T. Setoguchi, K. Okamoto, K. Eguchi, H. Arai, Effects of anode material and fuel on anodic reaction of solid oxide fuel cells, *J. Electrochen. Soc.* **139(10)** (1992) 2875-2880.

[45] Y. B. Lin, Z. L. Zhan, J. Liu, S. A. Barnett, Direct operation of solid oxide fuel cells with methane fuel. *Solid State Ionics* **176(23–24)** (2005) 1827-1835.

[46] N. Laosiripojana, W. Sutthisripok, S. Assabumrungrat. Synthesis gas production from dry reforming of methane over CeO_2 doped Ni/Al_2O_3: Influence of the doping ceria on the resistance toward carbon formation, *Chem. Eng. J.* **112(1-3)** (2005) 13-22.

[47] K. Kendall, C. M. Finnerty, G. Saunders, J.T. Chung, Effects of dilution on methane entering an SOFC anode. *J. Power Source*s **106(1-2)** (2002) 323-327.

[48] M. K. Bruce, M. V. D. Bossche, S. McIntosh. The influence of current density on the electrocatalytic activity of oxide-based direct hydrocarbon SOFC anodes, *J. Electrochen. Soc.* **155(11)** (2008) B1202-B1209.

[49] H. X. You, H. J. Gao, G. Chen, A. Abudula, X. W. Ding, The conversion among reactions at Ni-based anodes in solid oxide fuel cells with low concentrations of dry methane, *J. Power Sources* **196(5)** (2011) 2779-2784.

[50] G. L. Kellogg, T. T. Tsong, Pulsedlaser atomprobe fieldion microscopy, *J. Appl. Phys.* **51(2)** (1980) 1184-1193.

[51] Z. L. Zhan, Y. B. Lin, M. Pillai, I. Kimb, S. A. Barnetta, High-rate electrochemical partial oxidation of methane in solid oxide fuel cells, *J. Power Sources* **161(1)** (2006) 460-465.

[52] G. P. Wang, Basis of gas chromatography, Science Press, Beijing, 1986.

[53] M. C. Huang, T. J. Huang, Effect of addition method of gadolinia-doped ceria-added FeCr gas diffusion layer on performance of direct-methane solid oxide fuel cells, *J. Power Sources* **191(2)** (2009) 555-559.

[54] A. Abudula, Research of solid electrolyte fuel cell using hydrocarbon as fuel (Research on the SOFC (solid oxide fuel cell) for methane fuel, Tokyo University, 1997.

[55] X. L. Liu, J. F. Ma, W. H. Liu, G. Xu, H. J. Li, L. L. Yang, Study on the Fabrication of Mullite-Silica-rich Glass Material, *J. Chin. Ceram. Soc.* **(1) 2001** 84-87.

[56] A. A. Yaremchenko, V. V. Kharton, E. N. Naumovich, F. M. B. Marques, Physicochemical and Transport Properties of Bicuvox-Based Ceramics, *J. Electroceram.* **4(1)** (1999) 233-242.

[57] A. M. Hernández, L. Mogni, A. Caneiro, $La_2NiO_{4+\delta}$ as cathode for SOFC: Reactivity study with YSZ and CGO electrolytes, *Int. J. Hydrogen Energy* **35(11)** (2010) 6031-6036.

[58] Q. Li, H. Zhao, L. H. Huo, L. P. Sun, X. L. Cheng, J. C. Grenier, Electrode properties of Sr doped La_2CuO_4 as new cathode material for intermediate-temperature SOFCs, *Electrochem. Commun.* **9(7)** (2007) 1508-1512.

[59] M. Juhl, S. Primdahl, C. Manon, M. Mogensen, Performance/structure correlation for composite SOFC cathodes, *J. Power Sources* **61(1-2)** (1996) 173-181.

[60] K. K. Hansen, K. V. Hansen. A-site deficient $(La_{0.6}Sr_{0.4})_{1-\delta}Fe_{0.8}Co_{0.2}O_{3-\delta}$ perovskites as SOFC cathodes, *Solid State Ionics* **178(23-24)** (2007) 1379-1384.

[61] K. K. Hansen. The effect of A-site deficiency on the performance of $La_{1-\delta}Fe_{0.4}Ni_{0.6}O_{3-\delta}$ cathodes, *Mater. Res. Bull.* 45(2) (2010) 197-199.

[62] S. T. Aruna, M. Muthuraman, K. C. Patil. Synthesis and properties of Ni-YSZ cermet: anode material for solid oxide fuel cells, *Solid State Ionics* **111(1-2)** (1998) 45-51.

[63] M. Marinsek, K. Zupan, J. Maèek. Ni-YSZ cermet anodes prepared by citrate/nitrate combustion synthesis, *J. Power Sources* **106(1-2)** (2002) 178-188.

[64] T. Setoguchi, K. Okamoto, K. Eguchi, H. Arai, Effects of anode material and fuel on anodic reaction of solid oxide fuel cells, *J. Electrochem. Soc.* **139(139)** (1992) 2875-2880.

[65] D. W. Dees, T. D. Claar, T. E. Easler, D. C. Fee, F. C. Mrazek, Conductivity of Porous $Ni/ZrO_2-Y_2O_3$ Cermets, *J. Electrochen. Soc.* **134(9)** (1987) 2141-2146.

[66] E. Ivers-Tiffée, W. Wersing, M. Schießl, H. Greiner, Ceramic and Metallic Components for a Planar SOFC, *Phys. Chem. Chem. Phys.* **94(9)** (1990) 978-981.

[67] J. H. Lee, H. Moon, H. W. Lee, J. Kim, J. D. Kim, K. H. Yoon, Quantitative analysis ofmicrostructure and its related electrical property of SOFC anode, Ni-YSZ cermet, *Solid StateIonics* **148** (2002) 15-26.

[68] R. J. Gorte, J. M. Vohs, Novel SOFC anodes for the direct electrochemical oxidation of hydrocarbons. *J. Catal.* **216** (2003) 477-486.

[69] J. H. Jun, T. H. Lim, S. W. Nam, S. A. Hong, K. J. Yoon, Mechanism of partial oxidation of methane over a nickel-calcium hydroxyapatite catalyst, *Appl. Catal., A* **312(3)** (2006) 27-34.

[70] D. Mogensen, J. D. Grunwaldt, P. V. Hendriksen, K. Dam-Johansen, J.U. Nielsen, Internal steam reforming in solid oxide fuel cells: status and opportunities of kinetic studies and their impact on modelling, *J. Power Sources* **196(1)** (2010) 25-38.

[71] C. M. Grgicak, M. M. Pakulska, J. S. O'Brien, J. B. Giorgi, Synergistic effects of $Ni_{1-x}Co_x$-YSZ and $Ni_{1-x}Cu_x$-YSZ alloyed cermet SOFC anodes for oxidation of hydrogen and methane fuels containing H_2S, *J. Power Sources* **183(1)** (2008) 26-33.

[72] J. Ding, J. Liu, W. M. Guo. Fabrication and study on $Ni_{1-x}Fe_xO$-YSZ anodes for intermediate temperature anode-supported solid oxide fuel cells, *J. Alloys Compd.* **480(2)** (2009) 286-290.

[73] F. Besenbacher, I. Chorkendorff, B. S. Clausen, B. Hammer, A. M. Molenbroek, J. K. Norskov, I. I. Stensgaard, Design of a surface alloy catalyst for steam reforming, *Sci.* **279(5358)** (1998) 1913-1915.

[74] A. Sina, E. Kopnina, Y. Dubitskya, A. Zaopoa, A. S. Aricòb, D. L. Rosab, L. R. Gullob, V. Antonucci, Performance and life-time behaviour of NiCu-CGO anodes for the direct electro-oxidation of methane in IT-SOFCs, *J. Power Sources* **164(1)** (2007) 300-305.

[75] A. Rismanchian, J. Mirzababaei, S. S. C. Chuang, Electroless plated Cu-Ni anode catalyst for natural gas solid oxide fuel cells, *Catal. Today* **245** (2005) 79–85.

[76] K. Hamamoto, T. Suzuki, B. Liang, T. Yamaguchi, H. Sumi, Y. Fujishiro, B. Ingram, A. J. Kropf, J. D. Carter, Investigation of the microstructural effect of Ni-yttria stabilized zirconia anode for solid-oxide fuel cell using micro-beam X-ray absorption spectroscopy analysis, *J. Power Sources* **222** (2013) 15-20.

[77] G. Chen, Fabrication of cathod-supported SOFC with high performance and degration mechanism of Ni-base anodes at high current density, Hirosaki University, 2011.

[78] S. Mclntosh, R. J. Gorte, Direct hydrocarbon solid oxide fuel cells. Chem, *Rev.* **104** (2004) 4845-4865.

[79] A. Atkinson, S. Barnett, R. J. Gorte, J. T. S. Irvine, A. J. Mcevoy, M. Mogensen, S. C. Singhal, J. Vohs, Advanced anodes for high-temperature fuel cells, *Nat. Mat,* **3 (2004)** 17-27.

[80] Z. Xie, C. R. Xia, M. Y. Zhang, W. Zhu, H. T. Wang, $Ni_{1-x}Cu_x$ alloy-based anodes for low-temperature solid oxide fuel cells with biomass-produced gas as fuel, *J.Power Sources* **161**(2006) 1056-1061.

[81] C. Lu, W. L. Worrell, C. Wang, S. Park, H. Kim, J. M. Vohs, R. J. Goret, Development of solid oxide fuel cells for the direct oxidation of hydrocarbon fuels, *Solid State Ionics* **152(2)** (2002) 393-397.

[82] J. F. Li, Synthesis and catalytic oxidation performance of CeO_2-based Catalysts, East China University of Technology, 2012.

[83] N. V. Skorodumova, S. L. Simak, B. I. Lundqvist, I. A. Abrikosov, B. Johansson, Quantum origin of the oxygen storage capability of ceria, *Phys. Rev. Lett.* **89** (2002) 455-461.

[84] B. C. H. Steele, P. H. Middleton, R. A. Rudkin, Material science aspects of SOFC technology with special reference to anode development, *Solid State Ionics* **40(1)**(1990) 388-393.

[85] I. S. Metcalfe, P. H. Middleton, P. Petrolekas, B. C. H. Steele, Hydrocarbon activation in solid-state electrochemical-cells, *Solid State Ionics*, **57** (1992): 259-264.

[86] R. Craciun, B. Shereck, R. J. Gorte, Kinetic studies of methane steam reforming on ceria-supported Pd, *Catal. Lett.* **51(3-4)** (1998) 149-153.

[87] O. A. Marina, M. Mogensen, High-temperature conversion of methane on a composite gadolinia-doped ceria-gold electrode, *Appl. Catal. A* **189(1)** (1999) 117-126.

[88] H. U. Anderson, Review of p-type doped perovskite materials for SOFC and other applications, *Solid State Ionics* **52(1-3)** (1992) 33-41.

[89] S. Primdahl, J. R. Hansen, L. Grahl-Madsen, P. H. Larsen, Sr-doped $LaCrO_3$ anode for solid oxide fuel cells, *J. Electrochen. Soc.* **148(1)** (2001) A74-A81.

[90] G. Pudmich, B. A. Boukamp, M. Gonzalez-Cuenca, W. Jungen, W. Zipprich, F. Tietz, Chromite/titanate based perovskites for application as anodes in solid oxide fuel cells, *Solid State Ionics* **135(1-4)** (2000) 433-438.

[91] X. B. Zhu, Z. Lü, B. Wei, K. F. Chen, M. L. Liu, X. Q. Huang, W. H. Su, Enhanced performance of solid oxide fuel cells with Ni/CeO_2 modified $La_{0.75}Sr_{0.25}Cr_{0.5}Mn_{0.5}O_{3-\delta}$ anodes, *J. Power Sources* **190(2)** (2009) 326-330.

[92] J. Sfeir, P. A. Buffat, P. Mockli, N. Xanthopoulos, R. Vasquez, H. J. Mathieu, J. V. herle, K. R. Thampi, Lanthanum chromite based catalysts for oxidation of methane directly on SOFC anodes *J. Catal.* **202** (2001) 229-244.

[93] X. F. Zhu, Q. Zhong, X. J. Zhao, H. Yan, Synthesis and performance of Y-doped $La_{0.7}Sr_{0.3}CrO_{3-\delta}$as a potential anode material for solid oxygen fuel cells, *Appl. Surf. Sci.* **257(6)** (2011) 1967-1971.

[94] X. H. Dong, S. G. Ma, K. Huang, F. Chen, $La_{0.9-x}Ca_xCe_{0.1}CrO_{3-\delta}$ as potential anode materials for solid oxide fuel cells, *Int. J. Hydrogen Energy* **37(37)** (2012) 10866-10873.

[95] V. I. Sharma, B. Yildiz, Degradation mechanism in $La_{0.8}Sr_{0.2}CoO_3$ as contact layer on the solid oxide electrolysis cell anode, *J. Electrochem. Soc.* **157(3)** (2010) B441-B448.

[96] V. B. Vert, F. V. Melo, L. Navarrete, J. M. Serra, Redox stability and electrochemical study of nickel doped chromites as anodes for H_2/CH_4 fueled solid oxide fuel cells, *Appl. Catal., B* **115-116(15)** (2012) 346-356.

[97] Y. Tsvetkova, V. Kozhukharov, Synthesis and study of compositions of the La-Sr-Ti-O system for SOFCs anode development, *Mater. Des.* **30(1)** (2009) 206-209.

[98] A. Torabi, T. H. Etsell, Electrochemical behavior of solid oxide fuel cell anodes based on infiltration of Y-doped $SrTiO_3$, *J. Power Sources* **225** (2013) 51-59.

[99] Y. Sakaki, Y. Takeda, A. Kato, N. Imanishi, O. Yamamoto, M. Hattori, M. Iio, Y. Esaki, $Ln_{1-x}Sr_xMnO_3$ (Ln=Pr, Nd, Sm and Gd) as the cathode material for solid oxide fuel cells, *Solid State Ionics* **118(3-4)** (1999) 187-194.

[100] J. Jeong, A. K. Azad, H. Schlegl, B. Kim, S. W. Baek, K. Kim, H. Kang, J. H. Kim, Structural, thermal and electrical conductivity characteristics of $Ln_{0.5}Sr_{0.5}Ti_{0.5}Mn_{0.5}O_{3\pm\delta}$ (Ln: La, Nd and Sm) complex perovskites as anode materials for solid oxide fuel cell, *J. Solid State Chem.* **226** (2015) 154-163.

[101] J. H. Kim, X-ray photoelectron spectroscopy analysis of $(Ln_{1-x}Sr_x)CoO_{3-\delta}$ (Ln: Pr, Nd and Sm), *Appl. Surf. Sci.* **258(1)** (2011) 350-355.

[102] Y. H. Huang, R. I. Dass, Z. L. Xing, J. B. Goodenough, Double perovskites as anodes materials for solid-oxide fuel cells, *Sci.* **37(28)** (2006): 254-257.

[103] J. C. Ruiz-Morales, J. Canales-Vazques, C. Savaniu, D. Marrero-Lopes, W.Z. Zhou, T. S. Irvine, Disruption of extended defects in solid oxide fuel cell anodes for methane oxidation, *Nat.* **439(2)** (2006) 568-571.

[104] Y. Zheng, W. Zhou, R. Ran, Z. P. Shao, Perovskite as anode materials for solid oxide fuel cells, *Prog. Chem.* **20(2-3)** (2008) 413-421

[105] S. P. S. Shaikh, A.i Muchtar, M. R. Somalu. A review on the selection of anode materials for solid-oxide fuel cells. *Renew. Sust. Energ. Rev*. **51** (2015) 1-8.

[106] S. W. Tao, J. T. S. Irvine, A redox-stable efficient anode for solid-oxide fuel cells, *Nat. Mat.* **2** (2003) 320-323.

[107] M. Juhl, S. Primdahl, C. Manon, M. Mogensen, Performance/structure correlation for composite SOFC cathodes, *J. Power Sources* **61** (1996) 173-181.

[108] M. Brown, S. Primdahl, M. Mogensen, Structure/performance relations for Ni/YSZ anodes for SOFC, *J. Electrochem. Soc.* **147(2)** (2000) 475-48.

[109] H. Fridriksson, Study on Catalytic Reactions in Solid Oxide Fuel Cells with Comparison to Gas Phase Reactions in Internal Combustion Engines, Lund: Dept. of Energy Sciences, Faculty of Engineering Lund University, 2009.

[110] W. Zhu, C. Xia, J. Fan, R. Peng, G. Meng, Ceria coated Ni as anodes for direct utilization of methane in low-temperature solid oxide fuel cells, *J. Power Sources* **160(2)** (2006) 897-902.

[111] J. J. Haslam, A. Q. Pham, B. W. Chung, J. F. DiCarlo, R. S. Glass, Effects of the Use of Pore Formers on Performance of an Anode Supported Solid Oxide Fuel Cell, *J. Am. Ceram. Soc.* **88(3)** (2005) 513–518.

[112] M. Boaro, J. M. Vohs, R. J. Gorte, Synthesis of Highly Porous Yttria-Stabilized Zirconia by Tape-Casting Methods, *J. Am. Ceram. Soc.* **86(3)** (2003) 395–400.

[113] W. P. Pan, Z. Lü, K. F. Chen, X. B. Zhu, X. Q. Huang, Y. H. Zhang, B. Wei, W. H. Su, Paper-Fibres Used as a Pore-Former for Anode Substrate of Solid Oxide Fuel Cell, *Fuel Cells* **11(2)** (2011) 172–177.

[114] W. P. Pan, Z. Lü, K. F Chen, X. Q. Huang, B. Wei, W. Y. Li, Z. H. Wang, W. H. Su, Novel polymer fibers prepared by electrospinning for use as the pore-former for the anode of solid oxide fuel cell, *Electrochim. Acta*. **55(20)** (2010) 5538-5544.

[115] A. Sarikaya, V. Petrovsky, F. Dogan. Effect of the anode microstructure on the enhanced performance of solid oxide fuel cells, *Int. J. Hydrogen Energy* **37(15)** (2012) 11370-11377.

[116] H. Sumi, T. Yamaguchi, T. Suzuki, H. Shimada, K. Hamamoto, Y. Fujishiro, Effects of anode microstructures on durability of microtubular solid oxide fuel cells during internal steam reforming of methane, *Electrochem. Commun.* **49** (2014) 34-37.

[117] H. X. You, C. Zhao, B. Qu, G. Q. Guan, A. Abudula, Fabrication of $Ni_{0.5}Cu_{0.5}O_x$ coated YSZ anode by hard template method for solid oxide fuel cells, *J. Alloys Compd.* **669** (2016) 46-54.

[118] D. H. Dong, Y. Z. Wu, X. Y. Zhang, J. F. Yao, Y. Huang, D. Li, C. Z. Li, H. T. Wang, Eggshell Membrane-Templated Synthesis of Highly Crystalline Perovskite Ceramics for Solid Oxide Fuel Cells, *J. Mater. Chem.* **21(4)** (2011) 1028-1032.

[119] R. Pinedo, I. R. D Larramendi, I. G. D. Muro, M. Insausti, J. I. R. D. Larramendi, M. I. Arriortua, T. Rojo, Influence of colloidal templates on the impedance spectroscopic behaviour of $Pr_{0.7}Sr_{0.3}Fe_{0.8}Ni_{0.2}O_3$ for solid oxide fuel cell applications, *Solid State Ionics*. **192(1)** (2011) 235-240.

[120] Y. H. Koh, J. J. Sun, W. Y. Choi, H. E. Kim, Design and fabrication of three-dimensional solid oxide fuel cells, *J. Power Sources* **161(2)** (2006) 1023-1029.

[121] Z. Liu, B. Liu, D. Ding M. F. Liu, F. L. Chen, C. R. Xia, Fabrication and modification of solid oxide fuel cell anodes via wet impregnation/infiltration technique, *J. Power Sources* **237(3)** (2013) 243-259.

[122] D. Dong, Z. Wei, J. Gao, C. Xia, High performance electrolyte-coated anodes for low-temperature solid oxide fuel cells: Model and Experiments, *J. Power Sources* **179(1)** (2008) 177-185.

[123] F. Zhao, Z. Wang, M. Liu, L. Zhang, C. R. Xia, F. L. Chen, Novel nano-network cathodes for solid oxide fuel cells, *J. Power Sources* **185(1)** (2008) 13-18.

[124] H. X. You, C. Zhao, Y. J. Guan, G. Q. Guan, A. Abudula, Fabrication of composite anode GDC–SrMoO$_4$–YSZ by hard template method for solid oxide fuel cell, *J. Chin. Ceram. Soc.* **44(7)** (2016) 919-924.

Chapter 2

Experimental

2.1 Preparation of anode material

Raw materials. All the raw materials used to prepare SOFC in this thesis were listed in table 2.1.

Ni based anode materials. A series of methods were adopted to prepare different anode materials in this thesis. NiO mixed with YSZ or ScSZ powder was used as anode material (Chapter 3 and 4). The hard template method was adopted to prepare Ni_xCu_{1-x} (x=0.8, 0.5, and 0.2) alloy and fiber tubular YSZ materials. Fig. 2.1 and 2.2 shows the flow process of Ni_xCu_{1-x} (x=0.8, 0.5, and 0.2) alloy and fiber tubular YSZ preparation utilizing activated carbon fiber (ACF) as hard template, respectively. Meanwhile, Fig 2.3 and 2.4 describes the flow process of $Ni_{0.5}Cu_{0.5}O_x$ coated tubular YSZ and $Ni_{0.5}Cu_{0.5}Ba_{0.05}O_x$ coated tubular SDC preparation by hard template method combined with wet impregnation method, respectively. The preparations of anode materials described above would be introduced detailedly in corresponding chapter (Chapter 5, 6 and 7).
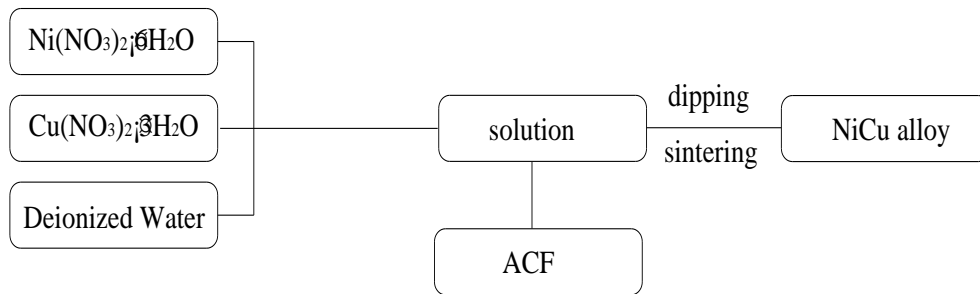
Fig. 2.1 The flow process of NiCu alloy preparation

Perovskite based anode material. GDC-SrMoO$_4$-YSZ was prepared by composite anode material hard template method combined with wet impregnation method. Fig. 2.5 presents the prepared flow process of GDC-SrMoO$_4$-YSZ composite anode material (Chapter 8).

Tab. 2.1 Experiment reagents for SOFC

Material	Manufacturer or distributor	Property
NiO powder	Japan SOEKAWA Co., Ltd.	1μm
YSZ powder(8mol% Y_2O_3)	TOSOH	1.5μm
SDC powder(20mol%Sm_2O_3)	TOSOH	1 μm
Yttria(Y_2O_3)	Sinopharm Chem. Reagent Co., Ltd.	GR
Cerium nitrate($Ce(NO_3)_3$)	Shanghai Chem. Reagent Co. of China Pharmaceutical (Group)	AR
Gadolinium oxide(Gd_2O_3)	Shanghai Chem. Reagent Co. of China Pharmaceutical (Group)	AR
Cerium carbonate($SrCO_3$)	Aladdin	99.95%
Ammonium molybdate tetrahydrate $((NH_4)_6Mo_7O_{24}\cdot4H_2O)$	Aladdin	99.9%
LSM($(La_{0.75}Sr_{0.25})_{0.95}MnO_{3\pm\delta}$)	Ningbo Institute of Industrial Technology, CAS	99.5%
Ethanol(C_2H_5OH)	Tianjin Damao Chem. Reagent Factory	AR
Zirconium nitrate $Zr(NO_3)4\cdot5H_2O$)	Sinopharm Chem. Reagent Co., Ltd.	AR
Nitrate (HNO_3)	Shenyang new reagent plant	AR
Nickel nitrate($Ni(NO_3)_2\cdot6H_2O$)	Tianjin Damao Chem. Reagent FTY	AR
Copper dinitrate ($Cu(NO_3)_2$)	Tianjin Damao Chem. Reagent FTY	99.5%
Barium nitrate ($Ba(NO_3)_2$)	Beijing Red Star Chemical Plant	AR
Cerium (III) nitrate hexahydrate ($Ce(NO_3)_3\cdot6H_2O$)	Shanghai Crystal Pure Biochem. Tech. Co., Ltd.	99.5%
samarium trinitrate ($Sm(NO_3)_3$)	Shanghai Crystal Pure Biochem.Tech. Co., Ltd.	99.9%
Ethyl cellulose	Station-packing Plant of Shanghai Chemical Reagent	AR
α -terpineol	Meredov Ferfume FTY of Sanming	AR
Polyvinyl butyral (PVB)	Station-packing Plant of Shanghai Chem. Reagent	AR
Acetone(CH_3COCH_3)	Shenyang New Reagent Plant	AR
Activated Carbon Fiber	Dalian University of Technology	SSA 1700
flour	Haining of COFCO	
Medical absorbent cotton	Taizhou Hengtai Dyeing Dressings Ltd.	

2.2 Fabrication of single cell

Electrolyte. Disks of 8 mol 5% Y_2O_3-ZrO_2 with a thickness of 0.5 or 1 mm and a diameter of 20 mm (8-YSZ; Tosoh) were used as electrolyte tablets in Chapter 3 and 4. Besides, in chapter 5, 6 ,7 and 8, electrolyte plate with a thickness of 0.5 mm and a diameter of 20 mm was prepared by pressing dried

YSZ powders (8mol% Y_2O_3- ZrO_2, Tosoh) after mixing with 3 wt.% polyvynil butyral (PVB) binder, followed by sintered at 1623 K in the air for 4 h.

Slurry coating method was adopted to prepare electrodes (anode and cathode). The mixture of α-terpineol and ethyl cellulose with a mass ratio of 4:1 was used as binders.
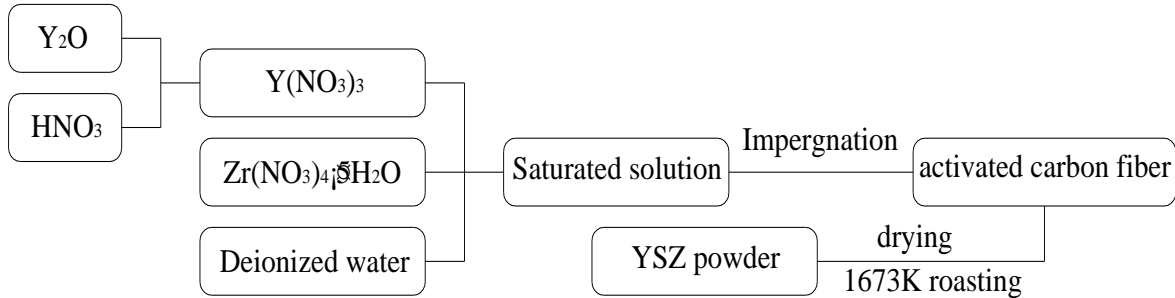
Fig. 2.2 The flow process of fiber tubular YSZ preparation
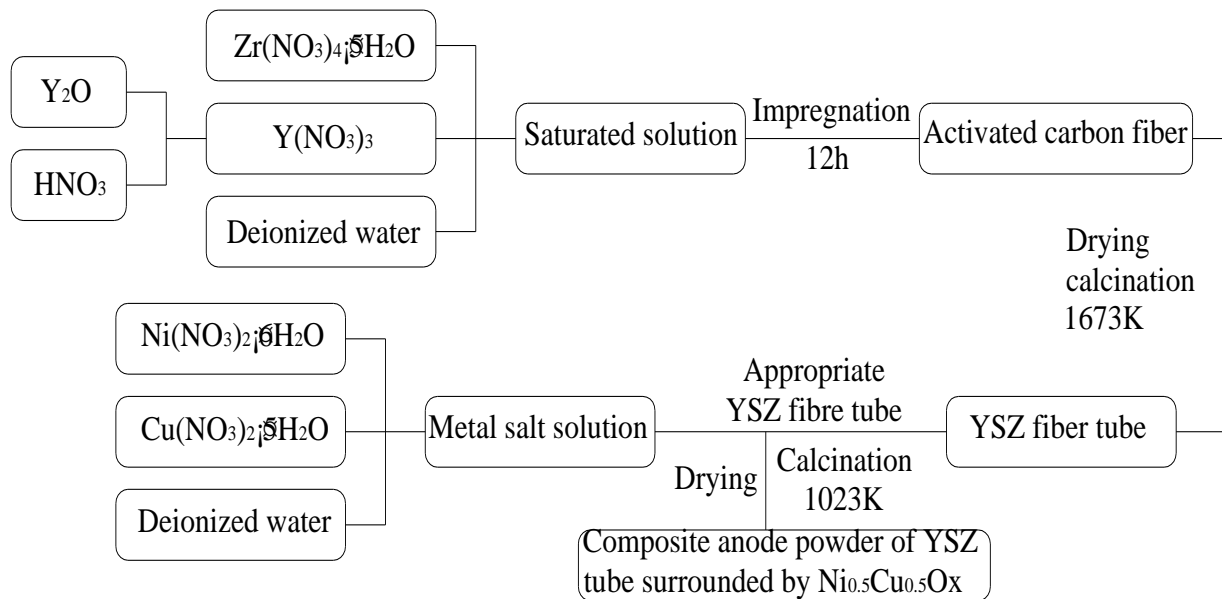
Fig. 2.3 The flow process of $Ni_{0.5}Cu_{0.5}O_x$ coated fiber tubular YSZ anode material preparation

Anode. An anode slurry, for example Ni-YSZ, was prepared by mixed NiO (Soekawa, Japan) and YSZ powders, in a mass ratio of 3:2, with 50 wt% binder (relative NiO and YSZ). The obtained slurry was coated onto the electrolyte substrate and sintered at 1673K for 2 h. Fig.2.6 (a) shows the flow process of conventional Ni-YSZ anode preparation described above.

cathode. Using a similar calcination method, the opposite side of the disk with anode was coated with $La_{0.85}Sr_{0.15}MnO_3$ and YSZ or ScSZ as a cathode material. The anode and cathode had the same size and were placed in the centre of the disk. The cathode was calcined under 1473℃ for 2h after the calcination of anode.
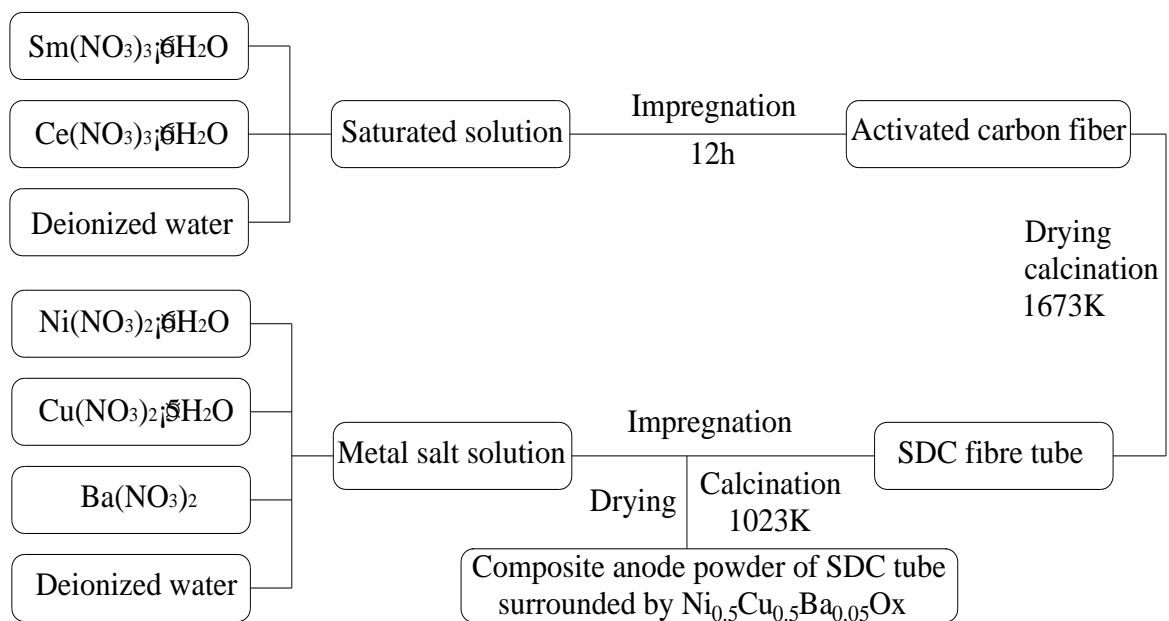
Fig. 2.4 The flow process of $Ni_{0.5}Cu_{0.5}Ba_{0.05}Ox$ coated fiber tubular SDC material preparation
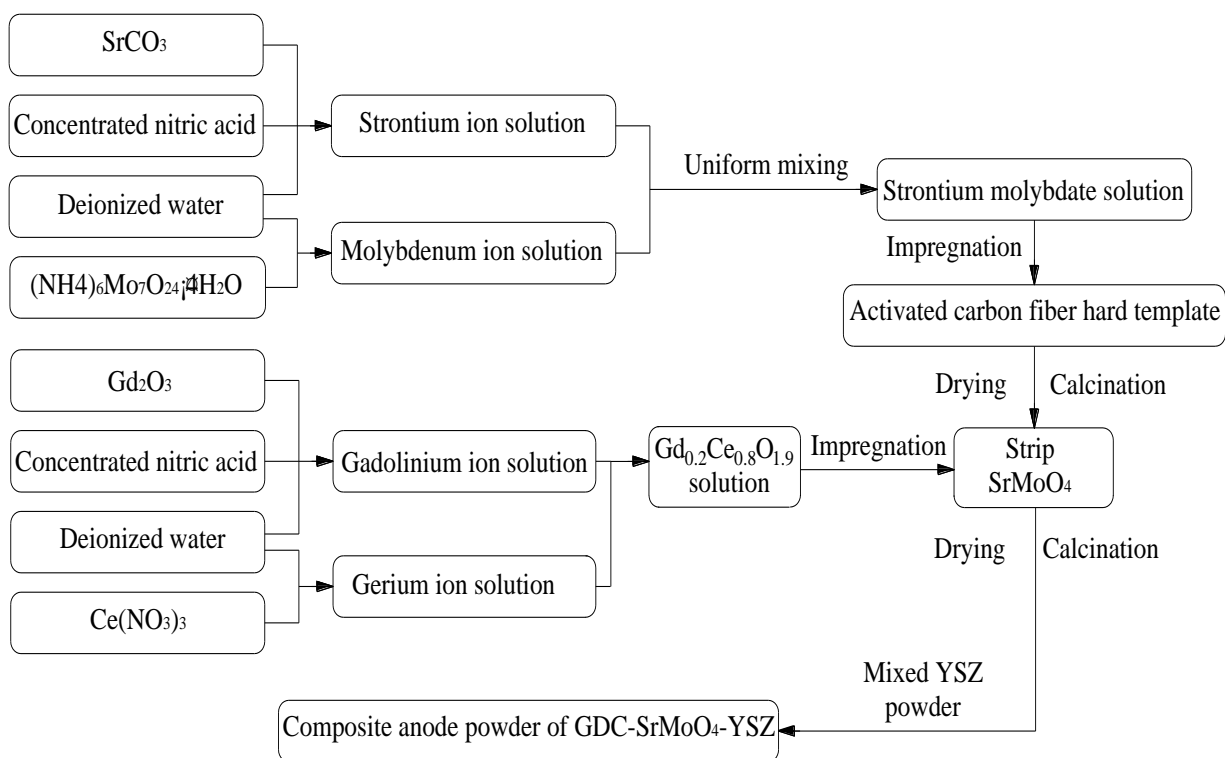
Fig. 2.5 The flow process of GDC-$SrMoO_4$-YSZ composite anode material preparation

The cathode of LSM is made according to Fig.2.6 (b). Fig 2.7 shows the photo for the as-prepared anode and. Cathode.
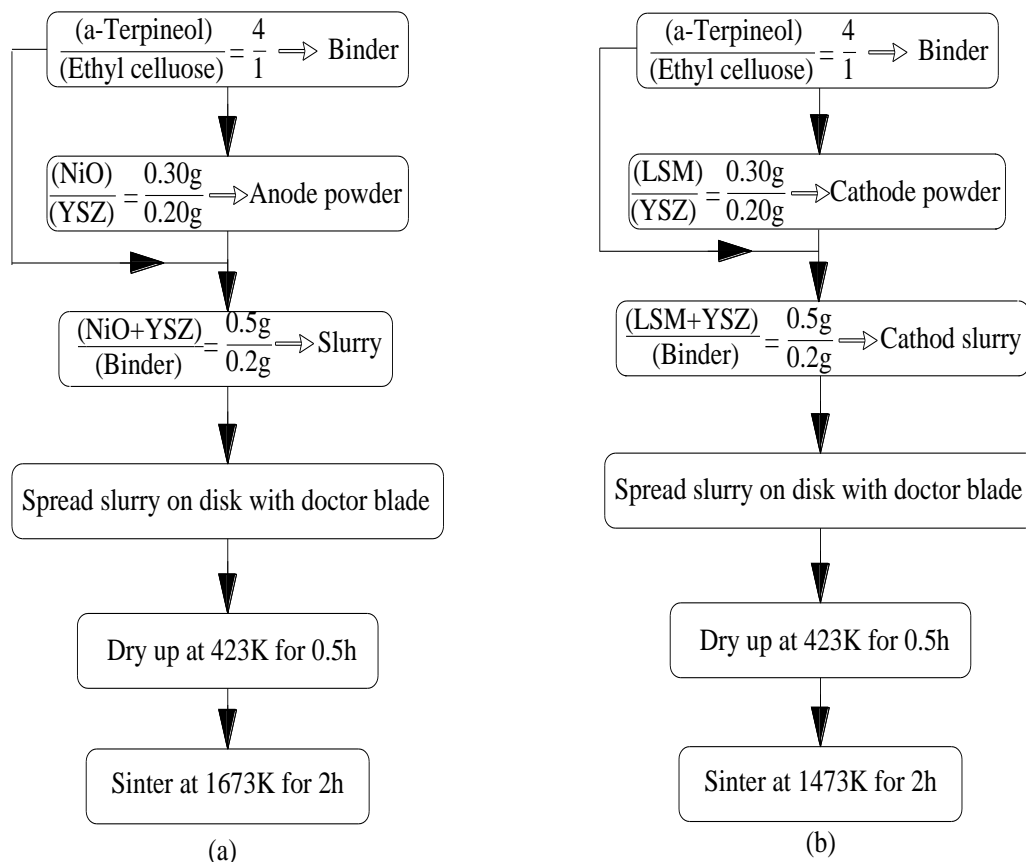
Fig. 2.6 The flow process of anode and cathode preparation (a) anode (b) cathode
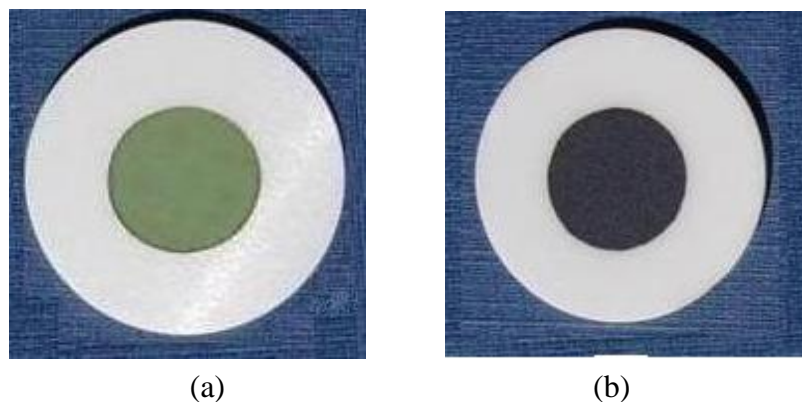
Fig. 2.7 A photo for as-prepared anode and cathode (a) anode (b) cathode

2.3 Experimental equipment

The equipment involved in this thesis is listed in Table2.2.

Especially, the Agilent GC 7890A gas chromatography system was used to identify the outlet gases of anode side on-line so that to investigate the reactions of dry methane on the anode at different current densities, as well as in different concentrations of dry methane. Before examination, the

42

chromatography was calibrated by two bottle of standard gas, and its calibration results were listed in Table 2.3. It demonstrates that it's the flow control accuracy was within ± 1% to guarantee the results accuracy. In this study, different concentrations of dry methane were used dry methane diluted by Ar.

Tab. 2.2 Experiment equipment for SOFC

Experiment equipment	Manufacturer	Model
High temperature resistance furnace with silicon molybdenum	Shanghai Yi Feng Furnace Co., Ltd.	SSX2-8-16C
Electronic analytical balance	Shanghai Balance Instrument Factory	JA2003N
Pressure die	Dalian University of Technology	Φ27.5mm
Hydraulic machine	Dingxin hydraulic machinery Plant of Dezhou	SYB
Dry oven	Shanghai Yiheng Scientific Instrument Co.	HZQ-F160A
Ultrasonic cleaning	Shanghai Kedao Ultrasonic Instrument Co., Ltd.	SK2200LH
Hydrogen gas tube furnace	Hefei Ke Jing Materials Technology Co., Ltd.	GSL-1600X
Chromatogram	Agilent Technologies, Inc.	GC 7890A
Electrochemical working apparatus	Shanghai Chen Hua Instrument Co., Ltd.	CH1604D
Potentiostat / galvanostat	Japan Hokuto Denko Corporation	HV-151
`Frequency Response Analyzer	AMETEK Advanced Measurement Technology	Solartron 1255B
Electrochemical Impedance Spectroscopy	AMETEK Advanced Measurement Technology	Solartron SI 1287A

2.4 Experimental set-up

Fig.2.8 shows theschematic diagram of SOFC performance testing system used in this thesis.Accordingly, Fig. 2.9 shows the photo of Norwegian Electro Ceramics AS (NorECS) SOFC testing rig used in Chapter 3 and 4 to investigate methane reactions on anode, and Fig. 2.10 shows the photo of SOFC testing rig to investigate the as-prepared anode materials for power generation test and long-term test in Chapter 5, 6, 7 and 8. Meanwhile, fig. 2.11 and 2.12 shows the structure of the two test rigs (SOFC test rig 1 and 2), respectively. The glass rings with diameter 20 mm and thickness 0.5 mm were used to seal the as-prepared single cell and Pt mesh or wires were adopted to collect the current. The designed heating rate was calculated to prevent SOFC fragmentation.

Tab.2.3 Chromatography calibration results and error for GC 960

composition	content / %	Calibration values / %			Relative error / %		
First bottle		first	second	third	first	second	third
CH_4	8.80	8.853	8.824	8.756	0.605	0.276	-0.499
H_2	30.31	31.087	29.531	29.798	2.564	-2.570	-1.688
CO	10.98	11.147	11.137	11.126	1.525	1.430	1.325
CO_2	9.12	9.081	9.069	9.019	-0.432	-0.564	-1.105
Second bottle		first	second	third	first	second	third
CH_4	17.85	17.822	17.726	17.725	-0.155	-0.694	-0.6986
H_2	16.35	16.870	16.816	16.656	3.182	2.852	1.872
CO	7.99	8.090	8.123	8.079	1.254	1.658	1.116
CO_2	16.99	16.850	16.744	16.673	-0.821	-1.450	-1.865
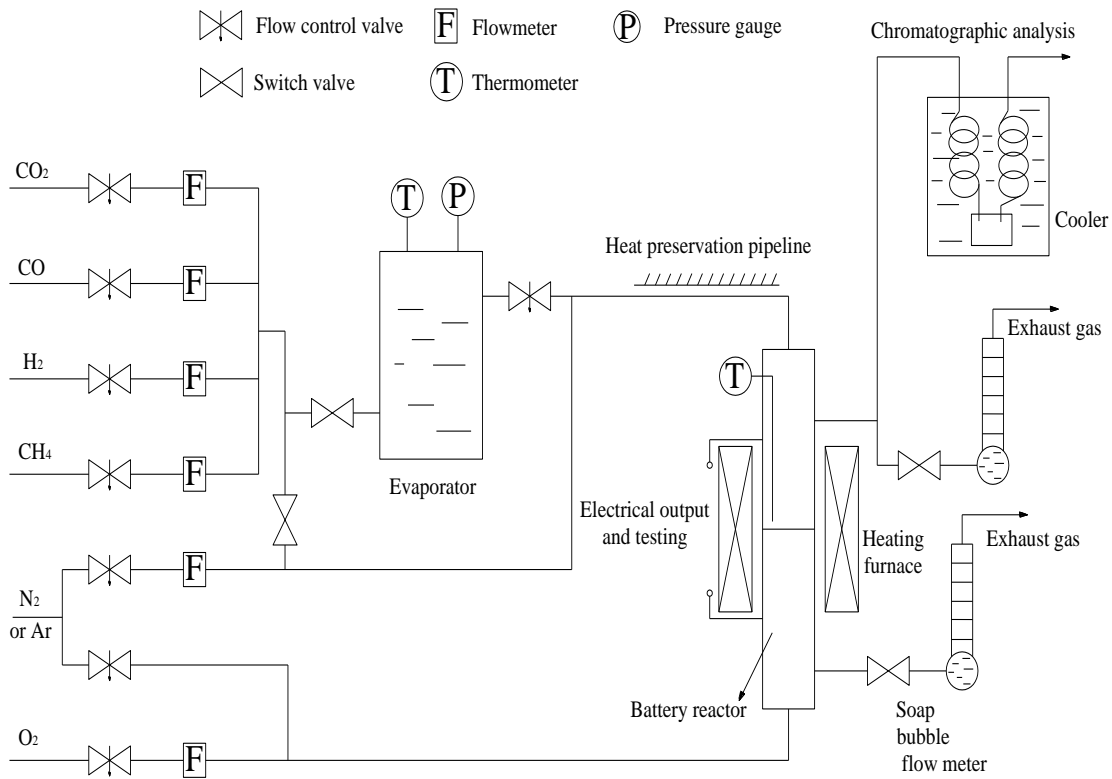
Fig. 2.8 Schematic diagram of SOFC performance testing system

Fig.2.9 Photo of the apparatus for researching reactions
at anode of dry methane

Fig.2.10 Photo of the apparatus for studying anode
materials

45
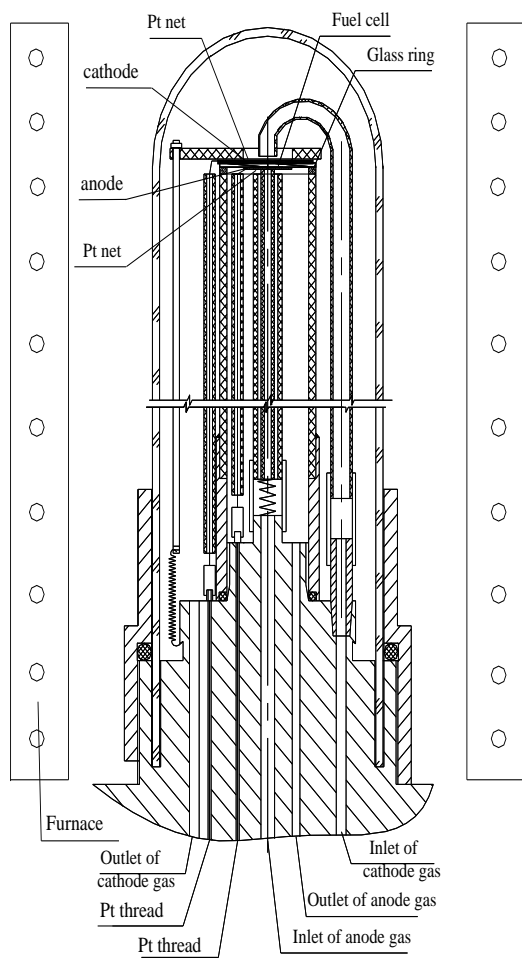
Fig. 2.11 Schematic structure of SOFC test rig 1
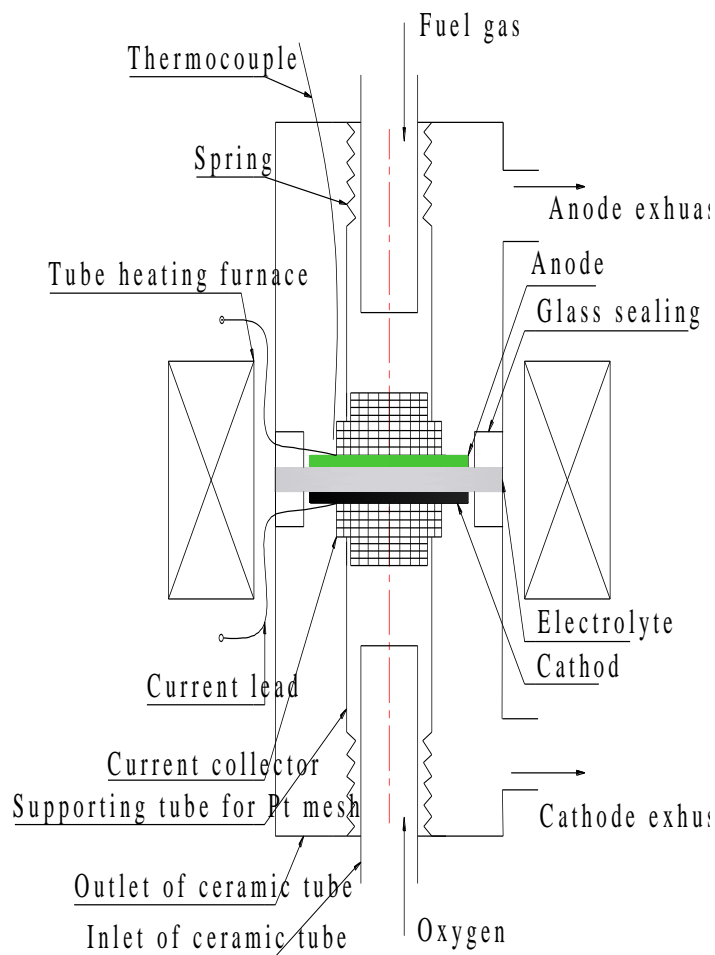
Fig.2.12 Schematic structure of the SOFC test rig 2

2.5 Characterization

X-ray diffractometer (XRD). XRD (SHIMADZU, XD-3A, Japan) was employed to analyze samples crystal phase and composition. Measurement condition was under 12kV voltage, 100mA current with a copper target, Ni filter, λa1 at 0.1541nm ray wavelength, angle 2θ in the measurement range from 20° to 80° by steps of 0.06°.

Scanning Electron Microscopy (SEM) and Energy Dispersive Spectroscopy (EDS). SEM (JEOL, JSM-5600LV, Japan) was adopted to examine the morphology and microstructure of the prepared material samples, as well as the single cell before and after the test. Besides, the elementary analysis of the anode after testing was performed by Energy Dispersive Spectroscopy (EDS) attached on SEM.

Automatic gas adsorption instrument. Automatic gas adsorption instrument (Quantachrome, Autosorb, USA) with Nitrogen as adsorption medium was used to examined pore volume, pore distribution and specific surface area of the sample material.

46

Electrochemical impedance spectroscopy (EIS). EIS is generally used to assess the cell performance. EIS measurements were performed over a frequency range from 0.1 Hz to 1 MHz with a excitation of 0.001 A using a frequency response analyzer (Solartron 1255B) and a potentiostat (Solartron 1287).

Chapter 3

The mathematical relationship between dry methane flux and current in the solid oxide fuel cells with Ni-YSZ anode

3.1 Introduction

Solid oxide fuel cells (SOFCs) operated directly by hydrocarbon fuels without external reformation is expected to be an important technology for power generation in the near future.

Carbon deposition during the reaction process is the primary issue for SOFCs with the direct use of hydrocarbon fuels. To overcome this problem, many researchers have been working on anti-coking anode materials. However, research on the anode reaction mechanisms of methane is also necessary. Many reactions may take place on the anode side, and various electrochemical reactions will generate different products and heat output. Therefore, appropriate thermal management in the fuel cells is required. In addition, synthesis gases, the reaction products of methane, are also raw materials for other chemical products. So, people show great interest in obtaining synthesis gases through the control of methane reactions in the process of generating electricity.

It is difficult to identify the electrochemical reactions of methane because of the coexistence of various gases on the anode side. Several authors [1-3] reported that the electrochemical reactions of methane at different current densities are controlled by multifarious factors. At a low current density (low oxygen stoichiometry), the anode reaction mechanism is dominated by methane cracking, while at a high current density (high oxygen stoichiometry), it is dominated by the total oxidation of methane. This change in mechanism was confirmed by M. K. Bruce by measuring the cell open-circuit voltage as fuel, testing CO_2 and H_2O's partial pressure and analyzing the SOFC product stream [1]. Kdendall [2] concluded that partial oxidation of methane (POM) occurs in pure methane under an open-circuit by comparing the measured OCV with the theoretical value.

Abudula [3] investigated the methane reactions in a Ni-YSZ anode cell with 4.2% dry methane. By analyzing the amount of electrons quantitatively, it was found that the partial electrochemical oxidation of methane (POM) took place at a low-current density, while the complete oxidation of methane (COM) occurs at a high current density. Zhan et al. [4] reported that the species and amount

of the outlet gases were mainly controlled by the ratio of O^{2-}/CH_4. The contents of H_2 and CO increased to a maximum value as O_2/CH_4 rose to approximately 0.7 and decreased as O_2/CH_4 increased further. The content of CH_4 decreased with the increase of O_2/CH_4. The concentration of CO_2 remained low at a low ratio of O_2/CH_4 but increased rapidly when O_2/CH_4 rose over 0.7.

Compared with the anode potential, the ratio of O^{2-}/CH_4 has a greater effect on the methane reactions. It was found that reactions of partial oxidation, $CH_4 +2O^{2-}\rightarrow CO+H_2O+H_2 +4e^-$, $CH_4 +3O^{2-}\rightarrow CO+2H_2O+6e^-$, and complete oxidation occurred to CH_4 at the Ni-based anodes in sequence while the current density increasing for low concentrations of dry methane by means of the comparison between the open-circuit voltages (OCV) and theoretical OCV, the quantitative analysis of elements at different current densities as well as the analysis of the activation energy of elementary reactions of CH_4 were investigated to identify the types of methane reactions[5].

It is impossible to apply methane in SOFC to fixed flux. The influence of dry methane flux on SOFC anodic reaction is mutually concerned issues. The quantitative analysis is absent now for methane flux and current density changed. In this paper, a serial different methane flux tests were arranged at different current densities on Ni-YSZ anodes. By analyzing the reactions on Ni-YSZ anode with different dry methane fluxes, the mathematical relationship between dry methane flux and SOFC operating current was obtained based on Faraday's first law and the mole relationship among the reactant species.

3.2 Experiment

Disks of 8mol% Y_2O_3-ZrO_2 (8-YSZ; diameter 20mm; thickness 0.5mm and 1mm), manufactured by Tosoh Company) were used as electrolytes. NiO and YSZ or ScSZ powders in a weight ratio of 3:2 were mixed and ground. 30 wt% (relative to anode composites materials) of pore-forming agents and adhesives consisting of α-terpineol and ethyl cellulose in a weight ratio of 4:1 were added into the mixture and the mixture was kept grounding. Then the anode slurry was prepared onto the electrolyte substrates by the slurry coating method, and the half cells were subsequently sintered at 1673K for 2h in air. The $La_{0.85}Sr_{0.15}MnO_{3-\delta}$ (LSM) cathodes were prepared using a similar method as that did to the anodes on the opposite side of the YSZ disk. The active area of the anodes and cathodes were 0.78cm^2, and the thicknesses of them were between 30μm and 50μm.

The cell was clamped in the same way as mentioned in Ref. [5]. The furnace was heated to 1273K electrically. For the reduction of NiO, pure hydrogen was fed to the anode chamber for 30 min, and then it was purged out with argon. Methane pumped into the anode was diluted into the required concentrations with 50mL STP min^{-1} argon. The anode gage pressure was 0.1 MPa. The residence

time for fuel gas in the anodes, assuming plug flow, was approximately 0.0027-0.0036 s. Pure O_2 was used as an oxidant with an inlet rate of 50mL STP min^{-1}. The measurements did not start until the OCV became stable. The anode outlet gases were measured in situ with the Agilent GC 7890A gas chromatography system. 15 min after the current was changed, the GC measurements were conducted.

3.3 Results and discussion

3.3.1 Electrical performance

Fig. 3.1 shows the typical I–V curves of the fuel cells with Ni-YSZ at 1000℃. Dry methane with different fluxes 4.464μmol·s^{-1}, 3.720μmol·s^{-1}, 2.232μmol·s^{-1} and1.488μmol·s^{-1} were used as fuel. All OCVs of SOFCs were higher than 1.45V, indicating that all cells were well sealed.
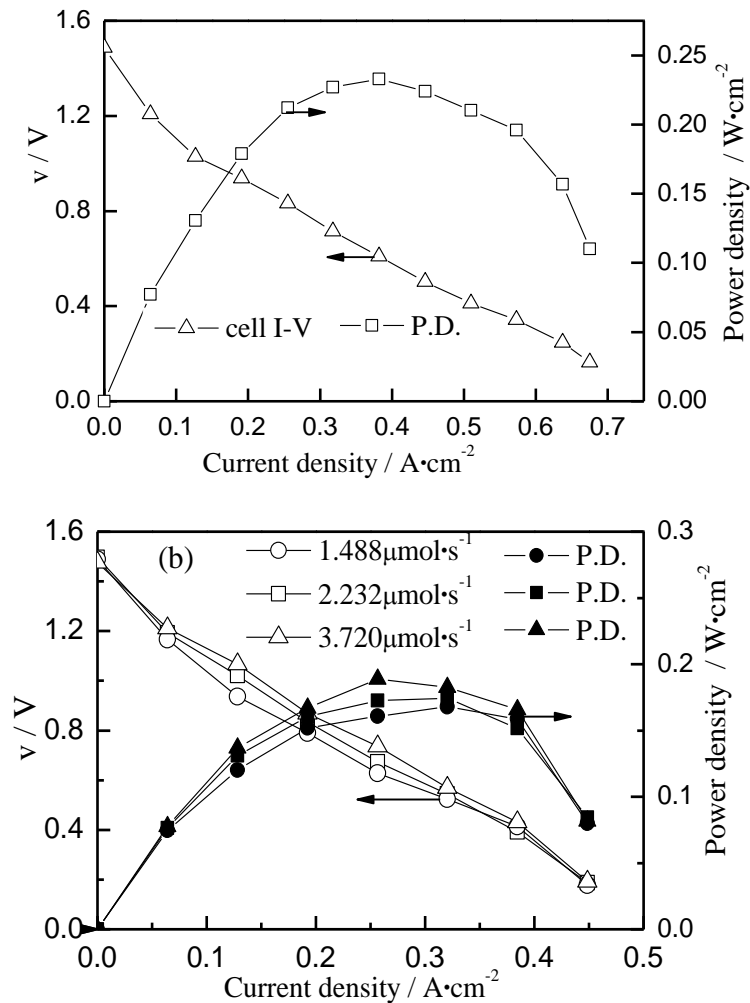
Fig.3.1 I-V and power density characteristics for different CH_4 flux on the cell with Ni-YSZ anode at 1273K (a)4.464μmol·s^{-1} CH_4 Ni-YSZ/YSZ(0.5mm)/LSM-YSZ (b)3.720μmol·s^{-1}, 2.232μmol·s^{-1} and 1.488μmol·s^{-1} CH_4 Ni-YSZ/YSZ(1mm)/LSM-YSZ

3.3.2 Analysis of outlet gases

Fig. 3.2 shows the production rates of anode outlet gases for SOFC with different methane flux.
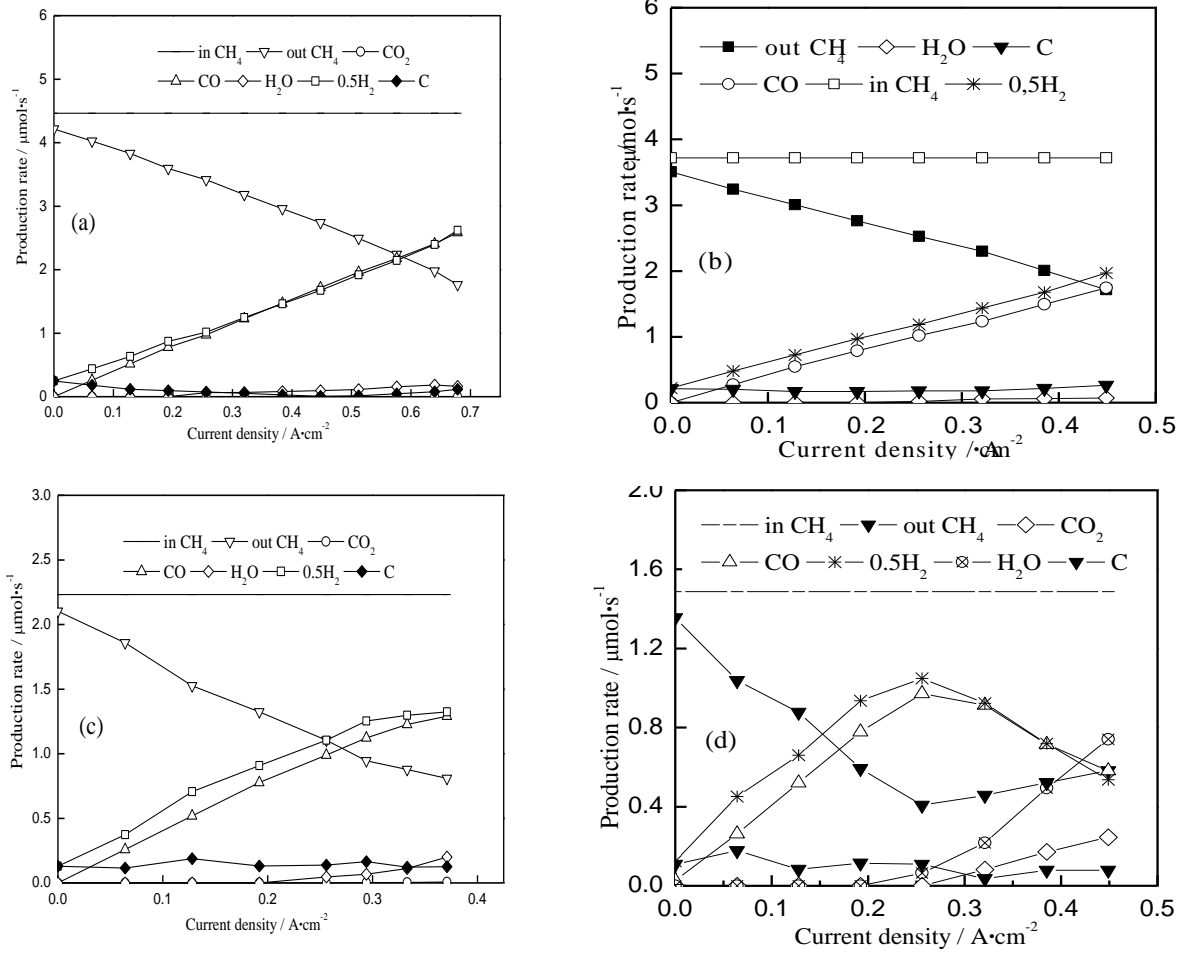
Fig. 3.2 The production rates for different methane flux on the cell with Ni-YSZ anode at 1273K (a) 4.464μmol·s⁻¹ (b) 3.720μmol·s⁻¹ (c) 2.232μmol·s⁻¹ (d) 1.488μmol·s⁻¹

The carbon deposition rate is calculated by the carbon balance equation:

$$v(C)_{dep} = v(CH_4)_{in} - v(CH_4)_{out} - v(CO)_{out} - v(CO_2)_{out} \tag{3.1}$$

where $v(C)_{dep}$ is the flux of deposited carbon per second, $v(CH_4)_{in}$ is the inlet flux of CH_4, $v(CH_4)_{out}$, $v(CO)_{out}$ and $v(CO_2)_{out}$ are the outlet fluxes of CH_4, CO and CO_2, respectively.

The flux of water is calculated from the hydrogen balance by the following equation:

$$v(H_2O)_{fH} = 2[v(CH_4)_{in} - v(CH_4)_{out}] - v(H_2)_{out} \tag{3.2}$$

The water generation rate can also be calculated by using the oxygen balance equation:

$$v(H_2O)_{fO} = v(O^{2-}) - v(CO)_{out} - 2 v(CO_2)_{out} \tag{3.3}$$

where $v(O^{2-})$ is the O^{2-} flux calculated from the current (I) passing through the electrolyte. The relation between the $v(O^{2-})$ and I is

$$v(O^{2--}) = I/(2F) \tag{3.4}$$

where, F is the Faraday constant. Here $v(H_2O)$ was calculated from the oxygen according to (3.3) due to the accurate current. All curves of H_2 in Figs. 3.2 and 3.3 were drawn with one-half calculated production rate.

The experimental phenomena and thermodynamic analysis indicate that, during the process of current increasing, which is the flow rate of the oxygen ion at the anode three-phase boundary is continuously increasing at the Ni-YSZ anode of SOFC, the following reactions [4]

$$CH_4 + O^{2-} \rightarrow CO + 2H_2 + 2e^- \tag{3.5}$$

$$CH_4 + 2O^{2-} \rightarrow CO + H_2 + H_2O + 4e^- \tag{3.6}$$

$$CH_4 + 3O^{2-} \rightarrow CO + 2H_2O + 6e^- \tag{3.7}$$

$$CH_4 + 4O^{2-} \rightarrow CO_2 + 2H_2O + 8e^- \tag{3.8}$$

occur in sequence for 1.488 $\mu mol \cdot s^{-1}$ dry methane

The partial oxidation reaction of methane is characterized in that, in addition to the unreacted methane, the anode exhaust gas only contains H_2 and CO; two reactions of methane occur:

$$CH_4 + 2O^{2-} \rightarrow CO + H_2 + H_2O + 4e^-$$

$$CH_4 + 3O^{2-} \rightarrow CO + 2H_2O + 6e^-$$
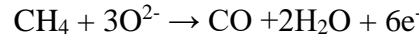
which is characterized by the anode exhaust gas containing H_2O. When CO_2 was detected in anode exhaust gases, the complete oxidation of methane (COM) took place.

For 4.464 $\mu mol \cdot s^{-1}$ dry methane, no CO_2 is detected in the exhaust gas during the whole testing, indicating that methane at this flow rate is not completely oxidized, and methane starts generating H_2O when the current density is 0.256 $A \cdot cm^{-2}$; for 3.720 $\mu mol \cdot s^{-1}$ dry methane, it starts generating H_2O when the current density is 0.256 $A \cdot cm^{-2}$, and no CO_2 is detected within the whole current density range; for 2.232 $\mu mol \cdot s^{-1}$ dry methane, it starts generating H_2O when the current density is 0.256 $A \cdot cm^{-2}$, and CO_2 is detected for the first time when the current density is 0.294 $A \cdot cm^{-2}$; for 1.488 $\mu mol \cdot s^{-1}$ dry methane, it starts generating H_2O when the current density is 0.256 $A \cdot cm^{-2}$, and CO_2 is detected for the first time when the current density is 0.321 $A \cdot cm^{-2}$.

Different methane fluxes tests show that the flow rate of dry methane has a greater impact on the anode reaction. High flow rate is equivalent to methane of high concentration, and only partial oxidation reaction of methane occurs at the SOFC anode for methane of high concentration, which is further proved by the experiment in literature [8-9], where the dry methane flow rate is 29.2%.

The chromatography detection of the anode exhaust gas at several flow rates in SOFCs experiment indicates that, if the methane flow rate is low, as the current density increases, the characteristic gases are produced in the sequence of CO, H_2O and CO_2 in the anode exhaust gas; and if methane flow rate is large, only CO and H_2O are produced in the anode exhaust gas according to the priority of CO and

H_2O.

3.3.3 Anode reaction mechanism when dry methane flow rate changes

The reaction when the dry methane flow rate changes should be in line with the basic principle of thermodynamics. Regardless of the changes in the methane flow rate, the reaction with small activation energy always proceeds before the reaction with high activation energy. Fig. 3.3 is the reaction path diagram of methane at the Ni-YSZ anode in the reference literature [6-8]. The figures above or below the line segment in Figure 3.3 are from the activation energy of relevant elementary reaction in literature [6], in $KJ \cdot mol^{-1}$. The O^{2-} entered and reaction products, excluding methane, are measured as per 1 mol.
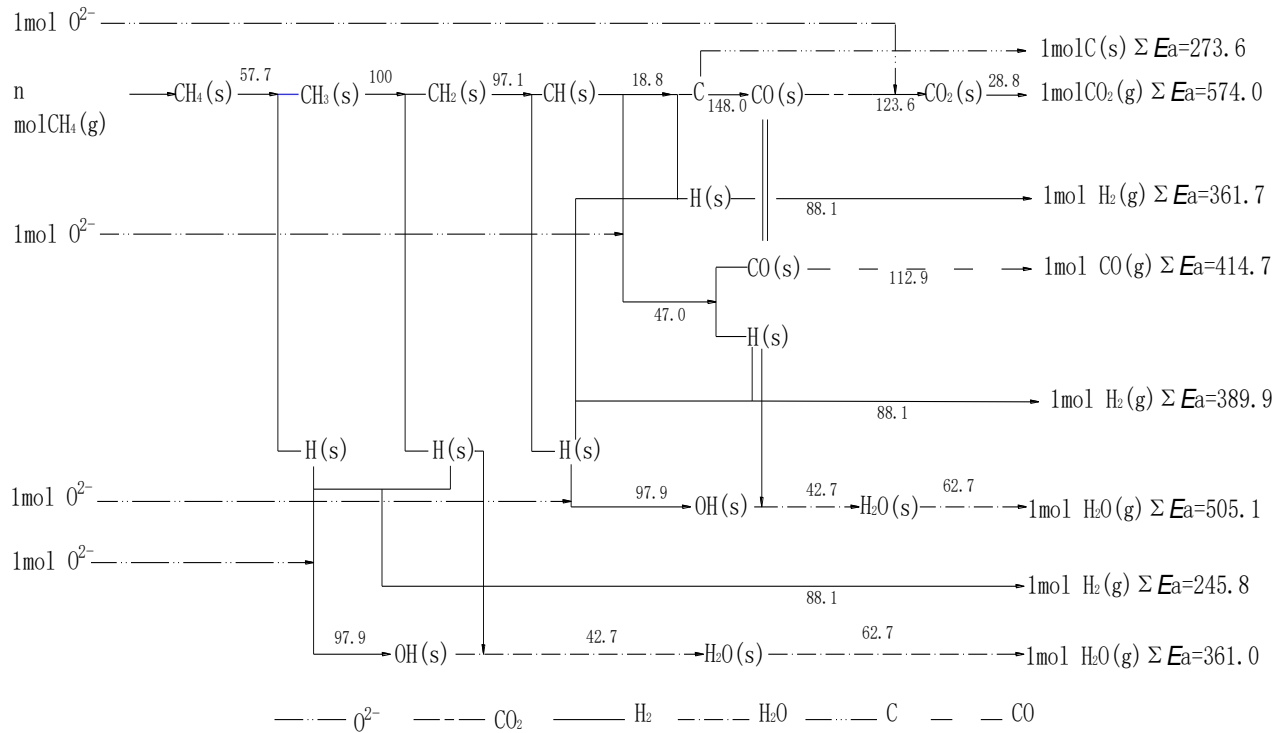
Fig. 3.3 The reactions routs of methane at the Ni-YSZ anode

Under the conditions of sufficiently large methane flow rate, no matter how large the current density is, in the oxidation of methane decomposition products, the reaction proceeds in the reaction path with minimum activation energy, and it produces CO and H_2 first. Although there is the overall activation energy ($\Sigma Ea_{(H2O)} = 361.0$ $KJ \cdot mol^{-1}$ and $\Sigma Ea_{(H2O)} = 505.1 KJ \cdot mol^{-1}$) for the formation of water, which is smaller than the overall activation energy ($\Sigma Ea_{(CO)} = 414.7 KJ \cdot mol^{-1}$) for the formation of CO, the reaction still proceeds in the reaction path with minimum activation energy in the intermediate process. The activation energy for the formation of CH(s) is $97.1 KJ \cdot mol^{-1}$, which is smaller than the activation energy (97.9 $KJ \cdot mol^{-1}$) for the formation of OH(s), and thus the reaction is developed

towards the final formation of CO.

Under the conditions of moderate methane flow rate, during the oxidation of the methane decomposition products, the reaction proceeds in the reaction path with minimum process activation energy first, it produces CO and H_2, and the methane decomposition products and O^{2-} are consumed in the process of CO formation; if there is surplus O^{2-} in the reaction process, the methane decomposition products continue to react with O^{2-} in the reaction path with minimum activation energy to generate H_2O, and the overall reaction is $CH_4 + 2O^{2-} \rightarrow CO + H_2 + H_2O + 4e^-$; if there is still surplus O^{2-}, the methane decomposition products continue to react with O^{2-} to generate H_2O, and the total reaction is $CH_4 + 3O^{2-} \rightarrow CO + 2H_2O + 6e^-$.

If the methane flow rate is small or the current density is large, in the oxidation of the methane decomposition products, after the reaction in which CO and H_2O are produced, there are still methane decomposition products available for the reaction, especially O^{2-} and CO(s). The overall reaction of methane is a fully oxidized reaction, which generates CO_2 and more H_2O.

3.3.4 Relationship between the methane flow and the current

The reactions of dry methane at anode of SOFCs are not only related to current density, but also to the flux of methane. It is necessary to summarize the regularity of dry methane reacted at the anode of SOFCs when current and the fluxes of methane are changing.

Ideally, in the unit time, 1 mol O^{2-} was required for 1 mol methane to occur POM; 2 mol O^{2-} were required for 1mol methane to take part in the reaction of $CH_4 + 2O^{2-} \rightarrow CO + H_2 + H_2O + 4e^-$; 3 mol O^{2-} were required for 1mol methane to take part in the reaction of $CH_4 + 3O^{2-} \rightarrow CO + 2H_2O + 6e^-$; when COM occurred, 4 mol O^{2-} were needed. In the case of low flux methane, the sequential reactions were carried out with the increased current density.

Based on Faraday's first law and relationships of the molar ratio between the reactions, when methane take part in partial oxidation reaction, the stoichiometry of O^{2-} and electrochemical oxidation methane must meet $v(O^{2-}) / \Delta v (CH_4) \leq 1$, i.e. $v(O^{2-}) \leq \Delta v(CH_4)$. $\Delta v(CH_4)$ is the methane amount which takes part in electrochemical oxidation reaction. Because $v(O^{2-}) = I/(2F)$, so $v(O^{2-}) \leq \Delta v(CH_4)$ converts to $I/(2F) \leq \Delta v(CH_4)$. Since the current change during the operation of cells, the O^{2-} transferred to the anode three-phase boundary changes. When the flow rate of methane is settled, the value of $v(O^{2-})/\Delta v(CH_4)$ formed is changeable. Accordingly, the molar ratio of reaction products is also changed, which will definitely cause changes in the reaction of methane. Therefore, when illustrating the flow rate of methane is high or low in a methane reaction, it is not an absolute quantity, but a relative quantity in the current changing process. Consequently, under the precondition that carbon deposition is not considered, the high flow capacity methane in the partial oxidation reaction of

methane must meet $\Delta v(CH_4) \geq I/(2F)$.

After POM, the reaction of $CH_4 + 2O^{2-} \rightarrow CO + H_2O + H_2 + 4e^-$ occurs when current is large enough and methane flux is relatively low. To have the reaction and the POM occurred, the stoichiometry of O^{2-} and electrochemical oxidation methane must meets $1 \leq v(O^{2-})/\Delta v(CH_4) \leq 3/2$, i.e. $2/3\, v(O^{2-}) \leq \Delta v(CH_4) \leq v(O^{2-})$. Because $v(O^{2-}) = I/(2F)$, $I/(3F) \leq \Delta v(CH_4) \leq I/(2F)$ is obtained.

The reaction of $CH_4 + 3O^{2-} \rightarrow CO + 2H_2O + 6e^-$ will take place, if the current continues to increase after POM and the reaction of $CH_4 + 2O^{2-} \rightarrow CO + H_2O + H_2 + 4e^-$. The reaction of $CH_4 + 3O^{2-} \rightarrow CO + 2H_2O + 6e^-$ will only occur when it meets the requirement $3/2 \leq v(O^{2-})/\Delta v(CH_4) \leq 2$, i.e. $I/(4F) \leq \Delta v(CH_4) \leq I/(3F)$.

The reaction of COM takes place, if the current continues to increase after POM, the reaction of $CH_4 + 2O^{2-} \rightarrow CO + H_2O + H_2 + 4e^-$ and the reaction of $CH_4 + 3O^{2-} \rightarrow CO + 2H_2O + 6e^-$ taken place for slow methane flux. The stoichiometry of methane electrochemical oxidized and O^{2-} should be $v(O^{2-})/\Delta v(CH_4) \geq 2$. Since $v(O^{2-}) = I/(2F)$, it can be concluded that $\Delta v(CH_4) \leq I/(4F)$. As long as $\Delta v(CH_4) < I/(4F)$, COM can occur in the process of which current continuously increasing when methane flow is fixed.

Fig. 3.4 shows the relation of the various reactions with the fluxes of methane and the quantity of O^{2-} at unit time for different methane flux.
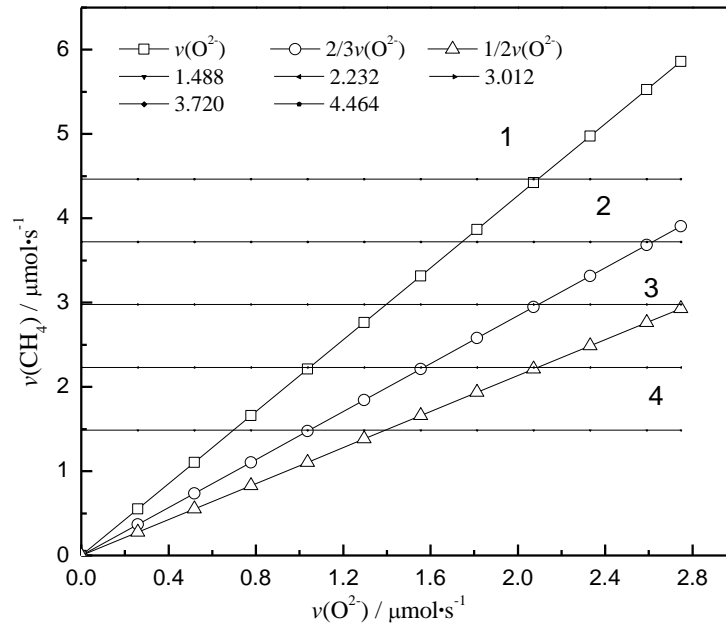
Fig. 3.4 The relationship between $v(CH_4)$ and $v(O^{2-})$

In Fig. 3.4, POM occurs in the area of 1, above the line of $v(O^{2-})$ region represent that methane flux

is bigger than needed O^{2-}. In the area of 2 of the line v (O^{2-}) and line $2/3v$ (O^{2-}) represents the flux of methane may taking place the reaction of $CH_4 +2O^{2-}\rightarrow CO + H_2 + H_2O +4e^-$, the reaction of $CH_4 + 3O^{2-}\rightarrow CO +2H_2O + 6e^-$ may occur when the flux of methane in the interval of line $2/3v$ (O^{2-}) and line $1/2v$ (O^{2-}) , and the flux of methane may takes place COM in the area below the line $1/2$ v (O^{2-}). The several horizontal lines in Fig. 3.4 represent the flow rate of the methane.

Oxygen ions may concentrate on some three phase boundarys for uneven anode, which could lead to the subsequent reaction occurred early. But even follow-up reactions occurred in advance, gas generated by reactions still following the sequence of CO, H_2O and CO_2.

3.4 Conclusions

Methane with different flux was fed to the anode chambers of Ni-YSZ/YSZ/LSM fuel cells to research the influence of methane flux to methane anode reaction. Based on Faraday's first law and relationships of the molar ratio between reactions, the methane participating in the electrochemical reactions with current has following conclusions. When $v(CH_4)\geq I/(4F)$，dry methane starts the electrochemical reactions in following sequence when the oxygen anion molar flow continue to increase at anode.

$CH_4 + O^{2-} \rightarrow CO + 2H_2 + 2e^-$

$CH_4 + 2O^{2-} \rightarrow CO + H_2O +H_2+ 4e^-$

$CH_4 + 3O^{2-} \rightarrow CO +2H_2O + 6e^-$

$CH_4 + 4O^{2-} \rightarrow CO_2 +2H_2O + 8e^-$

When $I/(4F)\leq v(CH_4)\leq I/(2F)$，the first two or three reactions occur in sequence when the oxygen anion molar flow continue to increase at anode. When $v(CH_4)\leq I/(2F)$，only the POM occurs.

The subsequent reactions occur in advance when the anode structure is uneven, which can lead to the oxygen anions focus in three-phase boundary. But even occur in advance, the reactions of methane with oxygen anion still generating CO, H_2O, and CO_2 in sequence.

References

[1] M. K. Bruce, M. van den Bossche, S. McIntosh, The influence of current density on the electrocatalytic activity of oxide-based direct hydrocarbon SOFC anodes, *J. Electrochem Soc*. **155(11)** (2008) B1202-B1209.

[2] K. Kendall, C. M. Finnerty, G. Saunders, J.T. Chung, Effects of dilution on methane entering an SOFC anode, *J. Power Sources* **106(1-2)** (2002) 323-327.

[3] A. Abudula, M. Ihara, H. Komiyama, K. Yamada, Oxidation mechanism and effective anode

thickness of SOFC for dry methane fuel, *Solid State Ionics* **86-88(Part 2)** (1996) 1203-1209.

[4] Z. Zhan, Y. Lin, M. Pillai, I. Kim, S. A. Barnett, High-rate electrochemical partial oxidation of methane in solid oxide fuel cells, *J. Power Sources* **161(1)** (2006) 460-465.

[5] H. X. You, H. J. Gao, G. Chen, A. Abudula,X. W. Ding, The conversion among reactions at Ni-based anodes in solid oxide fuel cells with low concentrations of dry methane, *J. Power Sources* **196(5)** (2011) 2779-2784.

[6] E. S. Hecht, G. K. Gupta, H. Zhu, A. M. Dean, J. R. Kee, L. Maier, O. Deutschmann, Methane reforming kinetics within a Ni-YSZ SOFC anode support, *Appl. Catal. A- Gen.* **295(1)** (2005) 40-51.

[7] T. H. Wu, H.Y. Wang, A study on the bond-order-conservation model of the mechanism of methane partial oxidation to syngas on Ni, *J. Zhejiang Norm. Univ. (Nat. Sci.).* **19(1)** (1996) 48-52.

[8] H.Y Zhu, R. J. Kee, M. R. Pillai, S. A. Barnett, Modeling electrochemical partial oxidation of methane for cogeneration of electricity and syngas in solid-oxide fuel cells, *J. Power Sources* **183(1)** (2008) 143-150.

Chapter 4

Influence of dry methane reactions on the cell output characteristics of solid oxide fuel cells

4.1 Introduction

Dry methane and oxygen ions that are derived from cathodes can produce a multitude of chemical reactions in a solid oxide fuel cell anode. The reaction of methane on the anode is also the oxidation reaction. The partial oxidation reaction of methane was founded by K. Kendall [1] under open circuit conditions, using the Nernst equation and by analyzing the open circuit voltage of this system. The study of anode reactions and electronic analysis of oxygen ions from anode exhaust gas by Abuliti [2] found that dry methane occurs from the partial oxidation reaction of $CH_4 + O^{2-} \rightarrow CO + 2H_2 + 2e^-$ when current density on the Ni-YSZ anode is low by using 4.2% dry methane. However, complete oxidation reactions have occurred with 4.2% high current density dry methane. The partial oxidation reaction of dry methane only occurred at the concentration of 29% dry methane under different current densities.

Some research found an effective measure for improving power generation performance by using a material with higher electric conductivity. The conductivity of 8% yttria-stabilized zirconia (YSZ) is $0.1S \cdot cm^{-1}$, which greatly influences cell performance. In order to avoid this influence on cell performance, it is necessary to adopt a new material with high electric conductivity in place of YSZ, such as scandia-stabilized zirconia (ScSZ), which has a conductivity of 0.3 [3].

On the Ni-ScSZ anode, 3% H_2O-CH_4 can be used in SOFC as a fuel [4]. Compared with the Ni-YSZ anode, the Ni-ScSZ anode exhibited lower overpotential and excellent durability. Gunji [5] et al. studied the depositional behavior of carbon on the Ni-ScSZ anode with 97% CH_4 + 3% H_2O as the fuel source. The cell voltage was reduced and unstable at 1073K. However, the cell performance began to increase in the initial 70h at 1173K and later became stable.

You [6] carried out experiments using low concentrations of dry methane on the Ni-YSZ and Ni-ScSZ anode, respectively, and measured the components of the anode exhaust gas and analyzed the produced characteristics of the anode exhaust gas. Combined with methane and oxygen ions reaction

kinetics, and with the current density traveling from low to high, the methane occurred following reactions on Ni based anodes in the following sequence: partial oxidation reaction, $CH_4 + 2O^{2-} \rightarrow CO + H_2O + H_2 + 4e^-$, $CH_4 + 3O^{2-} \rightarrow CO + 2H_2O + 6e^-$, and complete oxidation reaction. When the reaction changed, the output voltage of Ni-ScSZ anode cell was reduced.

Methane on the solid oxide fuel cell anode occurs with the partial oxidation reaction that resulted when the 1mol methane reaction released 2mol electron, the reaction of $CH_4 + O^{2-} \rightarrow CO + H_2 + 2e^-$ occurred. Methane on the SOFC anode occurs following the complete oxidation reaction [7-8] that 1mol methane reaction released 8mol electron, as the reaction of $CH_4 + 4O^{2-} \rightarrow CO_2 + 2H_2O + 8e^-$ occurred. The partial oxidation reaction and complete oxidation reaction can be carried out, not only in the nickel based catalyst, but also in cerium based [7] and Lanthanum chromite based catalysts [9]. According to the above two reactions, in order to use methane as the cell fuel in SOFC and make SOFC produce more power, a complete oxidation reaction with methane as a fuel source must be accomplished on the SOFC anode in order to obtain a high power generation performance.

To research methane reaction models and their influence on cell output characteristics in SOFC, experiments were carried out using different flows of dry methane on an Ni-ScSZ anode. Through researching the cell power performance and characteristics of the anode exhaust gas, we can analyze the characteristics of anodic oxidation reactions so that dry methane service can be used in SOFC reasonably.

4.2 Experiment

4.2.1 Single cell preparation

The solid electrolyte YSZ (8mol% Y_2O_3) substrate used in the experiments was purchased from Japan (Tosoh). The diameter and thickness of the YSZ substrate were 20.0 mm and 1.0 mm, respectively. The anode material used in the experiment was Ni-ScSZ, and was made by mixing and grinding NiO and ScSZ with a mass ratio of 3:2. 50% of binder and 10% of pore forming agent were added and grinded. Anode slurry grinded well was coated on one side of the electrolyte substrate, and then the electrolyte substrate was put into the high temperature heating furnace. The electrolyte substrate was calcined at 1673K for 2 hours and was slowly cooled. The anode area of the fuel cell was 0.78 cm^2. $La_{0.85}Sr_{0.15}MnO_{3-\delta}$ (LSM) was used as the cathode material and coated on the side opposite of the electrolyte substrate. The method used to coat the cathode material was the same as the anodic method, except the cathode calcining temperature was 1473K.

4.2.2 Cell power test

The method of cell clamping installation was the same as has been previously described in the literature [10]. During the cell test, the methane that passed into the anode was always diluted to the required concentration of 50ml·min^{-1} argon. Oxygen with a purity of 99.9% was passed into the cathode and its flux was 50ml·min^{-1}. The test was started after the open circuit voltage was stable. Agilent GC 7890A chromatography online was used to detect the anode exhaust gas in the experiment. After completing the experiment of one concentration of methane, argon gas was used to replace the anode chamber and measure the anode exhaust gas using chromatography until the anode exhaust gas was without fuel gas.

In order to assess the performance of the researched cell, ac impedance was used to test cell performance in open circuit. The AC impedance measurement device used in the test was Solartron 1255B+ Solartron SI 1287A. During open circuit test, an alternating current of 0.001 A was set and the frequency range was from 1000000Hz to 0.1 Hz.

4.3 Experimental results and discussion

4.3.1 Cell power performance

Fig. 4.1 depicts the power generation performance curve of Ni-ScSZ anode cells at 1273K, with 29.7% CH_4 +70.3% Ar, 10.7% CH_4 + 89.3% Ar, 7.41% + 92.59, 5.66% CH_4 +94.34% Ar and 3.85% CH_4 +96.15% Ar as fuel, respectively. Open circuit voltage of the cells was higher than 1.43V, which illustrates the quality seal of the cells. Fig. 4.2 shows the cell impedance spectra when open for different methane concentrations. The impedance of each cell under the open circuit showed little difference, suggesting the cell manufacturing process was essentially stable.

The maximum power density of the four cells was 0.275 W·cm^{-2}, 0.234 W·cm^{-2}, 0.229 W·cm^{-2} and 0.192 W·cm^{-2}, respectively. This confirms that the cells had good power performance at high methane concentration. For a cell methane concentration of 3.85%, the output power was low. However, when the cell in the current density was greater than 0.192 A·cm^{-2}, the output voltage dropped rapidly. A methane concentration of 5.66% also created a similar phenomenon when the cell in the current density was greater than 0.256A·cm^{-2}. As current density increased, the output voltage declined at a fast rate. During the cell test, a cell methane concentration of 7.41% of the cell appeared in the experiment (Fig. 4.3). As the current density approached 0.256 A·cm^{-2}, the voltage declined continuously through time, which prevented further measurements from being taken. The cell concentrations of 5.66% and 3.85% also showed similar problems in the test process of power generation performance, but did not hinder measurements from being taken.
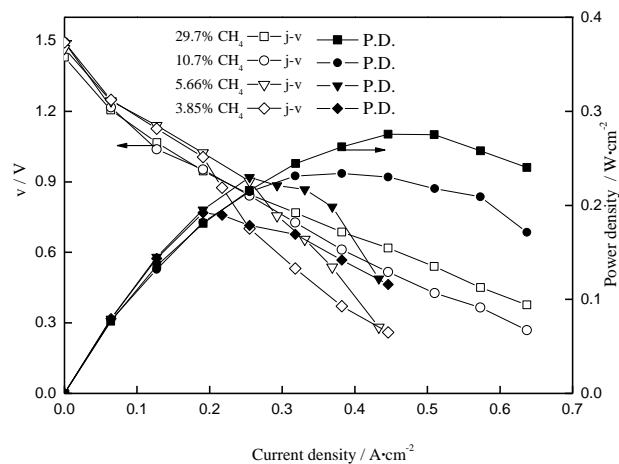
Fig. 4.1 J-V characteristics and power density with different methane concentrations at 1273K
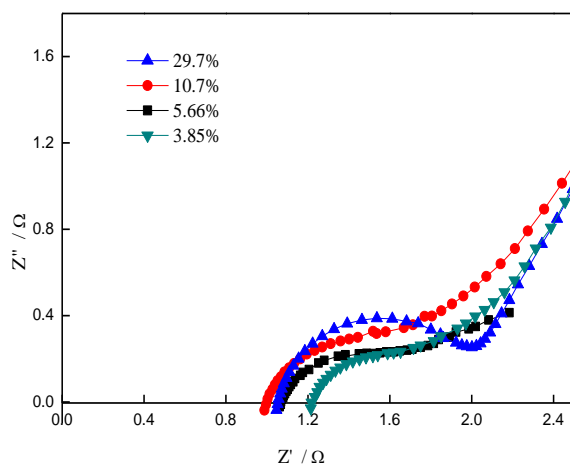
Fig. 4 2 Impedance spectra at open for the different methane concentrations at 1273K
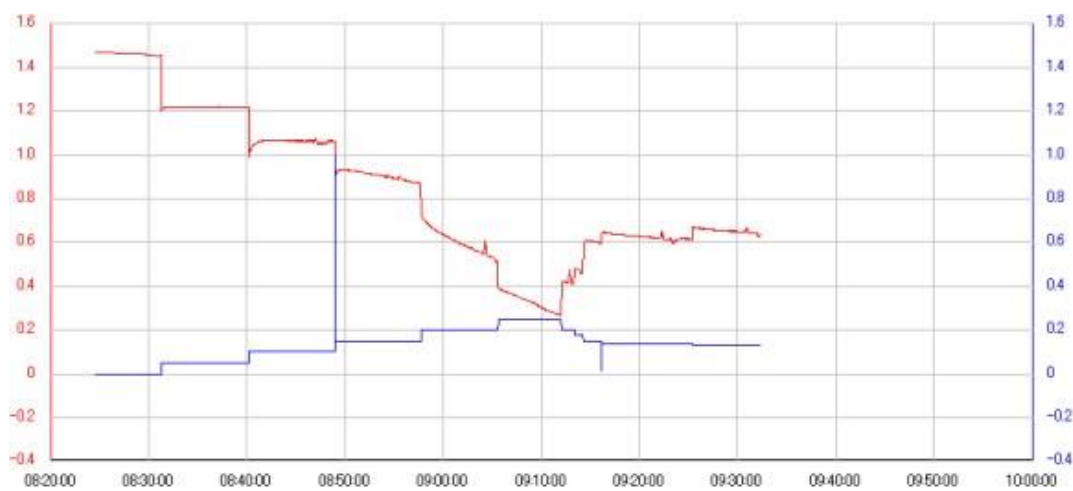
Fig. 4.3 The process of power generation of the cell with 7.41% CH$_4$

4.3.2 The anode exhaust gas

The anode exhaust gas is an important signal in determining the cell reaction. Fig. 4.4 shows the exhaust gas composition with different concentrations of methane after cell anode reaction and carbon precipitation after methane pyrolysis in the anode chamber at 1273K on the Ni-ScSZ anode. The water of reaction product was calculated in accordance with the method of the oxygen balance [6]. Fig. 4.4 shows a correlative relationship between releasing H_2 and CO and the relationship is represented with 0.5 times of H_2.
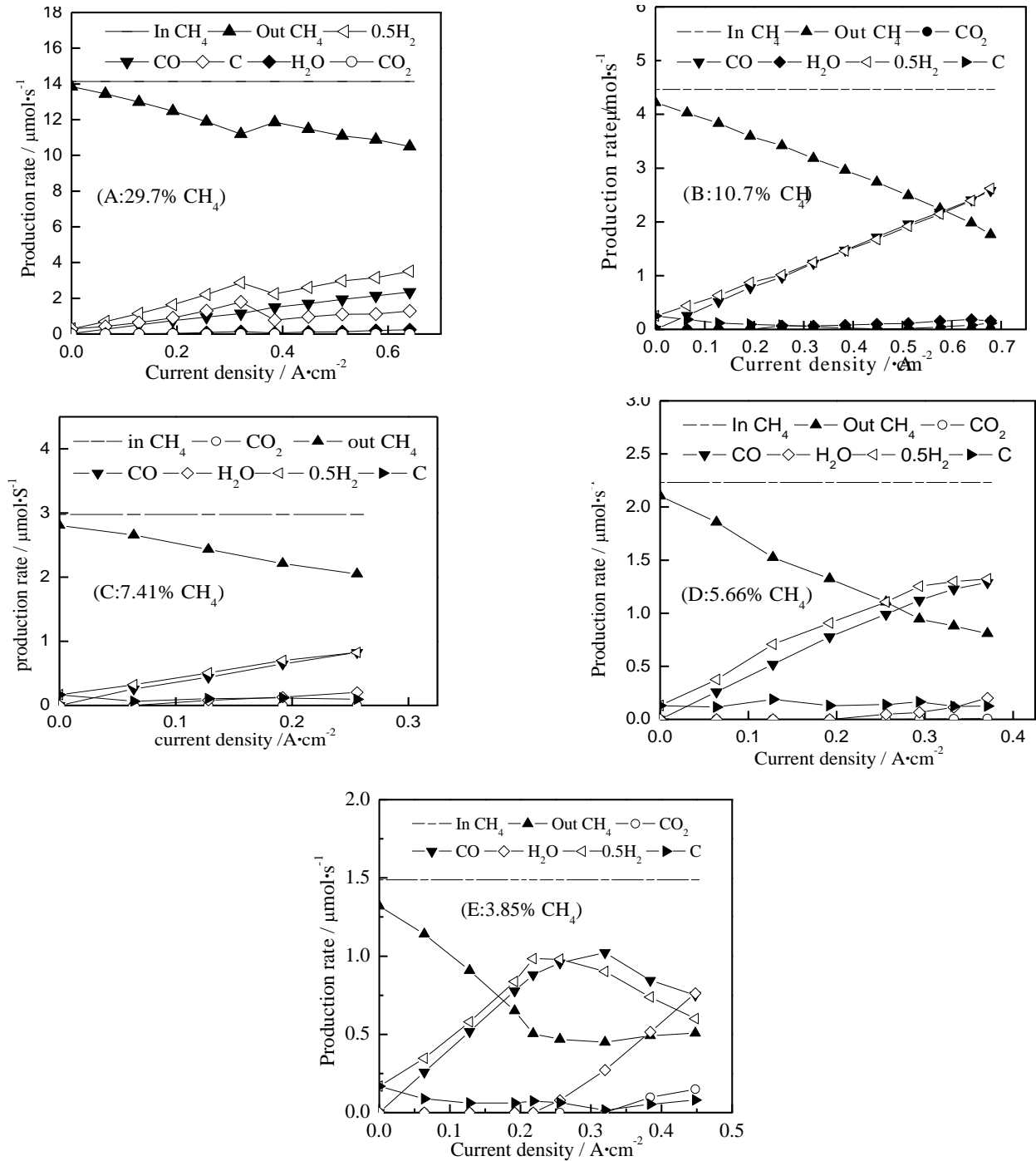
Fig. 4.4 The production rates for different methane concentration on the cell

62

With various concentrations of methane at a low current, the outlet methane continuously reduced with the increase of the current density (Fig. 4.4). Meanwhile, CO and H_2 exhaust gas increased with increasing current density.

For the 29.7% dry methane at a current density between 0.321 $A \cdot cm^{-2}$ and 0.386 $A \cdot cm^{-2}$, there was sudden change in the outlet methane (Fig. 4.4A). It first decreased suddenly, and then a subsequent increase in H_2 and H_2O created a similar change in the outlet methane. However, corresponded CO had no the trend following the increase of current density.

For the 10.7% dry methane, the outlet methane continuously decreased with the increase of the current density. The CO and H_2 in the exhaust gas increased with the increase of the current density when the current density was at 0.321 $A \cdot cm^{-2}$ and 0.256 $A \cdot cm^{-2}$, after the calculation the exhaust gas has a certain amount of water (Fig. 4.4B). When the current density was at 0.449 $A \bullet cm^{-2}$, trace amounts of CO_2 were measured in the exhaust gas. with Ni-ScSZ anode at 1273K

For the 5.66% dry methane, the outlet methane also continuously decreased with the increase of the current density, and CO and H_2 in exhaust gas increased with the increase of the current density (Fig. 4.4D). CO_2 was found in the exhaust gas when the current density was 0.385 $A \cdot cm^{-2}$. The exhaust gas began to produce water at the current density of 0.256$A \cdot cm^{-2}$.

For the 3.85% dry methane, increasing current density corresponded to rapidly decreasing outlet methane (Fig. 4.4E). CO and H_2 rapidly increased at first. After both reach a maximum production rate, the H_2 decreases beginning at current density more than 0.218 $A \cdot cm^{-2}$. The CO remained stable at a high level, until it began to gradually decrease. After the outlet methane was reduced to a lower level, little change was recorded. When the current density was low, CO_2 and H_2O did not appear in exhaust gas. When the CO and H_2 increased rapidly, H_2O first appeared in exhaust gas, and then CO_2 appeared. As the current density increased, the carbon precipitation reduced gradually. H_2O began to be produced in the current at a density of 0.385 $A \cdot cm^{-2}$, and CO_2 was measured in the current at a density of 0.384 $A \cdot cm^{-2}$.

For the 29.7% dry methane, irregularity of change in the outlet methane was similar to test results using a 14.8% concentration of dry methane on $Ni_{0.5}Cu_{0.5}$-CGO anode [11-12]. For 3.85% of dry methane the outlet methane also changed irregularly, suggesting the necessity of careful study in the future.

4.3.3 Anode reaction

With methane concentrations at 3.85% and 5.66%, the cell output voltage dropped rapidly. For concentrations of 29.7% and 3.85%, the anode exhaust residual methane changed irregularly with the

current density and this phenomenon was associated with the dry methane that reacted on anode of the cell.

For internal reforming and dry reforming of methane, the reaction residence time was a few seconds [13]. In the literature [14-16], according to the reaction thermodynamics, the multiple reaction steps of the activation energy were given describing methane and oxygen on the Ni-based anode. Drawing reaction route diagrams was shown in Fig. 4.5. The reaction activation energy and numerical value marked on the line in the figure was the activation energy of the step, the unit of which was $KJ \cdot mol^{-1}$.
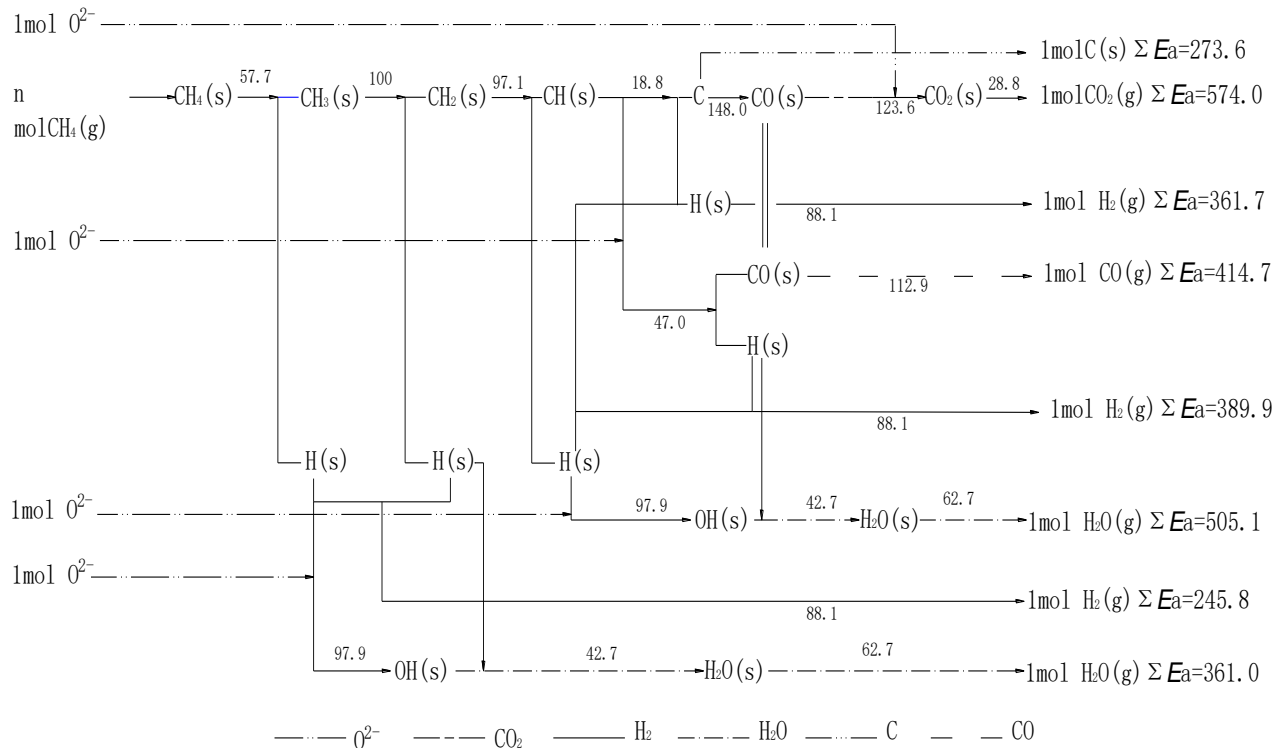
Fig. 4.5 The reactions routes of methane at the Ni base anode

Under specific reaction conditions, the main products of the reaction must be from a relatively stable process with the lowest activation energy. The dry methane reaction produced C, H_2, CO and H_2 in order along a continuous variation of the current density. CO, H_2 and H_2O, CO, CO_2 and H_2, and H_2O were produced at the same time. The activation energy for the precipitation of 1mol C (ΣEa) was 273.6 $KJ \cdot mol^{-1}$, and the activation energy of 1mol H_2 (ΣEa) by generating was 245.1 $KJ \cdot mol^{-1}$ and 361.7 $KJ \cdot mol^{-1}$ through different routes. Meanwhile, the activation energy of 1mol H_2O (ΣEa) by generating was 361.0 $KJ \cdot mol^{-1}$ and 505.1 $KJ \cdot mol^{-1}$ through different routes, the activation energy of

1mol CO (ΣEa) was 414.7 KJ·mol^{-1}, and the activation energy of 1mol CO_2 (ΣEa) was 574.0 KJ·mol^{-1}. Although the total activation energy forming water ($\Sigma Ea_{(H2O)}$ = 361.0KJ·mol^{-1} and $\Sigma Ea_{(H2O)}$ =505.1KJ·mol^{-1}) was less than total activation energy forming CO ($\Sigma Ea_{(CO)}$ =414.7KJ·mol^{-1}), the reaction was working towards forming CO. In the process, the reaction was carried out according to the minimum activation energy, so the activation energy of forming CH (s), that was 97.1KJ·mol^{-1}, was less than 97.9 KJ·mol^{-1}of forming OH (s). According to the principle of minimum activation energy, with the increase of the current density, corresponding O_2 increases and the reaction of generating CO and H_2 should occur after generating C by pyrolysis of methane. Then the reaction occurred with the reaction of generating CO, H_2 and H_2O, and finally, the reaction of forming CO_2.

Combined with exhaust gas measurement results after the anode reaction with different concentrations of dry methane as fuel in Fig. 4.4, the anode exhaust gas contained CO and H_2, which indicated that the cell anode occurred with the reaction of $CH_4 +O^{2-}\rightarrow CO+H_2 +2e^-$. The anode exhaust gas also contained CO, H_2 and H_2O, which indicated the reaction of $CH_4 +2O^{2-}\rightarrow CO+H_2 +H_2O +4e^-$ occurred at the cell anode. The anode exhaust gas also contained CO, H_2 and H_2O, that may occur in the reaction of $CH_4+ 3O^{2-} \rightarrow CO+2H_2O+6e^-$, which was reflected in Figure 4D. When the current density moved from 0.256 A·cm^{-2} to 0.32 A·cm^{-2}, the CO flux increased 0.066 μmol·s^{-1}, while the increment of H_2O was 0.273μmol·s^{-1}. With the increase of the current density, the production of water increased, indicating that it occurred from the reaction of $CH_4+ 3O^{2-} \rightarrow CO+2H_2O+6e^-$. When CO_2 was contained in the exhaust gas, it showed that the dry methane completed the oxidation reaction in the anode of cell.

Under ideal conditions, 1mol of methane occurring at partial oxidation reaction requires 1mol of O^{2-} and 1mol of methane requires 2mol O^{2-} in order for the reaction $CH_4+2O^{2-} \rightarrow CO+H_2+H_2O+4e^-$ to occur, per unit time. 1mol methane required 3mol O^{2-} to occur the reaction of $CH_4+3O^{2-} \rightarrow CO+2H_2O+6e^-$ while 1mol methane required 4mol O^{2-} to occur complete oxidation reaction. In the case of the low flow rate of methane, the above reactions occur in sequence with the increase of the current density.

When the flow of methane was small and remained unchanged, if the current density of the cell increased so as to increase O^{2-} in the process, and if the current density was low, namely less O^{2-}, the partial oxidation reaction of methane still followed. If the O^{2-} continuously increased, the subsequent reaction of consuming more oxygen negative ions was carried out. If the methane flowed at a medium rate, the methane was produced through a partial oxidation reaction and the reaction of consumed 2mol O^{2-} or 3mol O^{2-}. The methane only occurred from partial oxidation reaction at a high flow of methane.

In the Fig. 4.4A, for the 29.7% dry methane, there was a linear increase of CO corresponding to an increase in current density. When the current density was between 0.321 $A \cdot cm^{-2}$ and 0.386 $A \cdot cm^{-2}$, the outlet methane had a mutation and the phenomenon was associated with anode unevenness and anode reaction. Anode reactions occurred in the three-phase interface that consisted of a catalyst, an electrolyte and the fuel gas. Uneven three-phase interface caused the enrichment of the reaction medium in the anode. Once the enrichment reached a certain point, the anode reaction type may be changed. After the current density reached 0.321 $A \cdot cm^{-2}$, methane content increased slightly at the anode outlet because it was associated with a large number of methane pyrolysis products on the anode, including CH in the adsorption state and partial carbon. Part of the oxygen negative ions that were associated with the cathode were used to oxidize the product CH by methane cracking, which had existed on the three-phase interface of the anode. They were produced by the reaction that formed CO, rather than by the oxidization of a new methane cracking products directly. The reaction slightly increased the methane content of the anode while the methane conversion rate reduced. This process reduced the hydrogen produced by methane cracking. Therefore, when the current density was greater than 0.321 $A \cdot cm^{-2}$, the relative production rate of hydrogen in the CO production decreased.

When the current density for the low 3.85% concentration of dry methane was greater than 0.218 $A \cdot cm^{-2}$, the CH_4 flux in the outlet exhaust gas changed slowly between 0.65 $\mu mol \cdot s^{-1}$ and 0.45 $\mu mol \cdot s^{-1}$ (Fig. 4.4D). When the H_2 was reduced in the exhaust gas of the anode, there was an proportional increase in the water. As the CO_2 in the exhaust gas was produced and began to increase, the CO decreased proportionally and the CH_4 increased slowly. With the increase in oxygen ions that were transported to the anode, more oxygen ions became involved in the formation of H_2O and CO_2. The methane that originally produced CO can also be more involved in the reaction of the formation of CO_2 and H_2O, which made methane oxidation more thoroughly completed. The macroscopic experimental phenomena were that the methane of exhaust gas changed slowly with the increase of the current density.

4.3.4 Reasons for the voltage drop

Standard electric potentials for methane under complete oxidation, $CH_4 + O_2 \rightarrow CO + H_2 + H_2O$ and methane partial oxidation at 1273K were 1.067V, 1.204V and 1.444V, respectively [17]. Utilizing the Nernst equation of cell reactions to obtain the reaction of $CH_4 + 3/2O_2 \rightarrow CO + 2H_2O$ at 1273K, its standard electric potential was 1.085V. The reaction led to a continuous decline in the potential voltage of the cell throughout the power generation process. The reason for the decline was polarization and the anode occurs through a series of reactions: $CH_4 + 1/2O_2 \rightarrow CO + H_2$, $CH_4 + O_2$

$\rightarrow CO+H_2 +H_2O$ and $CH_4+ 3/2O^{2-} \rightarrow CO+2H_2O$. With the increase in the number of oxygen negative ions in the reaction, the open circuit voltages associated with standard electric potentials of this series of reactions were continuously reduced. The cell generated power under a current density, but the anode reaction can change abruptly when the current density is suddenly altered. These changes resulted in cell output voltage abruptly dropping. The performance changes were associated with the anode reaction in the methane concentration of 3.85% of the cell when current density was more than $0.192 \, A\cdot cm^{-2}$ (Fig. 4.1).

Another reason for a drop in the cell voltage is when it produces H_2O, as in Fig. 4.3. Gang Chen [11-12] researched degradation causes of Ni based anode electrode via repeated tests under higher current and analyzed anode material with XRD. Researches showed that with the constant consumption of methane in particular, the reaction produced H_2O, and the $p(H_2O)/p(CH_4)$ increased. This resulted in an active Ni of Ni based anode forming nickel hydroxide. Nickel hydroxide made the three-phase interface of anode reduction effective and decreased the cell performance.

In addition, when the reaction changed consuming less oxygen negative ions to consuming more oxygen negative ions when oxygen negative ions cannot be timely supplied, the concentration polarization of oxygen negative ions were greatly increased. A double electric layer was formed near the three-phase interface. When the reaction that requires more oxygen ions occurred, the oxygen negative ions of the three-phase interface weren't able to replenish at the same rate. The proportion of the fixed layer potential difference of the double electric layer increased in the whole potential difference, which led to the output voltage of the cell decreasing, as the reaction of the cell required more oxygen ions in its potential. In order to maintain the same reaction under the same current density, the concentration polarization changed from the proportion of fixed layer potential difference of double electric layer dominating in the whole potential difference to a fixed layer and the dispersive layer took effect simultaneously. As a result, the cell output potential decreased continuously under the fixed current density. Based on the analysis of the reaction activation energy, the activation energy of producing CO_2 was relatively high and subsequent reactions needed more oxygen ions. Hence, there may be higher potential difference for polarization activation.

4.4 Conclusion

These experiments were conducted in order to test power generation performance of the cell on a Ni-ScSZ anode with different concentrations of dry methane as fuel. By combining the measurements of the anode exhaust gas and through examination of the activation energy on the cell anode oxidation reaction, the results were analyzed for the anode oxidation reaction in power generation process.

Results showed that high concentrations of dry methane occurred following partial oxidation reactions on the cell anode. As the current density increased, there was a transition process from partial oxidation reaction to a complete oxidation reaction for low concentrations of dry methane. Although the partial oxidation reaction occurred with high concentrations of dry methane as fuel, good performance was able to be obtained. For low concentrations of dry methane, however, even if dry methane can occur following a complete oxidation reaction, H_2O was produced in transition of reaction and as a resultant of the reaction. The H_2O resulted in the increase of $p(H_2O)/p(CH_4)$. The polarization led to lower performance in a transition process of reaction.

References

[1] K. Kendall, C. M. Finnerty, G. Saunders, J.T. Chung, Effects of dilution on methane entering an SOFC anode, *J. Power Sources*.**106(1-2)** (2002) 323-327.

[2] A. Abudula, M. Ihara, H. Komiyama, K. Yamada, Oxidation mechanism and effective anode thickness of SOFC for dry methane fuel, *Solid State Ionics* **86-88(Part 2)** (1996) 1203-1209.

[3] O. Yamamoto, Y. Arati, Y. Takeda, N. Imanishi, Y. Mizutani, M. Kawai, Y. Nakamura, Electrical conductivity of stabilized zirconia with ytterbia and scandia, *Solid State Ionics* **79** (1995) 137-142.

[4] K. Ke, A. Gunji, H. Mori, S. Tsuchida, H. Takahashi, K. Ukai, Y. Mizutani, H. Sumi, M. Yokoyama, K. Waki, Effect of oxide on carbon deposition behavior of CH_4 fuel on Ni/ScSZ cermet anode in high temperature SOFCs, *Solid State Ionic* **177(5–6)** (2006) 541-547.

[5] A. Gunji, C. Wen, J. Otomo, T. Kobayashi, K. Ukai, Y. Mizutani, H. Takahashi, Carbon deposition behaviour on Ni–ScSZ anodes for internal reforming solid oxide fuel cells, *J. Power Sources* **131(1-2)** (2004) 285-288.

[6] H. X. You, H .J. Gao, G. Chen, A. Abudula, X. W. Ding, The conversion among reactions at Ni-based anodes in solid oxide fuel cells with low concentrations of dry methane, *J. Power Sources* **196(5)** (2011) 2779-2784.

[7] E. P. Murray, T. Tsai, S. A. Barnett, A direct-methane fuel cell with a ceria-based anode, *Nat.* **400(6745)** (1999) 649-651.

[8] J. Liu, S. A. Barnett, Operation of anode-supported solid oxide fuel cells on methane and natural gas, *Solid State Ionics* **158(1–2)** (2003) 11-16.

[9] J. Sfeir, P. A Buffat, P. Möckli, N. Xanthopoulos, R. Vasquez, H. J. Mathieu, J. Vanherle, K R. Thampi, Lanthanum Chromite Based Catalysts for Oxidation of Methane Directly on SOFC Anodes, *J. Catal.* **202(2)** (2001) 229-244.

[10] Z. Zhan, Y. Lin, M. Pillai, I. Kim, S. A. Barnett, High-rate electrochemical partial oxidation of

methane in solid oxide fuel cells, *J. Power Sources* **161(1)** (2006) 460-465.

[11] G Chen, Fabrication of cathod-supported SOFC with high performance and degration mechanism of Ni-base anodes at high current density, Hirosaki University, 2011.

[12] G Chen, G. Guan, Y. Kasai, H. X. You, A. Abudula, Degradation mechanism of Ni-based anode in low concentrations of dry methane, *J. Power Sources* **196(15)** (2011) 6022-6028.

[13] B. Qi, The Intrinsic Kinetics of Methane Steam Reforming and Reaction Performance Study in Micro-channel Reactor, Chongqing University, 2009.

[14] E. S. Hecht, G. K. Gupta, H. Zhu, A. M. Dean, J. R. Kee, L. Maier, O. Deutschmann, Methane reforming kinetics within a Ni-YSZ SOFC anode support, *Appl. Catal. A- Gen.* **295(1)** (2005) 40-51.

[15] H. Y Zhu, R. J. Kee, M. R. Pillai, S. A. Barnett, Modeling electrochemical partial oxidation of methane for cogeneration of electricity and syngas in solid-oxide fuel cells, *J. Power Sources* **183(1)** (2008) 143-150.

[16] T. Wu, H. Wang, A study on the bond-order-conservation model of the mechanism of methane partial oxidation to syngas on Ni, *J. Zhejiang Norm. Univ. (Nat. Sci.).* **19(1)** (1996) 48-52.

[17] X. Zhang, S. Ohara, H. Chen, T. Fukui, Conversion of methane to syngas in a solid oxide fuel cell with Ni-SDC anode and LSGM electrolyte, *Fuel*, **81(8)** (2002) 989-996.

Chapter 5

NiCu alloy anode material prepared with hard template method

5.1 Introduction

Solid oxide fuel cells (SOFCs) are a promising high efficient power generation tool by using hydrocarbon fuel since it can directly convert the chemical energy to electric energy. However, carbon deposition on the anode is a headache problem for the general anode material. In the present researches, perovskite [1,2] and fluorite structure [3] material are considered as good anode material, most of which require to add rare earth elements due to instability of the material. Nevertheless, China rare earth has being mined so continually that the amount of rare earth has being decreasing and the price has always being rising. The price of a gramme of perovskite and fluorite structure anode material with rare earth elements is 14 times of nickel based anode material in China. Therefore, it can be long-time and large-scale used for SOFC anode material. Ni-based anode material are widely applied due to its relatively stability, high catalytic activity and low cost. However, when hydrocarbon fuel is used, carbon deposition on the anode will occur because they can catalytically break C-H bonds [4-5]. Their catalytic performance is always unstable when they are used as the anode material [6]. But some research finds that carbon deposition phenomenon is caused by the methane that can't keep stable over 800K [7-8]. Methane pyrolysis becomes carbon, hydrogen or CH_x and carbon is deposited on the anode surface. Therefore, the high temperature has a great influence on the carbon deposition. Even with ABO_3 perovskite type composite material, cracking problems also exist.

It is reported that adding Cu to the Ni-based ceramic powders could improve the resistance to the carbon deposition [9-10]. Sin et al. tested long-term stability of a cell with NiCu-CGO anode working in dry methane at 1023K for 1300 h but found that the porosity declined because of the carbon deposition, resulting in the decrease of power performance [11]. The performance of Ni-Cu based anode should depend on the composition and microstructure. Conventional methods for preparing Ni-Cu based anode material include mechanical mixing method [12], sol-gel method [13] and chemical precipitation method [14]. In these methods, NiO-CuO mixture will be produced at first, followed by a reduction process in order to get NiCu alloy. Sometimes, NiCu alloy phase will not be obtained after the reduction process and the obtained powders have granular shape so that the porosity

of the anode is low.

Hard template method is an effective way to control the microstructure of the material. Using this method, it is possible to get three-dimensional microstructure with a high specific surface area in the obtained material. Dong et al. [15] prepared $Sm_{0.5}Sr_{0.5}CoO_3$ (SSC) electrolyte material with hollow fiber network structure using egg-shell-like film as the template. Comparing with the cell using the same electrolyte material prepared by sol-gel method, the maximum power density increased 44.5%. Pinedo et al. [16] prepared $Pr_{0.6}Sr_{0.4}Fe_{0.8}Co_{0.2}O_3$ cathode nanomaterial using thin polymer film as the template, and found that its specific resistance was as low as $0.12\Omega \cdot cm^2$. Activated carbon fiber (ACF) with pore diameters in the range of 10–30 μm is an excellent adsorption carbon material with high specific surface area and widely used in catalysis, medicine and other fields. It is expected to use it as template to prepare electrode material with excellent performance. Especially, ACF has reductive property like H_2; it is also expected to obtained metal alloy material directly if it is removed in an oxygen free environment. In the present study, NiCu alloy anode material with nano-porous three-dimensional microstructure was prepared using ACF as the hard template at different conditions. X-ray diffraction (XRD) and scanning electron microscope (SEM) were used to characterize the obtained material. YSZ electrolyte-supported planar single cell was fabricated using LSM as cathode and Ni_xCu_{1-x} alloy as anode and tested using methane as fuel at 1073K.

5.2 Experimental

5.2.1 Preparation of NiCu alloy powders using hard template method

NiCu alloy material was prepared using ACF (fibrous, specific surface area of 1300) as hard template. The ACF was dried at 393K for 1 h prior to use. Saturated mixture solution of $Ni(NO_3)_2 \cdot 6H_2O$ (>99.9%) and $Cu(NO_3)_2 \cdot 3H_2O$ (>99.9%) with a calculated molar ratio of Ni/Cu was prepared at first, then the dried ACF was added to the saturated solution on the basis of 0.2g ACF per milliliter solution and stirred for 30 min. The obtained slurry was dried in an oven at 373K for 5 h, and it was calcined in Ar gas flow at 1773K for 2 h. As such, NiCu/C alloy powders were obtained.

5.2.2 Fabrication of single cell and performance test

Electrolyte-supported single cell was fabricated as follows: Electrolyte plate with a thickness of 0.5 mm and a diameter of 20 mm was prepared by pressing dried YSZ powders (8mol% Y_2O_3- ZrO_2, Tosoh), followed by sintered at 1623 K in the air for 4 h. Both anode and cathode were prepared using slurry coating method. The slurry for the anode was prepared by mixing NiCu alloy powders with 50 wt% of binder, which was composed of α-pine oil and ethylcellulose with 4:1 mass ratio, and 10 wt%

of flour as pore-forming material. The slurry for the cathode was prepared using the similar method as the anode slurry by mixing LSM ($La_{0.85}Sr_{0.15}MnO_3$, Kojundo) with the 50 wt% of binder. After the slurry for the anode was coated on YSZ electrolyte, it was dried and sintered at 1373K in air. Thereafter, the cathode slurry was coated on YSZ electrolyte, and then sintered at 1173K in air. The final effective area of the anode was 0.785 cm^2 with a thickness of 0.07mm.

Before the performance test, the anode side was reduced using H_2 at first. 15 $cm^3 \cdot min^{-1}$ of CH_4 diluted by 15 $cm^3 \cdot min^{-1}$ of N_2 was used as the fuel. 30 $cm^3 \cdot min^{-1}$ of O_2 was provided in the cathode side. The performance test method is the same as our pervious study [17] and the test temperature was 1073K.

5.2.3 Physical characterizations

D/max–2400 X-ray diffractometer was employed to analyze crystal phase and composition. JSM-5600LV SEM was used to observe the morphology and microstructure of the sample before and after the test. CH604D electrochemical operating instrument was employed to measure the cell voltage, and the HV–151 potentiostat/constant current instrument was used to adjust the cell current.

5.3 Results and discussion

5.3.1 Phase analysis

Fig. 5.1 shows the XRD patterns of NiCu alloy powders with different Ni/Cu molar ratios prepared by the hard template method with a calcination temperature of 1773K.
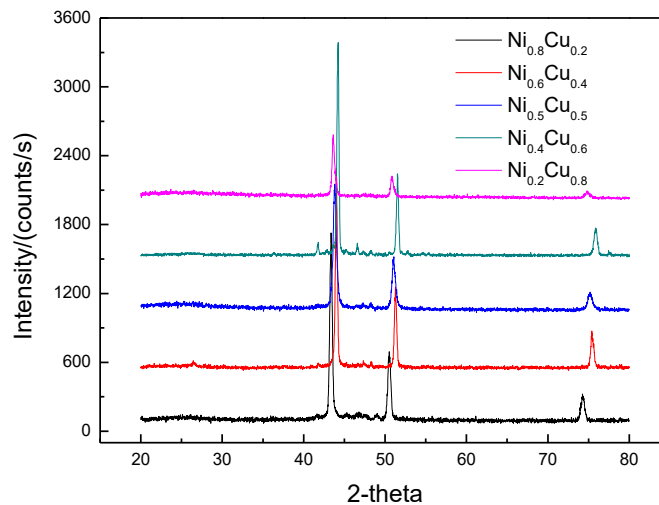
Fig.5.1 XRD patterns of NiCu alloys with different Ni/Cu molar ratios calcined at 1773K for 1h

One can see that NiCu alloys with cubic crystalline structure were well formed in all cases, indicating that ACF not only served as the template material but also as a reducing agent for the

formation of metal alloy. Herein, it should be noted that the main peaks shifted a little with the increase in Ni/Cu molar ratio, indicating minor structure change for different Ni/Cu molar ratios in the NiCu alloys. Fig. 5.2 shows the SEM image of NiCu alloy powders prepared with AFC as hard template. One can see that the prepared NiCu alloy material copied the microstructure of AFC with fiber tubular structure. In Fig. 5.2(b), cracked tubular structure and the fine particles exist, because NiCu alloy material was calcined in high temperature and the fibrofelt was cut into small pieces. It should be noted that a porous structure was also formed in the powders, which both were a supportive skeleton, and helped to enhance the electronic conductivity.
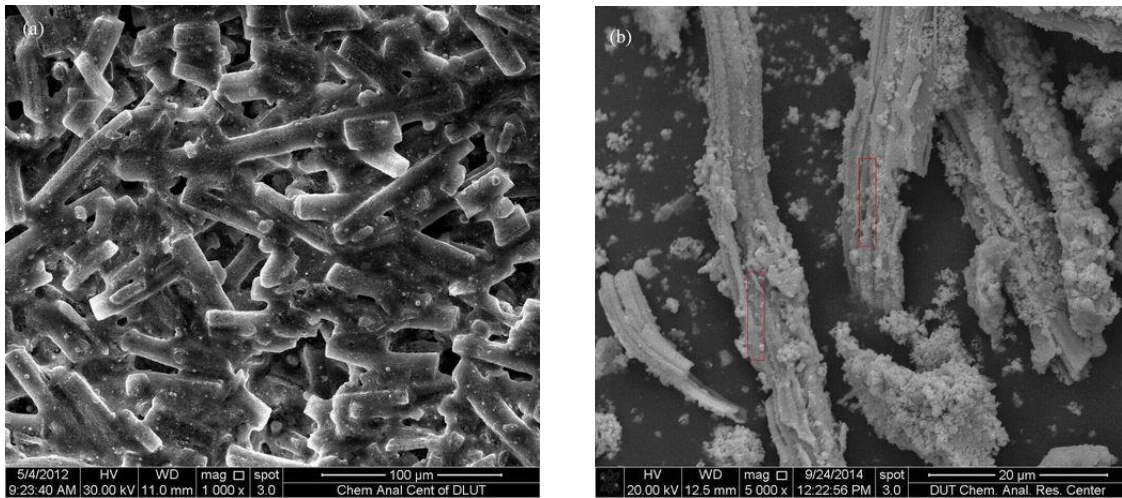
Fig.5.2 SEM images for NiCu alloy calcined at 1773K for 1h

Fig. 5.3 shows the SEM sectional image of the cell after coating anode material. One can see that the connection was close between anode and electrolyte, which explained that the oxygen ions through the electrolyte can be rapid reaction at the anode.
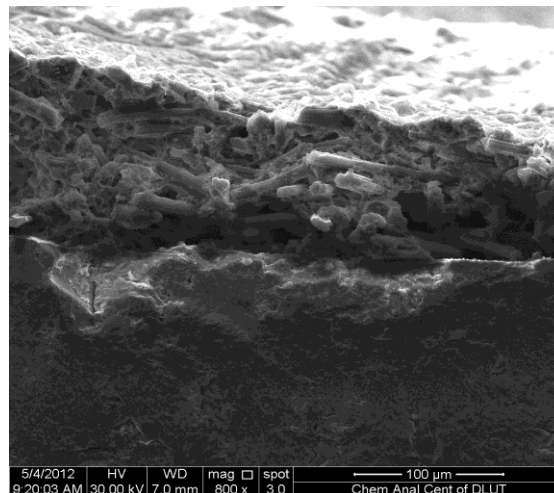
Fig. 5.3 SEM image for anode surface before reaction and used

5.3.2 Microscopic structure analysis

The anode sectional image shows NiCu alloy of fiber tubular structure was full of the entire cell anode, which improved the electron continuous conductivity. Hence, the microstructure was able to effectively increase the contact surface of catalytic metals and electrolyte, which was also conducive to forming up an independent conductive network with catalytic metals and electrolyte constituents, adding to the three phase boundary of the SOFC anode to improve the power generation performance.

The cell with Ni_xCu_{1-x}-YSZ(x=0.8, 0.5, 0.2) as anode has SEM on the anode surfaces before and after the experiment as shown in Fig.5.4. Fig. 5.4a and 5.4b are low magnification SEM images. The two figures show anode surface alloy material with different column structures have been destroyed due to long time in high temperature operation. When the anode was sintered in the air environment, NixCu1-x alloy reacted with oxygen to generate nickel oxide and copper oxide, which led to the volume of the micro tubular structure of the anode material increasing. While nickel oxide and copper oxide were reduced in the cell experiments, the volume of the tubular structure shrank and tubular structure was destroyed.
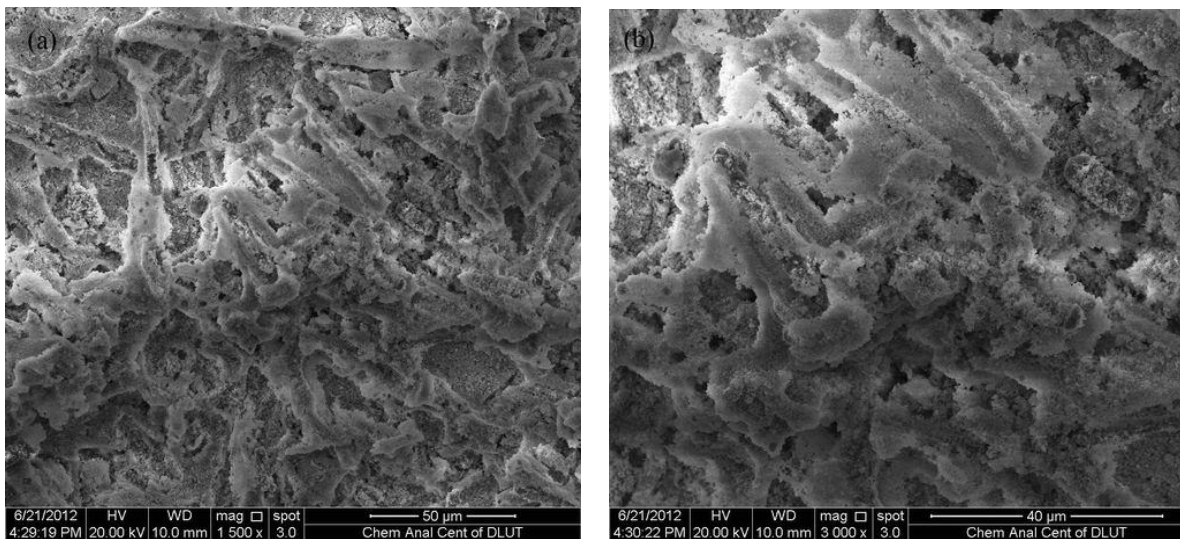
Fig.5.4 SEM for anode surface after the experiment

5.2.3 The cell performance

With YSZ as electrolyte, different proportions of NiCu alloys as anode material electrolyte supported cells were prepared. Fig. 5.5 shows the current density-voltage (J-V) curve and current density-power density (J-P) curve drawn of cells with CH_4 as fuel at 1073K.

Fig. 5.5 shows with the increase of Ni content in alloy material, power density of single cell increases. The maximum open circuit voltage and power density were 1.2005V and 315 mW·cm^{-2}

respectively. Compared with NiO as anode material, the power density of $Ni_{0.8}Cu_{0.2}$ alloy as anode material is higher. In the NiCu alloy, copper did not play a catalytic role, but the increase of Cu led to a corresponding reduction in nickel content. Compared with the pure Ni anode, NiCu alloy anode was beneficial to increase the three phase boundary and was more conducive to the reaction for the fuel gas and the anode to improve cell performance, because alloy material was fiber tubular structure. Even if the NiCu alloy anode has a certain content of Cu, the performance is still higher than that of the cell with Ni-YSZ as anode. Because the three-phase interface for reaction increases, the decrease of Ni content is offset.
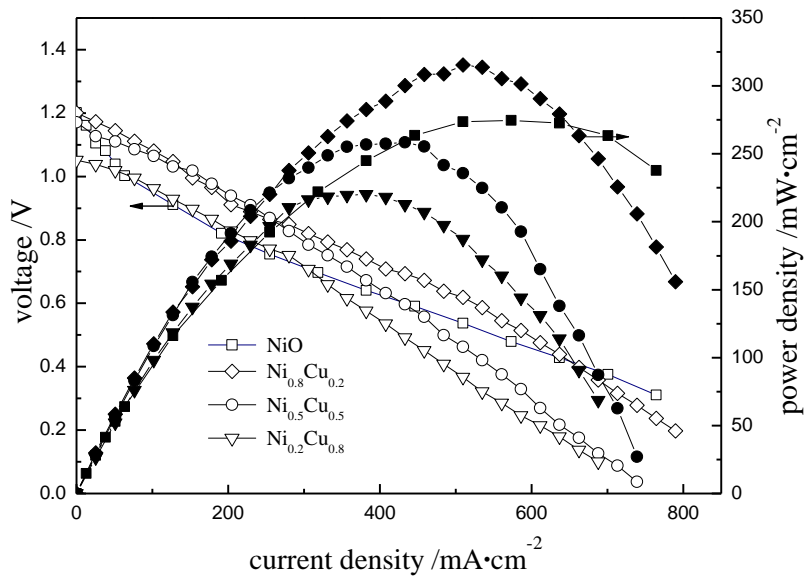
Fig.5.5 Current density and power density of the cells with different proportions of NiCu alloy at 1073K

5.3.4 Ten hous stability test

Fig. 5.6 shows, at 1073K, with CH_4 as fuel, the current density being 127.4 $mA \cdot cm^{-2}$ and Ni_xCu_{1-x}-YSZ(x=0.8, 0.5, 0.2) as anode material preparing electrolyte-supported cells, curve of voltage running 10 h.

Fig. 5.6 indicates that the single cell voltage with NiO-YSZ as anode decreases rapidly after running 100min, because the anode surface forms carbon deposition to clog anode pores. The single cell performance with Ni_xCu_{1-x}-YSZ(x=0.8, 0.5, 0.2) as anode material was stable after a long time test, which has shown strong anti-carbon deposition capacity. After adding copper, the cell anode had a good performance in anti-carbon deposition, because NiCu alloy prepared with the hard template method and anodic coating material were rich in pore so that the cell performance was improved. However, there is a voltage drop in Figure 6, because YSZ in anode material has no resistance to

carbon deposition [18]. It is noteworthy that copper content in the anode had little effect on the single cell, so the more nickel content can be selected to prepare anode material.
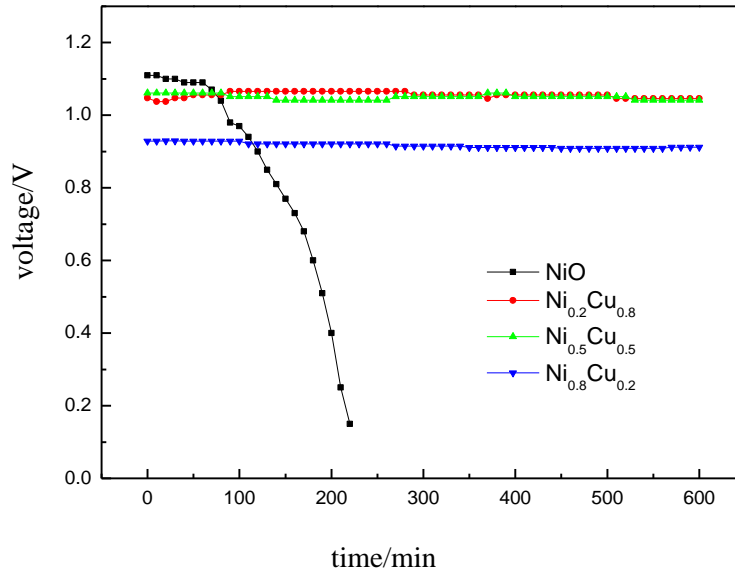
Fig. 5.6 The voltage with time for different anodes

5.4 Conclusions

With activated carbon fiber as template, Ni_xCu_{1-x} alloy anode material had been successfully prepared in the experiment with the hard template, to make up the cell anodes. The generation performance test on the cell with NiCu alloy as anode indicated that the anode alloy material forms complete cubic crystalline NiCu alloy structure and the micro structure was fiber tubular. There were abundant pore structures without agglomerations. With the increase of nickel content of Ni_xCu_{1-x} alloy material, power density of single cell also increased. The maximum power density of single cell with $Ni_{0.8}Cu_{0.2}$ alloy as anode material was 315 mW·cm^{-2}. Under the same conditions, power performance of Ni_xCu_{1-x} anode material for the single cell was better than that of NiO anode material, due to the change of the anode microstructure. Ni_xCu_{1-x} alloy can effectively improve the cell anodic anti-carbon deposition capacity. The microstructure of Ni_xCu_{1-x} alloy framework before and after the experiment has not changed whatsoever. Porous structure was remained and the appropriate channels for gas medium were formed, which helped increase the contact area between the catalytic metal and electrolyte, and has further bettered the cell performance. Therefore, the anode material prepared with the hard template method boasts of high electrical performance and stable microstructure, which is expected to be widely applied as SOFC anode material.

References

[1] S P Jiang, X J Chen, S H Chan, J. T. Kwok, GDC-Impregnated $(La_{0.75}Sr_{0.25})(Cr_{0.5}Mn_{0.5})O_3$ Anodes

for Direct Utilization of Methane in Solid Oxide Fuel Cells, *J. Electrochem Soc.* **153(5)** (2006) A850-A856.

[2] C. Jin, Z. Yang, H. Zheng, C, Yang，F. Chen, $La_{0.6}Sr_{1.4}MnO_4$ layered perovskite anode material for intermediate temperature solid oxide fuel cells, *Electrochem. Commun.* **14(1)** (2012) 75-77.

[3] X. F. Ye, S. R. Wang, Q. Hu, J. Y. Chen, T. L. Wen, Z. Y. Wen, Improvement of $Cu–CeO_2$ anodes for SOFCs running on ethanol fuels, *Solid State Ionics* **180(2-3)** (2009) 276-281.

[4] J. H. Jun, T. H. Lim, S. W. Nam, S. A. Hong, K. J. Yoon, Mechanism of partial oxidation of methane over a nickel-calcium hydroxyapatite catalyst, *Appl. Catal. A: Gen.* **312** (2006) 27-34.

[5] N. C. Triantafyllopoulos, S. G. Neophytides, The nature and binding strength of carbon adspecies formed during the equilibrium dissociative adsorption of CH_4 on Ni–YSZ cermet catalysts, *J. Catal.* **217(2)** (2003) 324-333.

[6] Y. H. Heo, J. W. Lee, S. B. Lee, T. H. Lim, S. J. Park, R. H. Song, C. O. Park, D. R. Shin, Redox-induced performance degradation of anode-supported tubular solid oxide fuel cells, *Int. J. Hydrogen Energy* **36(1)** (2011) 797-804.

[7] C. Guéret, M. Daroux, F. Billaud. Methane pyrolysis: thermodynamics, *Chem. Eng. Sci.* **52(5)** (1997) 815-827.

[8] P. Xiao, X. Ge, L. Zhang, J. M. Lee, J. Y. Wang, X. Wang, H_2 and CH_4 oxidation on $Gd_{0.2}Ce_{0.8}O_{1.9}$ infiltrated $SrMoO_3$-yttria-stabilized zirconia anode for solid oxide fuel cells, *Int. J. Hydrogen Energy* **37(23)** (2012) 18349-18356.

[9] A. Ringuedé, D. P. Fagg, J. R. Frade, Electrochemical behavior and degradation of (Ni, M)/YSZ cermet electrodes (M=Co, Cu, Fe) for high temperature applications of solid electrolytes, *J. Euro. Ceram. Soc.* **24(6)** (2004) 1355-1358.

[10] C. M. Grgicak, M. M. Pakulska, J. S. O'Brien, J. B. Giorgi, Synergistic effects of $Ni_{1−x}Co_x$-YSZ and $Ni_{1−x}Cu_x$-YSZ alloyed cermet SOFC anodes for oxidation of hydrogen and methane fuels containing H_2S, *J. Power Sources* **183(1)** (2008) 26-33.

[11] A. Sin, E. Kopnin, Y. Dubitsky, A. Zaopo, A. S. Aricò, D. L. Rosa, L. R. Gullo, V. Antonucci, Performance and life-time behaviour of NiCu-CGO anodes for the direct electro-oxidation of methane in IT-SOFCs, *J. Power Sources* **164(1)** (2007) 300-305.

[12] T. A. G. Restivo, S. R. H. de Mello-Castanho, Nickel-Zirconia cermet processing by mechanical alloying for solid oxide fuel cell anodes, *Anglais.* **185(2)** (2008) 1262-1266.

[13] J. Wang, C. Li, B. Xu, The basic principle of sol-gel method, development and application, *Chem. Ind. Eng.* **26(3)** (2009) 273-277.

[14] W. Ueda, M. Sadakane, H. Ogihara, Nano-structuring of complex metal oxides for catalytic oxidation, *Catal. Today* **132(1-4)** (2008) 2-8.

[15] D. Dong, Y. Wu, X. Zhang, J. F. Yao, Y. Huang, D. Li, C. Z. Li, H. T. Wang, Eggshell membrane-templated synthesis of highly crystalline perovskite ceramics for solid oxide fuel cells, *J. Mater. Chem.* **21(4)** (2011) 1028-1032.

[16] R. Pinedo, I. Ruiz de Larramendi, D. Jimenez de Aberasturi, I. G. D. Muro, J. I. R. D. Larramendi, M. I. Arriortua, T. Rojo, Synthesis of highly ordered three-dimensional nano structures and the influence of the temperature on their application as solid oxide fuel cel ls cathodes, *J. Power Sources*. **196(9)** (2011) 4174-4180.

[17] H. X. You, A. Abuliti, X. W. Ding, Y. H. Zhou, Reactions of Low and Middle Concentration Dry Methane over Ni/ YSZ Anode of Solid Oxide Fuel Cell, *J. Power Sources*. **165(2)** (2007) 722-727.

[18] C. W. Sun, J. Sun, W. Yang, Z. H. Ma, S. Li, C. N. Xian. S. F. Wang, R. J. Xiao, S. Q. Shi, H. Li, L. Q. Chen, Advances in carbon-based fuels SOFC anode materials, *Chin. Eng, Sci,* **15(2)** (2013) 77-87.

Chapter 6

Fabrication of $Ni_{0.5}Cu_{0.5}O_x$ coated YSZ anode by hard template method for solid oxide fuel cells

6.1 Introduction

Hydrocarbon fuels such as methane can be applied for solid oxide fuel cells (SOFCs). However, at a temperature over 800 K, methane decomposition reaction may occur which results in carbon deposition [1-2]. Therefore, coking problem should be solved when hydrocarbons are used as the fuel for SOFCs. It is reported that the preparation of anode with perovskite [3-4] and fluorite [5] structure materials or reducing the operating temperature are effective ways to avoid carbon deposition. Another good method is to change the microstructure of conventional anode to achieve a SOFC with a high performance. Rismanchian et al. [6] chemically plated Ni-based catalysts with Cu and used it as anode for SOFC and found that Cu had catalytic effect to hinder carbon deposition. Grgicak et al. [7] used Ni-Co and Ni-Cu alloy as anode materials and found that the alloy anode had great power generation ability and high sulfur resistance.

To solve the problems of carbon deposition and Ni sintering on Ni-based anode, it is necessary to optimize the microstructure of anode [8-9]. Sin et al. [10] tested long-term stability of a cell with NiCu-CGO anode working in dry methane at 1023 K for 1300 h and found that the porosity was declined due to the carbon deposition, which resulted in the decrease of power performance. Therefore, besides adding Cu at Ni-based anode for alleviating carbon deposition, it is also important to upgrade the microscopic pore structure of the anode. Zhang [11] demonstrated that the performance of the SOFC can be improved by optimizing the microstructure of anode with a higher porosity. An et al. [12] used YSZ nanoparticles coated spherical Ni as anode, which improved the properties of the fuel cell with good electrical conductivity and reduced polarization resistance. Li et al. [13] fabricated YSZ nano-fiber tubes by electrospinning and plated Ni layer on the fiber tube and used as anode material, and found that the performance of anode was improved to a great extent when comparing with the traditional Ni-YSZ milling anode. Low et al. [14] used Cu-coated Ni particles as anode material and found that the electronic conductivity and mechanical properties was promoted.

Anode porosity not only affects the power generation performance of fuel cell, but also has great effect on the anti-carbon deposition in the SOFCs [15]. Recently, the increase of the porosity in SOFC anode material has been pursued by many researchers [16-17]. It is well known that the porosity of anode can be improved by adding template materials such as polymers [18], graphite [19], or carbon dust [20] in the fabrication process. Srivastava et al. [21] added 15 wt.% graphite powder into NiO/YSZ to fabricate an anode with 32% porosity, which showed a high cell performance. An et al [22] prepared an anode-supported cell by adding different content of carbon powder as pore former, which also exhibited excellent performance.

Hard template method is an effective way to prepare porous microstructure material with high specific surface area. [23]   In this study, activated carbon fiber (ACF) was used as hard template, tubular YSZ powders were prepared at first, and then dipped in salt solutions containing various concentrations of Ni and Cu species by wet impregnation method to fabricate $Ni_{0.5}Cu_{0.5}O_x$ coated tubular YSZ powders, which were used as anode materials. The performance of obtained SOFCs based on the obtained anode materials was tested under dry methane and wet methane (3% H_2O). It is expected to create a novel porous structure for general anode and obtain excellent cell performance with high anti-coking property.

6.2 Experimental

6.2.1 Preparation of anode materials

ACF (specific surface area of 1700m$^2 \cdot$g^{-1}) was employed as hard template to prepare tubular YSZ material. The process of fabrication was as follows. Y_2O_3 and $Zr(NO_3)_4 \cdot 5H_2O$ in a molar ratio of 23:2 were weighed and introduced separately into two beakers, A and B. The excessive concentrated nitric acid (HNO_3) was added into the beaker A to prepare a solution of $Y(NO_3)_3$, which was then poured into the beaker B. Afterwards, appropriate amount of deionized water was added into the beaker B for preparation of the saturated solution which use $Y(NO_3)_3$ as a reference. The calculated amount of ACF dried in an oven for 1 h at 393 K, and added into the as-prepared saturated solution and stirred for 30 min. Then, the solution was evaporated at 373 K for 4-5 h. Finally, the dried ACF was calcined at 1673 K for 2 h, and the tubular YSZ powder was obtained.

The preparation process of the composite anode material of $Ni_{0.5}Cu_{0.5}O_x$ coated tubular YSZ was as follows. $Ni(NO_3)_2 \cdot 6H_2O$ and $Cu(NO_3)_2 \cdot 5H_2O$ in a molar ratio of 1:1 was dissolved in proper amount of deionized water and ethanol and an emerald green solution was obtained. The relevant amount of tubular YSZ power with a mass ratio of the calcined metal oxide to YSZ of 3:2 was introduced into the aforementioned solution, and heated at 323 K for 6 h with stirring. Finally, the green and loose

solid mixture was calcined in air at 1073 K for 2 h. As such, the composite anode material of $Ni_{0.5}Cu_{0.5}O_x$ coated tubular YSZ powder was obtained.

6.2.2 Fabrication and measurement of single cell

YSZ electrolyte-supported single cell was prepared as follows. Electrolyte substrate with a thickness of 0.5 mm and a diameter of 20 mm was prepared by pressing YSZ powders (8 mol% Y_2O_3-ZrO_2, Tosoh) with 3 wt% polyvinyl butyral (PVB, relative to YSZ), followed by sintered at 1673 K for 4 h in air. Both anode and cathode were prepared by slurry coating method [24]. The mixture of α-terpineol and ethyl cellulose with a mass ratio of 4:1 was used as binders. LSM (CAS, China) and YSZ powders in a weighted ratio of 3:2 were mixed with 40 wt% binder (relative to LSM and YSZ) as cathode slurry, which was coated on the as-prepared electrolyte substrate and sintered at 1373 K for 2 h in air. As-prepared composite anode material with 40 wt% binder (relative to anode material) was coated on the other side of the electrolyte substrate and sintered at 1273 K for 2 h in air.

As-prepared single cells were mounted in a test rig as reported previously in Chapter 2. Electrochemical performance test was performed at 923, 973, 1023, and 1073 K, respectively using a CHI660C electrochemical workstation system (CHI604D, Shanghai Chen Hua Instrument Co., Ltd.) with HV–151 potentiostat constant current instrument. In the power generation performance tests with hydrogen, the flow rates of dry H_2 and O_2 were 80 $cm^3 \cdot min^{-1}$ and 30 $cm^3 \cdot min^{-1}$, respectively. Similarly, in the tests of power generation performance in methane, the flow rates of N_2, O_2 and CH_4 were 30 $cm^3 \cdot min^{-1}$, 30 $cm^3 \cdot min^{-1}$ and 20 $cm^3 \cdot min^{-1}$, respectively.

X-ray diffractometer (SHIMADZU, XD-3A, Japan) was employed to analyze crystal structure. Measurement condition was under 12 kV voltage, 100 mA current with a copper target, Ni filter, λa1 at 0.1541 nm ray wavelength, angle 2θ in the measurement range from 20° to 80° by steps of 0.06°. The morphology and microstructure of the prepared material sample was examined by scanning electron microscopy SEM (JEOL, JSM-5600LV, Japan) before and after the test. Automatic gas adsorption instrument (Quantachrome, Autosorb, USA) with nitrogen as adsorption medium was used to examined pore volume, pore distribution and specific surface area. The porosity is equaled to the ratio of the pore volume and the total volume of the material.

6.3 Results and discussion

6.3.1 Phase analysis

Fig. 6.1a shows XRD patterns of the composite anode material of $Ni_{0.5}Cu_{0.5}O_x$ coated tubular YSZ. It can be seen that the diffraction peak of composite material is sharp with high intensity, which

illustrates that the degree of crystallinity of the prepared material is relatively high. Compared with the standard spectrum of $Zr_{0.92}Y_{0.08}O_{1.96}$ (YSZ, PDF#48-0224), all the corresponding characteristic peaks prove that tubular YSZ materials with high purity have been produced by hard template method. Also, diffraction peaks corresponding to NiO (PDF#65-2901) and CuO (PDF#48-1548) were also found. Fig 6.1b shows the XRD patterns of the prepared anode material after reduction in hydrogen. Characteristic peaks of $Ni_{0.5}Cu_{0.5}$-YSZ are identical to Cu pattern (PDF#04-0836), Ni pattern (PDF#87-0712) and YSZ pattern (PDF#48-0224), indicating that Ni-Cu metallic oxide particles in $Ni_{0.5}Cu_{0.5}O_x$-YSZ can be reduced to Ni-Cu alloy particles.
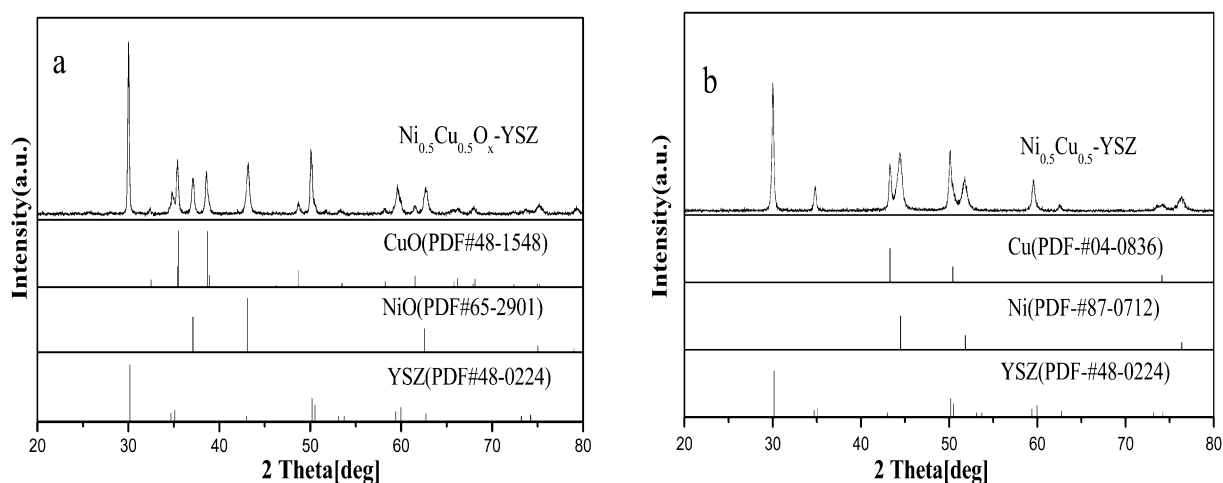
Fig. 6.1 XRD patterns of the composite anode materials before and after reduced by H_2:
(a) $Ni_{0.5}Cu_{0.5}O_x$-YSZ; (b) $Ni_{0.5}Cu_{0.5}$-YSZ

6.3.2 Microscopic structure analysis

Fig. 6.2 shows the SEM images of composite anode material with $Ni_{0.5}Cu_{0.5}O_x$ coated tubular YSZ utilizing ACF as hard template. One can see that the as-prepared YSZ has successfully copied the microstructure of ACF to form a tubular form with a diameter of 4μm as shown in Fig. 6.2(a). As a template material, ACF can be burned out completely in air atmosphere so that the tubular YSZ was successfully formed. Fig. 6.2 also demonstrates that there were many tiny particles attached on tubular YSZ scaffolds owing to the calcining of tubular YSZ impregnated with $Ni(NO_3)_2$ and $Cu(NO_3)_2$ saturated solution in air atmosphere, which caused the formations of NiO and CuO particles on the tubular YSZ. One can see that the metallic oxide particles with a uniform size of about 90 nm were distributed on the tubular YSZ surface randomly. On the other hand, it should be noted that some tubular YSZ particles are broken due to the vigorous stirring during the preparation process.
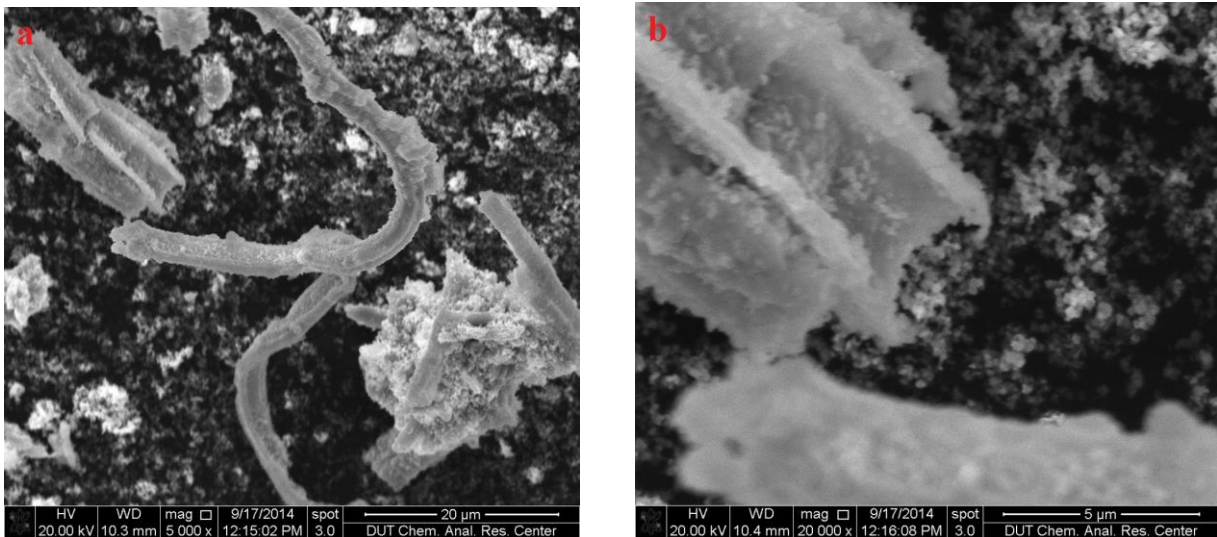
Fig. 6.2 SEM images of $Ni_{0.5}Cu_{0.5}O_x$ coated tubular YSZ material

As shown in the enlarged image (Fig. 6.2(b)), Ni-Cu metallic oxide granules also existed inside the tubular YSZ, which proves the hollow structure of the tubular YSZ, which could increase the specific surface area. On the other hand, the contact of Ni-Cu metallic oxide particles with YSZ could improve the power generation performance by raising TPB in the SOFC anode. These results indicate that the composite anode material with Ni-Cu metallic oxide coated tubular YSZ has been successfully prepared by hard template method followed by wet impregnation process.

6.3.3 Performance test of power generation by single cell

Fig. 6.3 describes the power generating performances of the prepared single cell worked with hydrogen fuel.
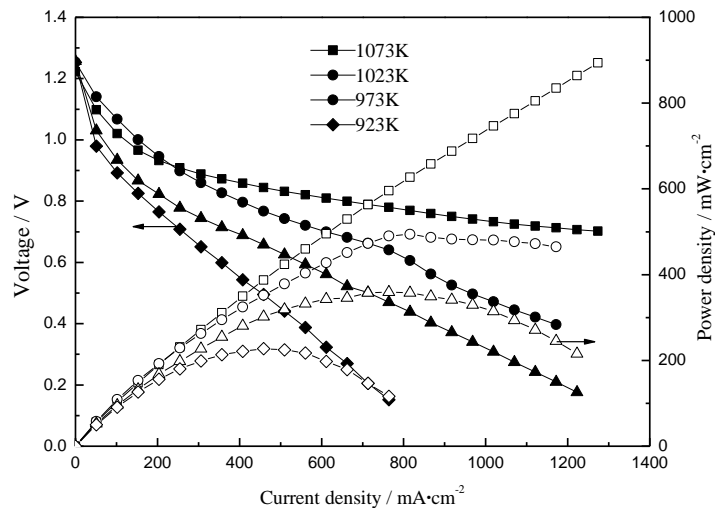
Fig. 6.3 The power generating performances of the prepared single cell with H_2 fuel

The open circuit voltages were 1.222, 1.254, 1.257 and 1.253 V at temperatures of 1073, 1023, 973 and 923 K, respectively. All the open circuit voltages were higher than 1.2 V, which indicates that the single cell was well fabricated. Meanwhile, its maximum power densities were 900, 493.90, 359.16 and 227.19 mW·cm^{-2} at 1073, 1023, 973 and 923 K, respectively.

Furthermore, the porosity of the half single cell with $Ni_{0.5}Cu_{0.5}O_x$ coated tubular YSZ as anode before test was 34.72%. It indicates that due to the improvement on anode microstructure by the pore-creating method, the power generation performance of single cell was improved to a great extent when comparing with the conventional method.

Fig. 6.4 shows the power generation performances of the fabricated single cells in dry methane. Similarly, the open circuit voltages were 1.18, 1.13, 1.02 and 0.91 V at the temperatures of 1073, 1023, 973 and 923 K, respectively. Accordingly, the maximum power densities were 315.52, 213.81, 144.83 and 101.14 mW·cm^{-2}, respectively. Previous theoretical researches indicated that adding Cu into the Ni-based ceramic powders would decrease the power density [25-27]. However, in this study, it is found that the cell remained its good performance thanks to the multi gas passages in the porous anode of the single cell.
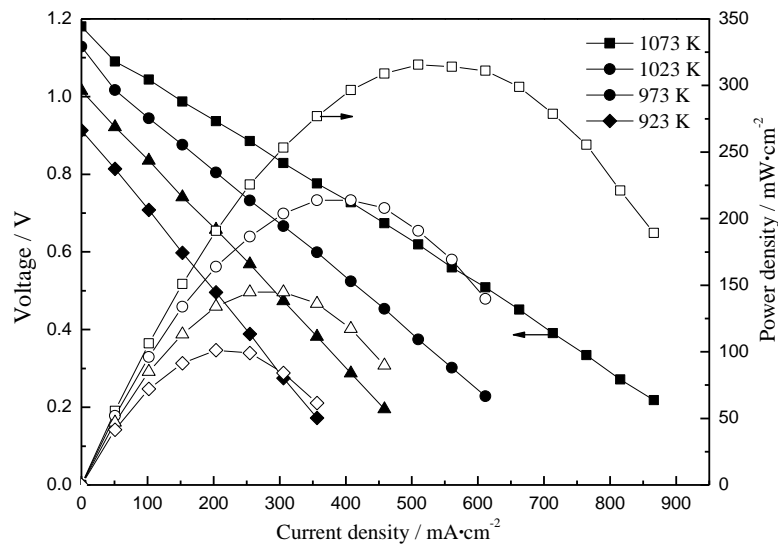
Fig.6.4 The power generating performances of the prepared single cell with the fuel of dry methane

6.3.4 The influence of moisture on single cell performance

With wet methane (3% H_2O) as fuel, the power generation performance of single cell prepared with $Ni_{0.5}Cu_{0.5}O_x$ coated tubular YSZ as anode under temperature ranging from 923 K to 1073 K is shown in Fig. 6.5. Compared to the previous experiment using dry methane as fuel, the open circuit voltages of single cell with wet methane decreased a little to 1.04, 1.01, 0.97 and 0.96 V, respectively. The

decrease should be caused by the methane reforming reaction in the anode due to the addition of water vapor into dry methane [28]. Accordingly, the maximum power densities were decreased to 241.77, 195.18, 116.76 and 59.07 $mW \cdot cm^{-2}$ from 1073 K to 923 K respectively. Although the reaction between methane and steam produced H_2 and CO, the existing of CH_4, H_2O and CO_2 diluted the concentration of H_2 for participating in the power generation. Besides, both reforming reaction and electrochemical oxidation occurred on the catalyst, which reduced the efficiency of H_2 electrochemical reaction on the catalyst. Therefore, it is difficult to achieve the performance as high as using pure H_2 as fuel. However, the addition of steam should be essential in inhibiting carbon deposition. Also, it could result in higher power density [29].
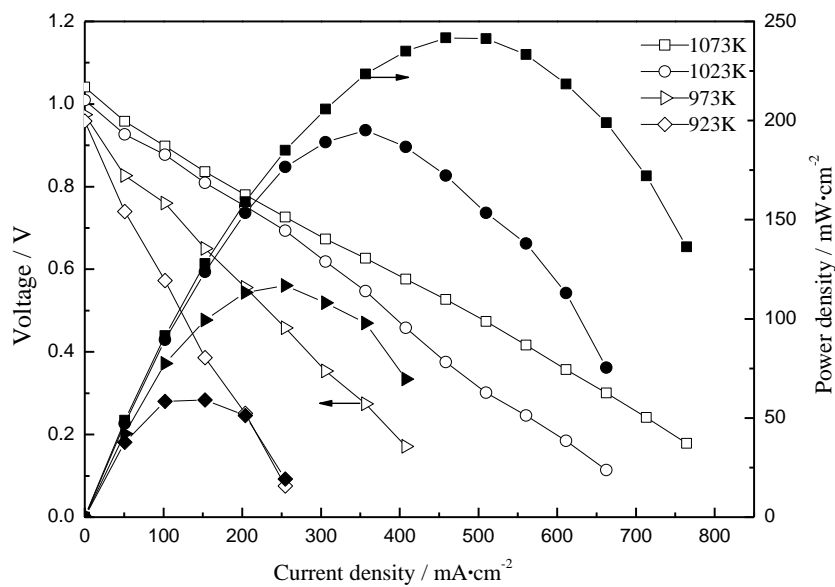
Fig.6.5 The power generation performances of the prepared single cell
under wet methane (3% H_2O)

6.3.5 Long-term stability test

The long-term stability of the electrolyte-supported cells with the as-prepared $Ni_{0.5}Cu_{0.5}O_x$/tubular YSZ as anode material was tested. Fig. 6.6 displays its voltage variation curve measured under the condition of 1073 K with a current density 127.4 $mA \cdot cm^{-2}$ for 100 h by using dry methane and wet methane (3% H_2O) as fuels respectively. The initial voltages of the single cells in dry and wet methane were 0.8697 and 1.005V, respectively, which maintained within the voltage value of power generation performance test. It indicates that the long-term performance test caused no damage to the cells. After running for 100 h, it is obvious that the voltage of single cell with wet methane remained approximately the same due to the steam reforming reaction caused by the addition of water vapor.

85

However, with dry methane as fuel, the voltage of single cell dropped to 0.952 V, which is about 5.27% voltage drop.

Herein, for single cell with wet methane, its voltage was lower than the one with dry methane at the beginning of the long-term stability test due to the addition of water vapor. Its voltage stayed relatively stable at the first 30 h. However, the voltage dropped a little between 25 and 31 h, which was resulted from the decrease of methane pressure during the test. After the pressure was recovered, from 31 to 64 h, the performance was improved smoothly. Constantly, after running for 70 h, the variation curve of voltage maintained smoothly and steady. This result indicates that the presence of 3% H_2O could alleviate carbon deposition and improve the anti-carbon deposition capacity of Ni based composite anode.
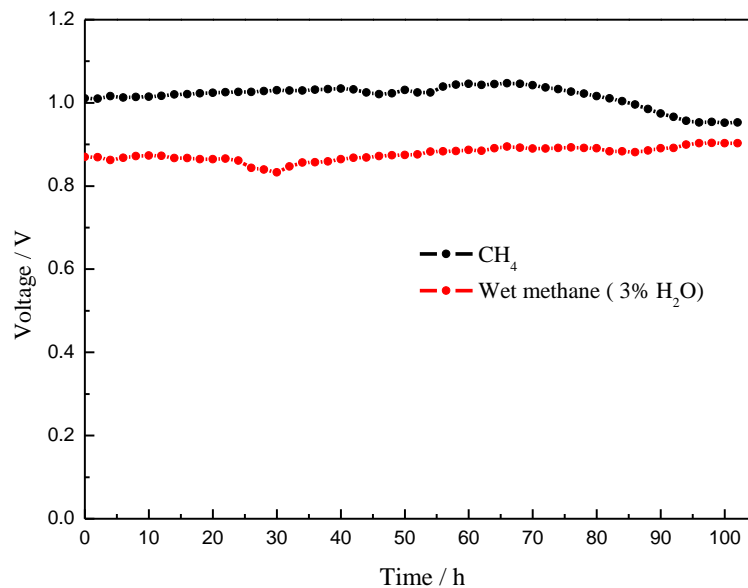
Fig. 6.6 The voltage change with time for the single cell worked in different fuels

In contrast, for the single cell with dry methane, its voltage remained relatively stable until 70 h. It indicates that the carbon deposition caused by dry methane cracking was not obvious. However, after the 70 h test, the voltage began to decrease obviously. This should be due to the carbon deposition on TPB, which could result in the blockage of gas passage that weaken the electrochemical performance.

6.3.6 Analysis of carbon deposition phenomenon for single cell

Fig. 6.7 displays the photos of carbon deposition under the two conditions. For dry methane, as shown in Fig.6.7 (a) and (b), the carbon deposition was quite serious. It can be clearly seen from Fig.6.7 (a), in which a large amount of coke was found to be deposited on the anode surface. Fig.6.7 (b) shows that the inner wall of the tubular particles was also covered by coke.

It indicates that the carbon deposition would occur on the whole anode under high temperatures so that the pores in the anode would prone to be blocked. Herein, although the addition of Cu into Ni based ceramic powders was reported to be able to avoid the carbon deposition, considerable amounts of coke would still deposit after testing the single cell for a relatively long period, which might block the pore channels and lower the porosity of the anode.
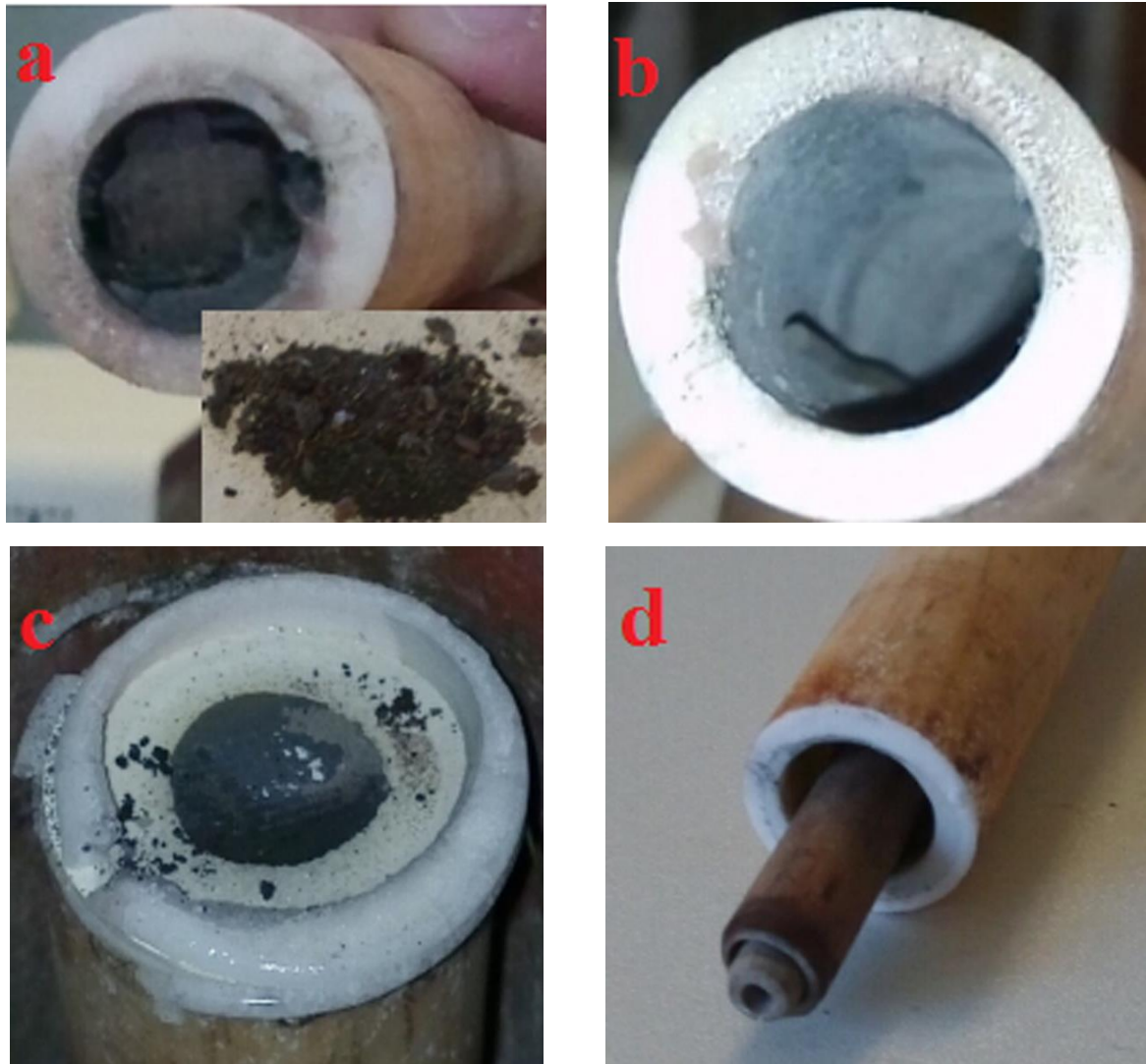
Fig.6.7 Photos of carbon deposition phenomenon on the prepared single cell under different fuels after running for 100 h: (a), (b) dry methane; (c), (d) wet methane ($3\%H_2O$)

Fig.6.7 (c) and (d) show the carbon deposition for wet methane after the cell has been run for 100 h. Compared with the one under dry methane, the amount of carbon deposition clearly decreased since the addition of water vapor can alleviate the production of coke and thereafter speed up the reaction rate. It is proved that the presence of 3% H_2O is an efficient way to inhibit carbon deposition.

6.3.7 SEM and EDS analysis for single cells after experiment

Fig.6.8 shows the SEM images of the surface and cross section of single cell using $Ni_{0.5}Cu_{0.5}O_x$ coated tubular YSZ as anode and fueled by dry methane for 100 h. Fig.6.8 (a) of the anode surface presents reduced metal particles of $Ni_{0.5}Cu_{0.5}$, which could enlarge the specific surface area of anode. On the other hand, the tubular YSZ remained a stable microstructure after the long-term test.

Fig.6.8 Morphologies of surface and cross section of cell with $Ni_{0.5}Cu_{0.5}O_x$ coated tubular YSZ anode after long-term test in dry methane: (a) anode surface; (b) cross section; (c) enlarged view of cross section

Fig.6.8 (b) is a cross-sectional SEM image of the single cell after the long-term test. One can see that the anode layer connected densely with the YSZ electrolyte supporter. Especially, the tubular YSZ also existed on the interface of the anode and the electrolyte, and attached with each other tightly. The tubular YSZ spread uniformly in the anode to form a three-dimensional electrode, which provided continuous and connected transport pathways for fuel gas fluently diffusing to the anode reaction zone. Meanwhile, the tubular YSZ coated by $Ni_{0.5}Cu_{0.5}$ alloy particles increased the contact area with electrolyte and fuel gas. As a result, more TPB sites were generated for improving the power generation performance.

Fig.6.8(c) presents one end of the tubular YSZ in the anode. The inside of tubular YSZ was filled with abundant $Ni_{0.5}Cu_{0.5}$ metal particles. The metal particles not only coated on the external surface, but also spread all over their inner surface. It indicates that the anode with such a three-dimensional microstructure could provide high specific surface and be benefit for electrochemical reaction.

The SEM images of surface and cross section of the single cell worked in wet methane (3% H_2O) for 100 h are presented in Fig.6.9. By comparing with the results in Fig.6.8, the difference of the microstructure was no obvious. Similar to the anode microstructure after worked in dry methane for 100 h, the anode still maintained its original structure. It proves that the addition of steam in the fuel can inhibit the carbon deposition.
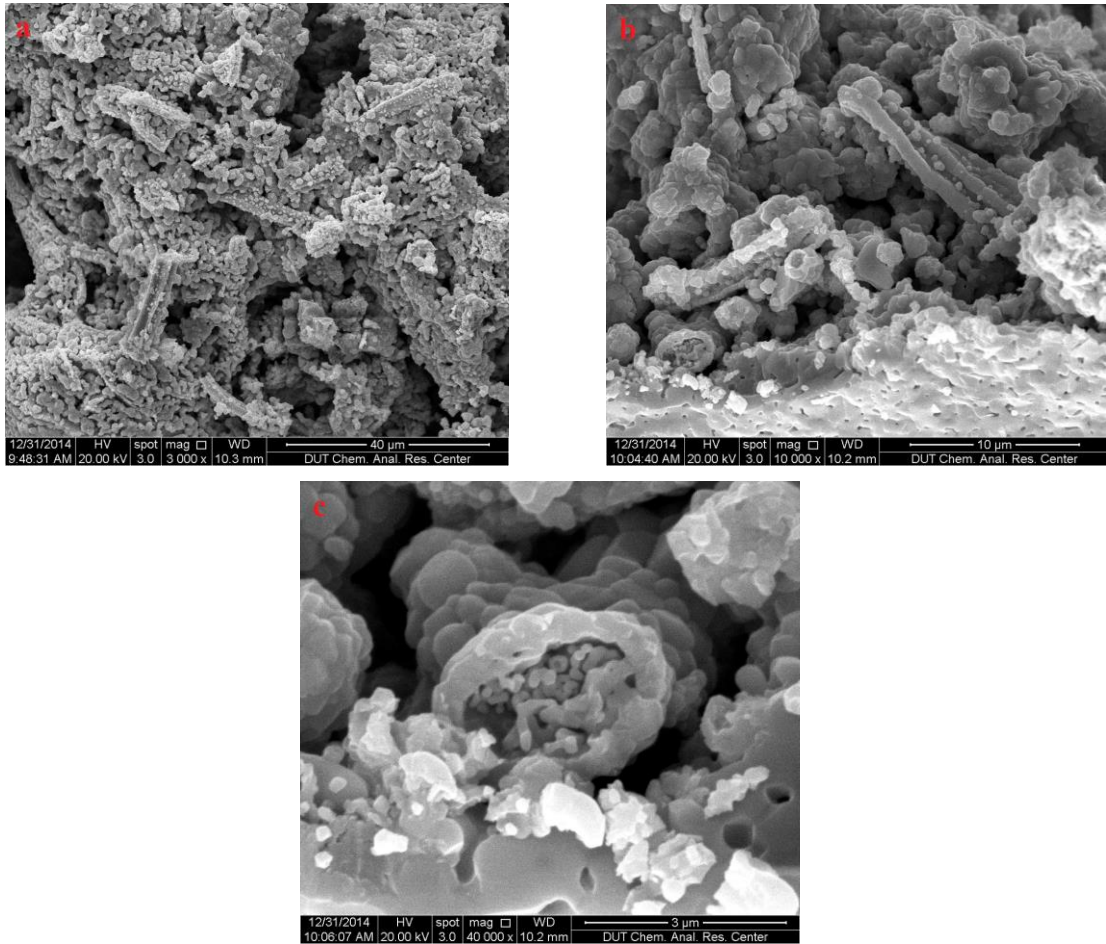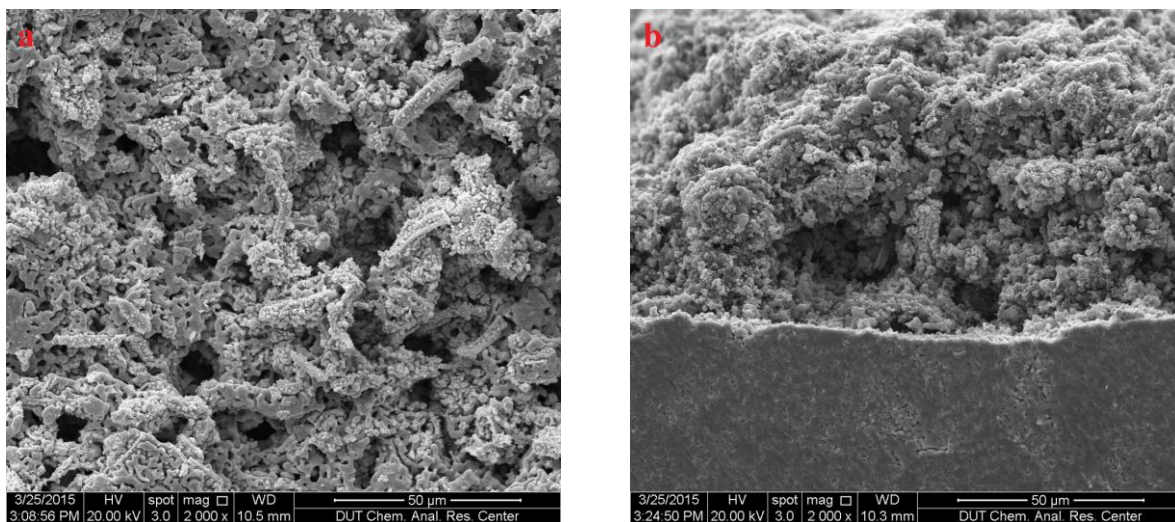

Fig.6.9　Morphologies of surface and cross section of cell with $Ni_{0.5}Cu_{0.5}O_x$ coated tubular YSZ anode after long-term test in wet methane for 100 h:(a) anode surface; (b) cross section

Fig. 6.10 shows the contrastive EDS images of single cells with $Ni_{0.5}Cu_{0.5}O_x$ coated tubular YSZ as anode worked in dry methane and wet methane for 100 h. In the case of dry methane, as shown in Fig.6.10 (a), the anode material layer fell off from the single sell after disassembly due to the severe carbon deposition. In addition, its surface should be covered by carbon since no Ni and Cu elements were detected. The relative amount of carbon deposition reached 37.98% in 100 h. It is believed that the real relative amount of deposited carbon should be higher than this value because EDS can only detect the elements on the surface. In contrast, in the case of wet methane, as shown in Fig.6.10 (b), the amount of carbon deposition was 33.46%, which proved that the presence of 3% H_2O can decrease carbon deposition and enable long-term stability. Meanwhile, a high content of Ni, Cu, Zr, O and other elements were detected as from the red box area in top right corner of Fig.6.10 (b), which indicated

that the prepared single cell with $Ni_{0.5}Cu_{0.5}O_x$ coated tubular stable YSZ as anode had a steady structure for power generation.

Spectrum a

Element	Wt %	At %
C K	16.92	37.98
O K	26.97	45.44
Zr L	56.11	16.58
Total	100.00	

30μm

Full Scale 2732 cts   Cursor 17.746 (1 cts)   keV

Spectrum b

Element	Wt %	At %
C K	10.71	33.46
O K	10.35	24.27
Ni K	31.65	20.23
Cu K	25.10	14.83
Zr L	13.51	5.56
Au M	8.68	1.65
Total	100.00	

60μm

Full Scale 5705 cts   Cursor 16.647 (13 cts)   keV
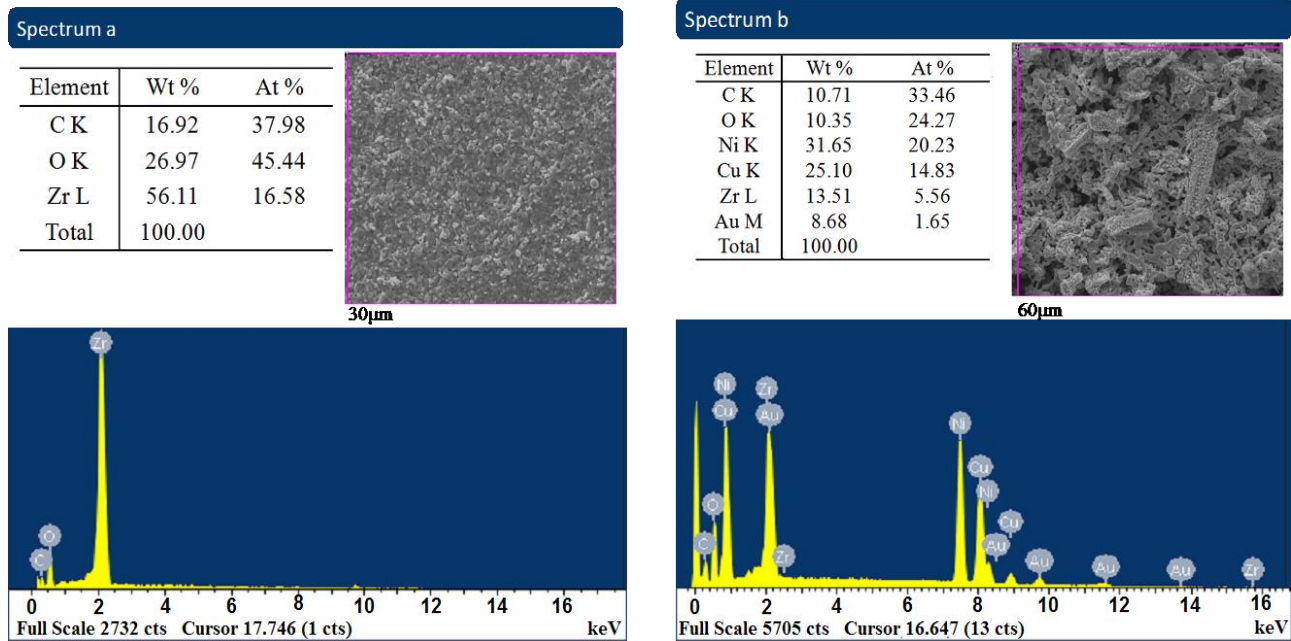
Fig.6.10 Energy spectrums of single cell worked in different fuels for 100 h:(a) dry methane; (b) wet methane (3%H_2O)

6.4 Conclusions

In this study, the hard template method combining with wet impregnation method was adopted to prepare anode material of $Ni_{0.5}Cu_{0.5}O_x$ coated tubular YSZ. The single cell with this kind of material as anode was tested by its power generation performance and a 100 h long-term stability. After the long-term test, the microstructure and components in the anode were analyzed by SEM and EDS. The following results were obtained:

(1) Fueled by H_2, the single cell showed excellent power generation performance and the maximum power density was higher than 900 mW•cm^{-2} at 1073 k, which indicated that $Ni_{0.5}Cu_{0.5}O_x$ coated tubular YSZ can improve the anode microstructure and electrical performance. For the same single cells fueled by dry and wet methane (3% H_2O) respectively, at 800℃, the maximum power densities were 315.52 mW·cm^{-2} and 241.77 mW·cm^{-2}, respectively.

(2) By comparing the results of the 100 h long-term stability tests under dry methane and wet methane (3% H_2O) respectively, the single cell with dry methane showed an obvious voltage drop of 5.27% but the one with wet methane showed the more stable property. It illustrated that wet methane had an obvious impact on inhibiting carbon deposition on the anode.

(3) From the SEM images of internal and external surfaces of $Ni_{0.5}Cu_{0.5}$ metal particles coated

tubular YSZ, it was found that the porous structure was quite steady. Such a three-dimensional microstructure with high specific surface and long channel for fuel transport in the anode was expected to increase TPB and to improve its electric properties and carbon deposition resistance.

(4) The analysis of carbon deposition phenomenon and energy spectrum (EDS) indicated that compared with the one under dry methane, the amount of carbon deposition decreased obviously under wet methane (3% H_2O), which proved that the presence of 3% H_2O had an effective impact on limiting carbon deposition and enabling long-term work.

Reference

[1] C. Gueret, M. Daroux, F. Billaud, Methane pyrolysis: thermodynamics, *Chem. Eng. Sci*. **52(5)** (1997) 815-827.

[2] P. Xiao, X. M. Ge, L. Zhang, J. M. Lee, J. Y. Wang, X. Wang, H_2 and CH_4 oxidation on $Gd_{0.2}Ce_{0.8}O_{1.9}$ infiltrated $SrMoO_3$-yttria-stabilized zirconia anode for solid oxide fuel cells, *Int. J. Hydrogen Energy* **37(23)** (2012) 18349-18356.

[3] D. Dong, Y. Z. Wu, X. Y. Zhang, J. F. Yao, Y. Huang, D. Li, C. Z. Li, H. T. Wang, Eggshell membrane-templated synthesis of highly crystalline perovskite ceramics for solid oxide fuel cells, *J. Mater. Chem*. **21(4)** (2011) 1028-1032.

[4] K. B. Yoo, B. H. Park, G. M. Choi, Stability and performance of SOFC with $SrTiO_3$-based anode in CH_4 fuel, *Solid State Ionics* **225(14)** (2012) 104-107.

[5] S. P. Jiang, X. J. Chen, S. H. Chan, J. T. Kwok, GDC-impregnated $(La_{0.75}Sr_{0.25})(Cr_{0.5}Mn_{0.5})O_3$ anodes for direct utilization of methane in solid oxide fuel cells, *J. Electrochem. Soc*. **153(5)** (2006) A850-A856.

[6] A. Rismanchian, J. Mirzababaei, S. S. Chuang, Electroless plated Cu–Ni anode catalyst for natural gas solid oxide fuel cells, *Catal. Today* **245** (2015) 79-85.

[7] C. M. Grgicak, M. M. Pakulska, J. S. O'Brien, J. B. Giorgi, Synergistic effects of $Ni_{1-x}Co_x$-YSZ and $Ni_{1-x}Cu_x$-YSZ alloyed cermet SOFC anodes for oxidation of hydrogen and methane fuels containing H_2S, *J. Power Sources*, **183(1)** (2008) 26-33.

[8] Q. A. Huang, R. Hui, B. Wang, A review of AC impedance modeling and validation in SOFC diagnosis, *Electrochim. Acta*. **52(28)** (2007) 8144-8164.

[9] L. Liu, G. Y. Kim, A. C. Hillier, Microstructural and electrochemical impedance study of nickel–$Ce_{0.9}Gd_{0.1}O_{1.95}$ anodes for solid oxide fuel cells fabricated by ultrasonic spray pyrolysis, *J. Power Sources* **196(6)** (2011) 3026-3032..

[10] A. Sin, E. Kopnin, Y. Dubitsky, A. Zaopoa, A. S. Aricòb, D. L Rosab, L. R. Gullob, V. Antonucci, Performance and life-time behaviour of NiCu–CGO anodes for the direct electro-oxidation of methane in IT-SOFCs, *J. Power Sources* **164(1)** (2007) 300-305.

[11] L. Zhang, F. Chen, C. Xia, Spin-coating derived solid oxide fuel cells operated at temperatures of 500℃ and below, *Int. J. Hydrogen Energy* **35(24)** (2011) 13262-13270.

[12] Y. T. An, B. H. Choi, M. J. Ji, H. J. Hwang, New fabrication technique for a Ni–YSZ composite anode from a core–shell structured particle, *Solid State Ionics.* **207(207)** (2012) 64-68.

[13] L. Li, P. Zhang, R. Liu, S. M. Guo, Preparation of fibrous Ni-coated-YSZ anodes for solid oxide fuel cells, *J. Power Sources* **196(3)** (2011) 1242-1247.

[14] Q. X. Low, W. S. Huang, X. Z. Fu, J. Melnik, K. T. Chuang, A. R. Sanger, Copper coated nickel foam as current collector for H_2S-containing syngas solid oxide fuel cells, *Appl. Surf. Sci.* **258(3)** (2011) 1014-1020.

[15] N. Ai, Z. Lü, J. Tang, K. Chen, X Huang, W Su, Improvement of output performance of solid oxide fuel cell by optimizing Ni/samaria-doped ceria anode functional layer, *J. Power Sources* **185(1)** (2008) 153-158.

[16] H. Taira, M. Iha, H. Takagi, Solid oxide fuel cell and manufacturing method thereof: *U.S. Patent* 5,531,019. 1996-7-2.

[17] L. K. Chiang, H. C. Liu, Y. H. Shiu, C. H. Lee, R. Y. Lee. Thermal stress and thermo-electrochemical analysis of a planar anode-supported solid oxide fuel cell: Effects of anode porosity, *J. Power Sources* **195(7)** (2010) 1895-1904.

[18] J. C. Ruiz-Morales, J. Canales-Vázquez, J. Peña-Martínez, D. Marrero-López, J. T. S. Irvine, P. Núñez, Microstructural optimisation of materials for SOFC applications using PMMA microspheres, *J. Mater. Chem.* **16** (2006) 540-542.

[19] M. Prestat, A. Morandi, A. Heel, L. Holzera, P. Holtappelsa, T. J. Graulea, Effect of graphite pore former on oxygen electrodes prepared with $La_{0.6}Sr_{0.4}CoO_{3-\delta}$ nanoparticles, *Electrochem. Commun.* **12(2)** (2010) 292-295.

[20] F. Zhao, A. V. Virkar, Dependence of polarization in anode-supported solid oxide fuel cells on various cell parameters, *J. Power Sources* **141(1)** (2005) 79-95.

[21] P. K. Srivastava, T. Quach, Y. Y. Duan, R. Donelson, S. P. Jiang, F. T. Ciacchi, S. P. S. Badwal, Electrode supported solid oxide fuel cells: Electrolyte films prepared by DC magnetron sputtering, *Solid State Ionics* **99(3)** (1997).311-319.

[22] C. M. An, J. H. Song, I. Kang, N. Sammes, The effect of porosity gradient in a Nickel/Yttria Stabilized Zirconia anode for an anode-supported planar solid oxide fuel cell, *J. Power Sources* **195(3)** (2010) 821-824.

[23] H. Y. Chen, B. Shen, Z. Z. Zhang, Progress in studying the resistance to carbon deposition of methane reforming with carbon dioxide, *Shanghai Chem. Ind.* **30(8)** (2005) 25.

[24] H. X. You, A. Abuliti, X. W. Ding, Y. H. Zhou, Reactions of low and middle concentration dry methane over Ni/YSZ anode of solid oxide fuel cell, *J. Power Sources* 1**65**(2) (2007) 722-727.

[25] K. Cheng, H. Chen, W. J. Weng, C. L. Song, P. Y. Du, G. Shen, G. R. Han, Effects of dual Cu incorporation on carbon deposition in SDC anode, *J. Alloys Compd.* **541** (2012) 65-69.

[26] H. S. Hong, S. Lee. Fabrication and characterization of 900℃-sintered Ni/Cu/YSZ cermet high temperature electrolysis cathode material prepared by high-energy ball-milling method . *J. Alloys Compd.* **538** (2012) 201-204.

[27] E.W. Park, H. Moon, M. Park, S.H. Hyun. Fabrication and characterization of Cu–Ni–YSZ SOFC anodes for direct use of methane via Cu-electroplating. *Int. J. Hydrogen Energy*. **34(13)** (2009) 5537-5545.

[28] P. Vernoux, M. Guillodo, J. Fouletier, A. Hammou. Alternative anode material for gradual methane reforming in solid oxide fuel cells. *Solid State Ionics*. **135(1)** (2000) 425-43.

[29] M. Li, B. Hua, S. P. Jiang, J. Pu, B. Chi, L. Jian. BaZr$_{0.1}$Ce$_{0.7}$Y$_{0.1}$Yb$_{0.1}$O$_{3-\delta}$ as highly active and carbon tolerant anode for direct hydrocarbon solid oxide fuel cells. *Int. J. Hydrogen Energy*. **39(28)** (2014) 15975-15981.

Chapter 7

Coking tolerance improvement of $Ni_{0.5}Cu_{0.5}Ba_{0.05}$ coated SDC composite anode by hard template method for solid oxide fuel cells

7.1 Introduction

Solid Oxide Fuel Cells (SOFCs) have attracted widespread interests as power generation device that can directly convert the chemical energy to electric energy with low emissions, high efficiency and fuel flexibility. Hydrogen usually produced from steam-reforming reaction of hydrocarbons is most widely used fuel for SOFCs. Therefore, hydrocarbon fuels such as methane can be directly used to replace the expensive hydrogen fuel, which can significantly reduce system complexity, energy costs and increase cell efficiency [1-2]. However, Carbon deposition occurs mainly on anode surface due to methane decomposition reaction at a temperature over 800 K, resulting in the deactivation and damage of anode, causing a notable degradation of the cell [3-4]. Therefore, coking problem should be solved when hydrocarbons are used as the fuel for SOFCs.

To date, various new anode including Perovskite structure and ceria-based anode materials were investigated to prevent carbon formation [5-6]. Compared with them, the conventional anode consisting of nickel and yttria-stabilized zirconia (YSZ) still attracted widely attention due to its high conductivity for current collection and good catalytic activity for fuel oxidation [7]. Therefore, it is necessary for preparing Ni based anode with enhanced carbon tolerance [8]. It is reported that alloying Ni with Cu [9-10], Co [11], Fe [12] and another metal, or adding alkaline earth oxides such as MgO, CaO and BaO in Ni catalysts [13], could effectively enhance the carbon tolerance of Ni based anodes. Rismanchian [14] developed a Ni-Cu alloy as anode catalyst which could suppress carbon formation for hydrocarbon fuels. Rosa prepared the cell with barium-doped $Ni_{0.53}Cu_{0.47}$-CGO as anode and investigated its performance and stability in dry methane, and found that the cell showed a good stability for 200 h [15]. Sin investigated the durability of a cell with NiCu-CGO as anode under dry methane for 1300 h at 1023 K, and the results showed that the anode porosity was decreased due to carbon formation, which caused the damage on its integrated structure and the reduction of cell performance [16]. Thus, besides adding Cu and other metals in Ni catalysts to suppress carbon

formation, it is also essential to upgrade the microscopic pore structure of the anode [17].

It is well known that adding the pore former into the raw anode materials is one of the most effective methods to improve anode microstructure [18]. The pore formers including starch, flour, graphite and carbon dust can be burned off during high temperature-treatment, leaving pores in the anode [19]. Pan added paper-fibers into NiO-YSZ to prepare porous anode, which showed a high cell performance [20]. Srivastava used 15wt %(relative to anode) graphite powder as NiO-YSZ anode pore former, and found that the additive graphite can improve cell performance [21]. Sarikaya modified the anode structure by using Polymethyl methacrylate (PMMA) as pore former, and the cell also exhibited high performance [22]. Although anodes prepared with pore former additive can improve the cell performance and durability, the pores formed in anodes materials are isolated and discontinuous that may set back the diffusion of fuel gas and gas products, thus stop the cell performance from further improvement.

Compared with the addition of the pore former, hard template method has typical advantage in its shape and structure to prepare porous microstructure material with high specific surface; and the prepared material can copy the template structure after the template is burned off. [23] While wet impregnation method can produce anode materials with different metal ions doping; and the prepared materials can enhance the contact between catalyst and electrolyte [24]. In this study, with activated carbon fiber felt (ACFF) as a hard template, the tubular $Sm_{0.2}Ce_{0.8}O_{1.9}$(SDC) electrolyte materials were prepared as anode skeleton first, and then impregnated in salt solutions containing various concentrations of Ni, Cu and Ba species to fabricate $Ni_{0.5}Cu_{0.5}Ba_{0.05}O_x$ coated tubular SDC materials, which used as the ultimate anode materials. Meanwhile, for a comparison, $Ni_{0.5}Cu_{0.5}Ba_{0.05}O_x$ with powder structure was prepared by sol-gel method and then mixed with SDC powder as anode material. Electrolyte-supported single cells were fabricated using the obtained two anode materials, and their performances, evaluated by the current density, and long-term stability, were tested under dry methane.

7.2 Experimental

7.2.1 Preparation of anode materials

ACFF (specific surface area of 1700 m^2 g^{-1}) was used as hard template to prepare tubular SDC material. ACFF was dried in an oven for 2h at 373K. $Sm(NO_3)_3 \cdot 6H_2O$ and $Ce(NO_3)_3 \cdot 6H_2O$ in a molar ratio of Sm to Ce of 1:4 were weighed and added to a beaker and then deionized water was added to generate a saturated solution, using $Sm(NO_3)_3$ as a reference. Then, the dried ACFF was weighed and

added into the as-prepared saturated solution; and the mixture was stirred for 30 min, and maintained at the condition for 12 h; then, the mixture is put into the oven at 373K for 5 h for solvents evaporation. Finally, the impregnated ACFF was sintered at 1673K for 2 h to obtain tubular SDC (Samarium oxide stabilized ceria) material.

The preparation process of the composite anode material of $Ni_{0.5}Cu_{0.5}O_x$ coated tubular SDC was as follows. $Ni(NO_3)_2 \cdot 6H_2O$, $Cu(NO_3)_2 \cdot 5H_2O$ and $Ba(NO_3)_2$ in a molar ratio of 0.5:0.5:0.05 were first mixed and dissolved in proper amount of deionized water and ethanol and an emerald green solution was obtained. The relevant amount of tubular SDC power with a mass ratio of the calcined metal oxide to YSZ of 3:2 was introduced into the aforementioned solution, and heated at 323K for 6 h with stirring. Finally, the green and loose solid mixture was calcined in air at 1023K for 2 h. As such, the composite anode material of $Ni_{0.5}Cu_{0.5}O_x$ coated tubular SDC powder was obtained. For a convenience, $Ni_{0.5}Cu_{0.5}Ba_{0.05}O_x$/SDC was used to represent the as-prepared composited anode material.

Correspondingly, the $Ni_{0.5}Cu_{0.5}Ba_{0.05}O_x$ anode powders used sol-gel method was prepared for a comparison. $Ni(NO_3)_2 \cdot 6H_2O$, $Cu(NO_3)_2 \cdot 5H_2O$ and $Ba(NO_3)_2$ in a molar ratio of 0.5:0.5:0.05 were first mixed and dissolved in deionized water and Citric acid was then added to the solution at a molar ratio of mental ions to Citric acid of 1:2. And ethanol and PVA were added as dispersing agent to form an emerald green solution. The pH value of the solution used was adjusted to 7 by adding further amounts of NH_4OH solution. The solution was heated and stirred for 4 h at 353K to form a sol, followed by dried for 2 h at 393K to obtain a gel. The gel mixture was calcined in air at 1073K for 2 h, and finally, $Ni_{0.5}Cu_{0.5}Ba_{0.05}O_x$ powder material was obtained. The as-prepared $Ni_{0.5}Cu_{0.5}Ba_{0.05}O_x$ and SDC (20mol% Sm_2O_3, Tosoh) in a weight ratio of 3:2 were mixed and ground in an agate mortar for 2h to prepare homogenous powders. Similarly, $Ni_{0.5}Cu_{0.5}Ba_{0.05}O_x$-SDC was used to represent the mixed materials.

7.2.2 Fabrication and measurement of single cell

YSZ electrolyte-supported single cells were prepared as follows. Electrolyte substrate with a thickness of 0.5 mm and a diameter of 20 mm was prepared by pressing YSZ powders with 3wt% (relative to YSZ) polyvinyl butyral (PVB), followed by sintered at 1673 K for 4 h in air. Both anode and cathode were prepared by slurry coating method. Ethyl cellulose and α-terpineol with a mass ratio of 1: 4 was mixed as binders. A cathode slurry was prepared by mixed $La_{0.85}Sr_{0.15}MnO_3$ (LSM, CAS, China) and YSZ powders, in a mass ratio of 3:2, with 40 wt% binder (relative LSM and YSZ). The obtained slurry was coated onto the electrolyte and sintered at 1373K for 2 h. A anode slurry was

prepared by mixed the as-prepared anode material with 40wt% binder (relative to anode material) and then applied on the other side of electrolyte and sintered at 1273 K for 2 h. As such, the single cells of $Ni_{0.5}Cu_{0.5}Ba_{0.05}O_x$-SDC | YSZ | LSM-YSZ and $Ni_{0.5}Cu_{0.5}Ba_{0.05}O_x$/SDC | YSZ | LSM-YSZ were obtained. The effective area of the anode and cathode was 0.78 cm^2.

As-prepared single cells were mounted in a test rig as reported previously in Chapter 2. Pt mesh and glass ring was used to collect the current and seal the cell, respectively. Electrochemical performance test was performed at the temperature ranged from 923 to 1073 K in increments of 50 K. In the power generation performance tests with hydrogen, the flow rates of dry H_2 and O_2 were 80 cm^3·min^{-1} and 30 cm^3·min^{-1}, respectively. Similarly, in the tests of power generation performance in methane, the flow rates of N_2, O_2 and CH_4 were 30 cm^3·min^{-1}, 30 cm^3·min^{-1} and 20 cm^3·min^{-1}, respectively.

X-ray diffraction (XRD, SHIMADZU, XD-3A, Japan) with Cu Kα radiation was applied to analyze anode structure. The morphology and microstructure of the material and the cell after testing were examined by scanning electron microscope (SEM, Jeol, JSM-5600LV, Japan). The elementary analysis of the anode after testing was performed by Energy Dispersive Spectroscopy (EDS) attached on SEM.

7.3 Results and discussion

7.3.1 Characterization of anode material

Fig. 7.1(a) shows XRD patterns of the composite anode material of $Ni_{0.5}Cu_{0.5}Ba_{0.05}O_x$ prepared by sol-gel method. One can see that the diffraction peaks in the XRD pattern were identical to NiO pattern (PDF#65-2901) and CuO pattern (PDF#48-1548), indicating the as-prepared $Ni_{0.5}Cu_{0.5}Ba_{0.05}O_x$ material was mainly composed of NiO and CuO.

The tubular SDC electrolyte shown in Fig. 7.1(b), prepared by hard template, was identical to $Sm_{0.2}Ce_{0.8}O_{1.9}$ pattern (PDF#75-0158).Its diffraction peak was sharp with high intensity, and no unwanted phase was found, suggesting that the SDC with fluorite structure was successfully prepared.

Fig. 7.1(c) shows XRD patterns of the composite anode material of $Ni_{0.5}Cu_{0.5}Ba_{0.05}O_x$ coated tubular SDC, diffraction peaks corresponding to NiO (PDF#65-2901) and CuO (PDF#48-1548) were found, indicating Ni-Cu metallic oxide particles are successfully prepared by wet impregnation method followed by calcining.

Herein, no BaO phase with relative intensity was examined and observed in all the XRD patterns, which was coincident with the results studied by Rosa et al. [15, 25-26] as reported previously. The main reason is the additive amount of BaO was extremely low. According to the EDS analysis of the

anode surface after testing shown in Fig 7.2, it can be seen that the Ba element does exist in the two anode surface; and this indicates that BaO was successfully impregnated into the as-prepared anodes.

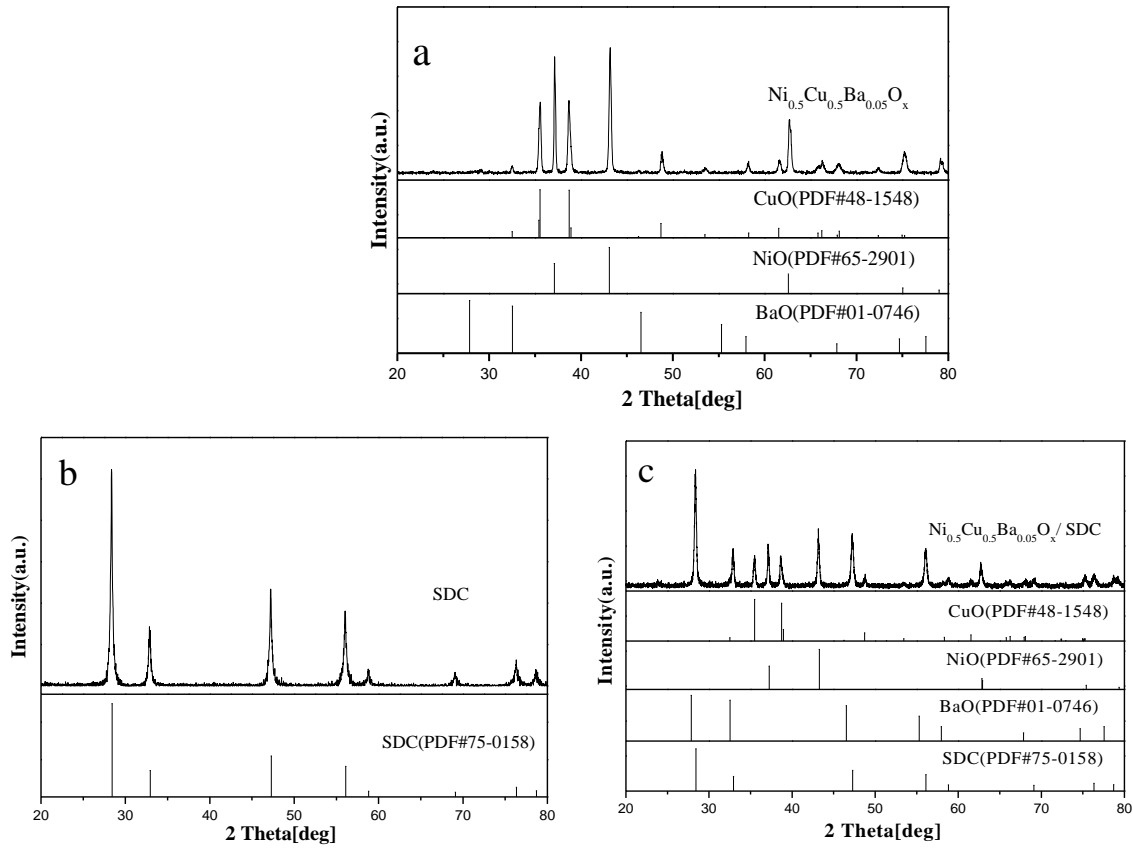Fig. 7.1 XRD patterns of the as-prepared anode material with different methods
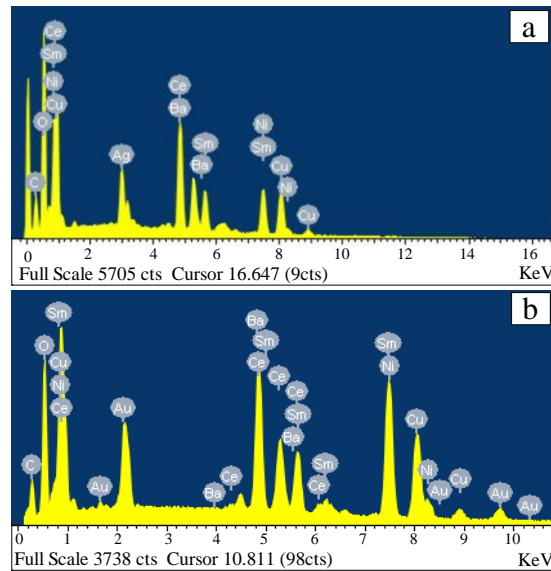(a): $Ni_{0.5}Cu_{0.5}Ba_{0.05}O_x$; (b): SDC; (c): $Ni_{0.5}Cu_{0.5}Ba_{0.05}O_x$ coating tubular SDC

Fig. 7.2 EDS analysis for different anodes of unit cell after experiment
(a): $Ni_{0.5}Cu_{0.5}Ba_{0.05}O_x$-SDC; (b): $Ni_{0.5}Cu_{0.5}Ba_{0.05}O_x$/SDC

7.3.2 Microscopic structure analysis

Fig.7.3 shows the constrative SEM morphologies of the correspondingly as-prepared anode materials. As seen from Fig.7.3 (a), the $Ni_{0.5}Cu_{0.5}Ba_{0.05}O_x$ material prepared by sol-gel method shown a particle structure and some of them agglomerated together. Herein, the composite anode material of $Ni_{0.5}Cu_{0.5}Ba_{0.05}O_x$ coated tubular SDC electrolyte prepared by ACFF as template shown in Fig.7.3 (b). Self-made SDC electrolyte show tubular shape with a diameter of 7 μm, indicating the as-prepared SDC has successfully copied the microstructure of ACFF. One can see that there were many fine particles evenly distributed on tubular SDC skeletons, which illustrates catalytic particles successfully coated SDC electrolyte by wet impregnation method followed by calcining. The dense contact of catalytic metallic oxide particles with SDC extended the active reaction sites in the SOFC anode, leading to improve the power generation performance.
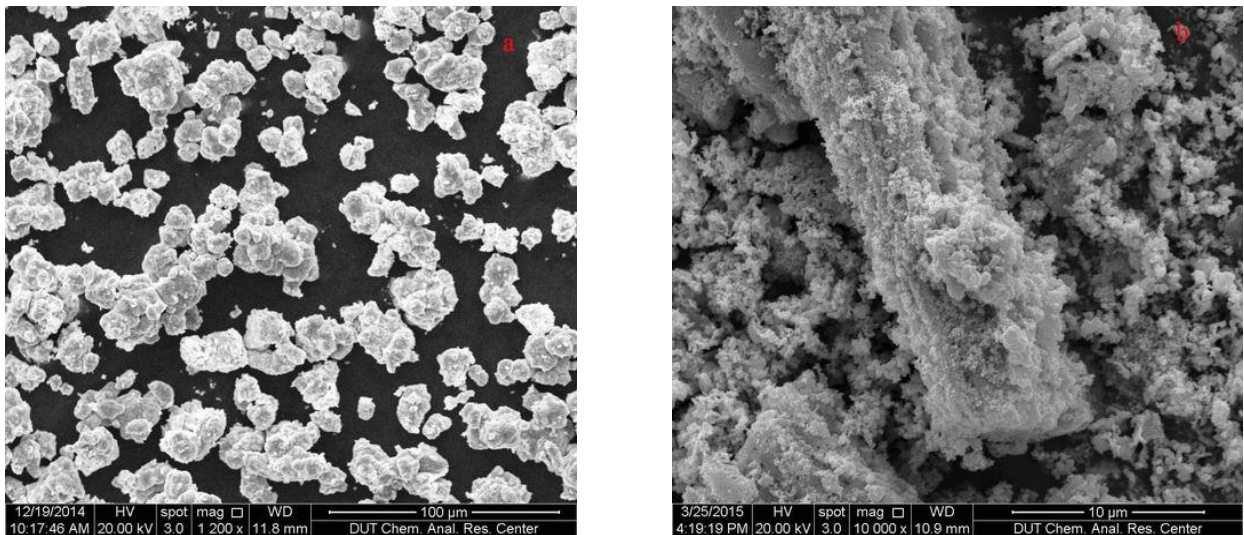
Fig. 7.3 SEM images of the anode material prepared by different methods
(a): $Ni_{0.5}Cu_{0.5}Ba_{0.05}O_x$; (b): $Ni_{0.5}Cu_{0.5}Ba_{0.05}O_x$ coating tubular SDC

7.3.3 Cell performance test

Fig.7.4 shows the typical current–voltage characteristics and the corresponding power densities with a configuration of $Ni_{0.5}Cu_{0.5}Ba_{0.05}O_x$-SDC | YSZ | LSM-YSZ operated with hydrogen and dry methane as fuels at various temperatures. For hydrogen in Fig .4(a), the open-circuit voltages (OCVs) of the cell were 1.167, 1.117, 1.111 and 1.103 V at 1073, 1023, 973 and 923 K, respectively, which were close to the theoretical values calculated by Nernst equation, indicating that the unit cell was well fabricated and sealed. Meanwhile, its maximum power densities were 622.50, 444.58, 298.64 and 170.68 mW·cm^{-2} at 1073, 1023, 973 and 923 K, respectively. Similar with hydrogen, fueled in dry methane, as shown in Fig.7.4 (b), the OCVs were 1.012, 0.961, 0.911 and 0.853V. Accordingly, the

maximum power densities were 324.99, 201.99, 133.18 and 92.23 mW·cm^{-2}, respectively.
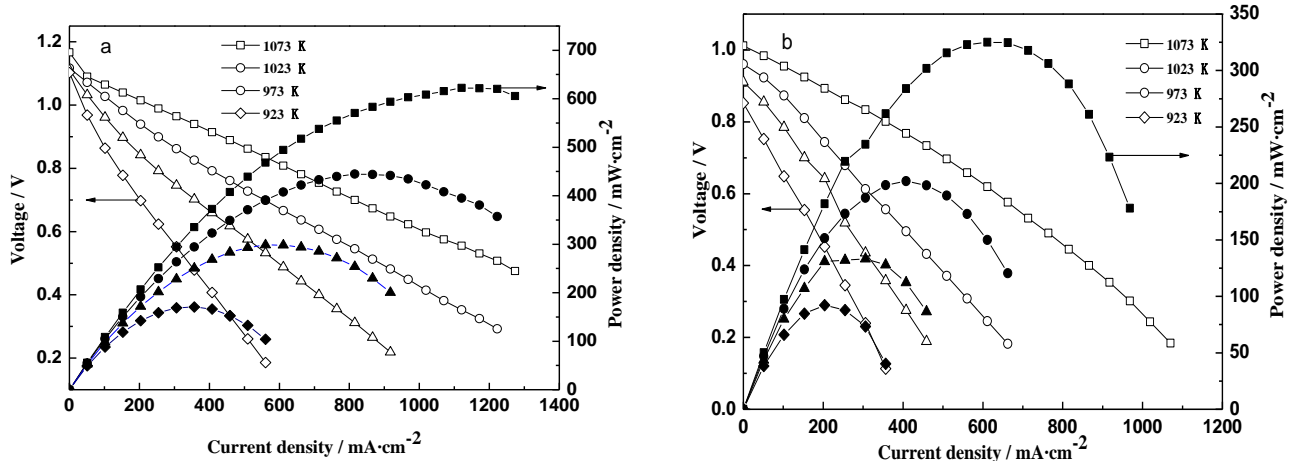
Fig. 7.4 Power generating performances of unit cell with Ni$_{0.5}$Cu$_{0.5}$Ba$_{0.05}$O$_x$-SDC as anode
(a): in hydrogen; (b): in dry methane

Fig.7.5 shows the shows the typical current–voltage characteristics and the corresponding power densities measured at various temperatures with a configuration of Ni$_{0.5}$Cu$_{0.5}$Ba$_{0.05}$Ox/SDC when hydrogen and dry methane as fuel. For hydrogen in Fig .6(a), the OCVs of the cell were 1.207, 1.211, 1.214 and 1.213V at 1073, 1023, 973 and 923 K, respectively. All the OCVs were close to 1.200V, suggesting that the cell consisting of such anode was also well sealed. Correspondingly, the maximum power densities were 535.18, 403.08, 245.72 and 157.61 mW·cm^{-2}, respectively. For dry methane in Fig .7.5(b), the OCVs of the cell were 1.077, 1.022, 1.001 and 0.989V at 1073, 1023, 973 and 923 K, respectively. Accordingly, the maximum power densities were decreased to 384.54, 240.79, 118.01 and 55.78 mW·cm^{-2} from 1073 to 923 K respectively.

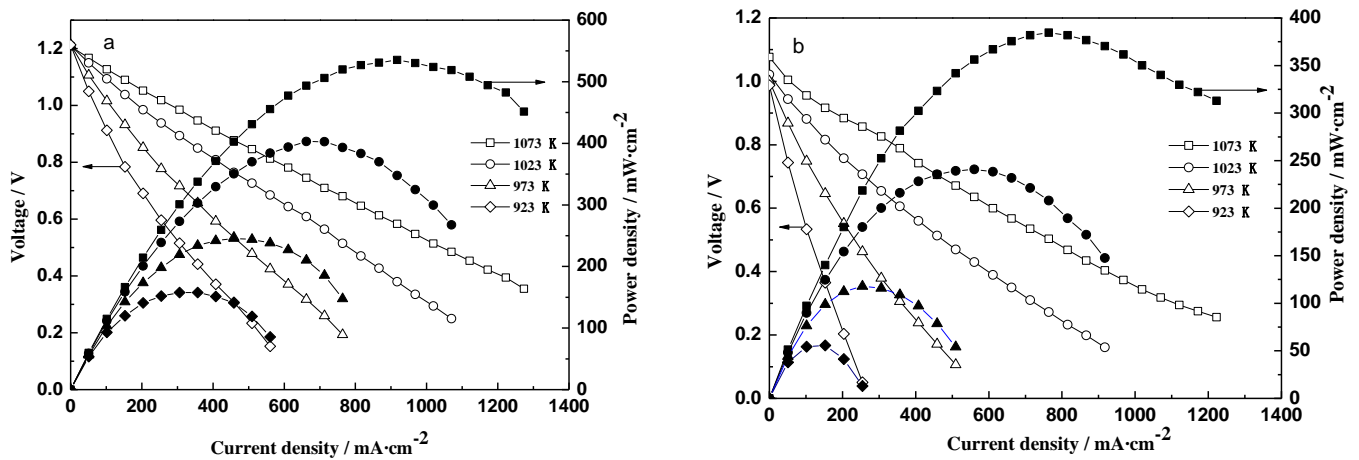Fig. 7.5 Power generating performances of unit cell with Ni$_{0.5}$Cu$_{0.5}$Ba$_{0.05}$O$_x$/SDC as anode
(a): in hydrogen; (b): in dry methane

Compared with the aforementioned output performance characteristics of the cells with configuration of $Ni_{0.5}Cu_{0.5}Ba_{0.05}O_x$-SDC | YSZ | LSM-YSZ and $Ni_{0.5}Cu_{0.5}Ba_{0.05}O_x$/SDC | YSZ | LSM-YSZ in dry methane, the following results were obtained: there was a difference of two anodes with identical raw materials but prepared by different methods. For example, the OCV and power density of the $Ni_{0.5}Cu_{0.5}Ba_{0.05}O_x$/SDC anode were higher than the $Ni_{0.5}Cu_{0.5}Ba_{0.05}O_x$-SDC anode, and its increasing of maximum power density was reached 15.49% at 1073 K. As seen from Fig. 7.5(b), the power density decreased slowly with the current density increase when the power density was reached maximum. The main reason was the prepared method of two anodes was different, resulting in the big microstructure difference of anode. One presented particles, and the other displayed tubular structure, causing a certain gap of the as-prepared cell performance.

7.3.4 Long-term stability test

Fig.7.6 shows the terminal voltage of as-prepared cells operated with a constant current density of 127.4 $mA \cdot cm^{-2}$ as a function of time when dry methane was used as the fuel at 1073 K. The cells with $Ni_{0.5}Cu_{0.5}Ba_{0.05}O_x$-SDC and $Ni_{0.5}Cu_{0.5}Ba_{0.05}O_x$/SDC as anodes were measured for 10 h and 100 h, respectively. The voltages of two cells were continuously variable during long-term stability test, indicating that the aforementioned performance test caused no damage to the cells.
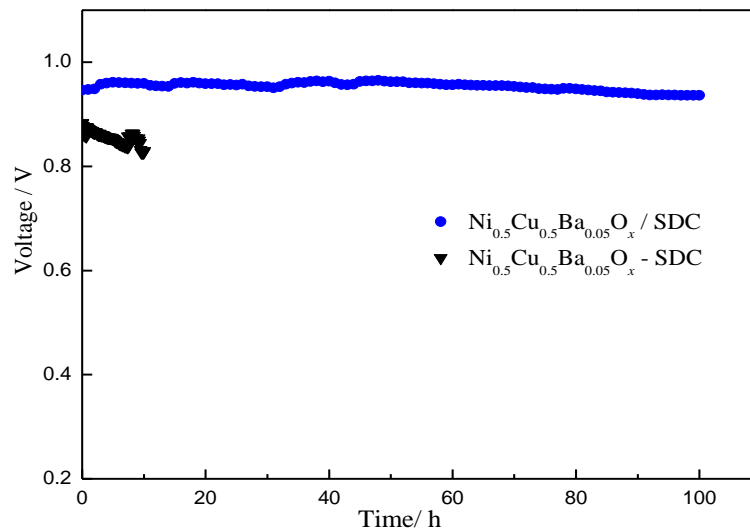
Fig. 7.6 Voltage change with time for the as-prepared unit cells

For comparison, the $Ni_{0.5}Cu_{0.5}Ba_{0.05}O_x$-SDC anode dropped rapidly in dry CH_4 through 10 h operation. Its initial and terminal voltage was 0.8820 V and 0.8300 V, respectively, which was about 5.60% voltage drop. At 10 h, the voltage still showed a decreasing trend, implying that the anode was severely deactivated. Therefore, the $Ni_{0.5}Cu_{0.5}Ba_{0.05}O_x$-SDC anode prepared by directly mixing raw

powders exhibited a poor coking resistance, due primarily to carbon buildup and deposition of the anode.

Herein, for the cell with $Ni_{0.5}Cu_{0.5}Ba_{0.05}O_x$/SDC anode, its initial voltage was reached 0.9467 V. The voltage showed a relatively narrow change, which was resulted from the pressure change of methane during test. However, after running 48 h, its voltage was decreased, due primarily to methane decomposition and carbon buildup on the anode.

After operation of 100 h, the voltage was drop to 0.9366 V, which is about 1.07% voltage drop. There was no significant cell initial voltage drop, which indicated that $Ni_{0.5}Cu_{0.5}Ba_{0.05}O_x$ coated tubular SDC prepared by hard template combined with wet impregnation method could enhance cell stability and improve the anti-carbon deposition capacity of Ni based composite anode.

7.3.5 SEM analysis for single cells after test

Fig 7.7 shows the SEM images of the surface and cross section of two tested cell with such anodes after long-term stability test. Fig. 7.7(a) of the $Ni_{0.5}Cu_{0.5}Ba_{0.05}O_x$-SDC anode surface displays the agglomerative particles and narrow pores were form among the anode. Fig. 7.7(b) is the cross-sectional SEM image of the cell with such anode. One can see that the anode layer connected densely with the YSZ electrolyte supporter. However, the agglomerated anode particles resulted in the insufficient porosity in anode layer, hindering the fuel transport and reaction gas diffusion. The pores in the anode were prone to be blocked, resulting in the degradation of cell performance, which was consistent of the long-term stability test.

In contrast, for the cell with $Ni_{0.5}Cu_{0.5}Ba_{0.05}O_x$/SDC as anode, as shown in Fig.7.7(c) and 7.7(d), the tubular SDC electrolyte uniformly distributed and some of them cross-connected to form a porous skeletal structure of anode with high specific surface area. Furthermore, the coated the tubular SDC was evenly coated by reduced catalyst particles to form a densely electrical conductive network, leading to extend anode active reaction sites. Fig. 7.7(d) is a cross-sectional SEM image of the single cell after the long-term test. It can be seen that the porous anode layer and dense SDC electrolyte substrate are well-connected. Also, a uniform distribution of the tubular SDC in anode layer is facilitated to form a three-dimensional electrode to provide continuous and connected gas transport pathways, which is beneficial for rapid diffusion of reactants getting in and the byproducts getting out of the anode reaction areas. The tubular SDC coated by catalytic mental particles increased the land area with electrolyte and fuel gas. As a result, more three phase boundaries are generated for electrochemical reaction to enhance the cell output performance. Therefore, the tubular SDC coated by $Ni_{0.5}Cu_{0.5}Ba_{0.05}O_x$ as anode had high advantage in the microstructure and maintaining stable cell

performance.
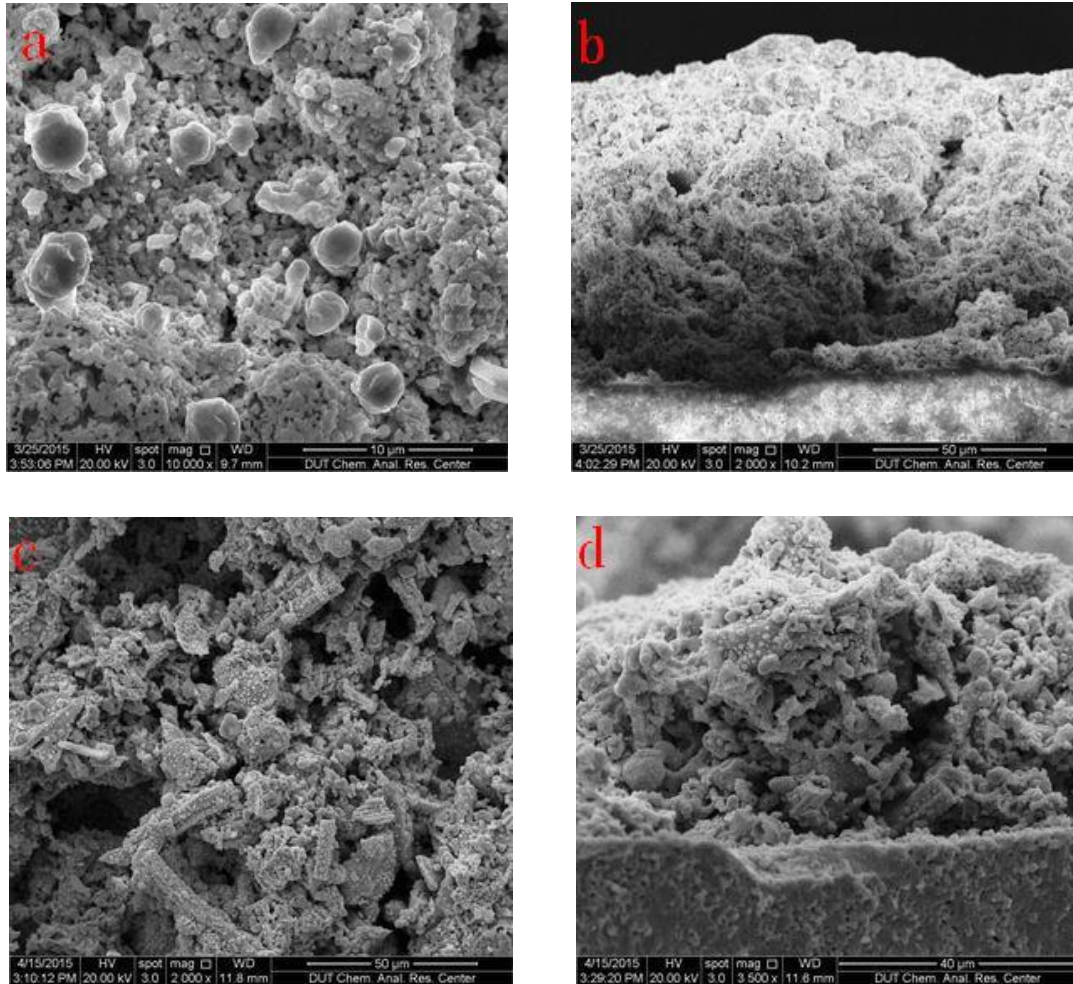
Fig. 7.7 SEM images of the different anode surface and cross section after the experiment (a),(b): $Ni_{0.5}Cu_{0.5}Ba_{0.05}O_x$-SDC; (c),(d): $Ni_{0.5}Cu_{0.5}Ba_{0.05}O_x$/ SDC

7.3.6 Carbon phenomenon and EDS analysis for single cells after experiment

Fig. 7.8 displays the photos of carbon deposition after long-term operation. A amount of coke was found to be deposited on the two cells anode surface, which illustrated dry methane was decomposed in anode chamber at 1073K.

For $Ni_{0.5}Cu_{0.5}Ba_{0.05}O_x$-SDC anode, as show in Fig. 7.8(a), the carbon deposition on anode was prone to block the pores and hinder the rapid diffusion of fuel gas to TPB that weaken the electrochemical performance. Herein, the $Ni_{0.5}Cu_{0.5}Ba_{0.05}O_x$/SDC anode, cover by carbon deposition on surface, still showed no deactivation, due to its fabrication of three-dimensional porous structure, which contributed to the enhancement of cell stability during long-term operation.
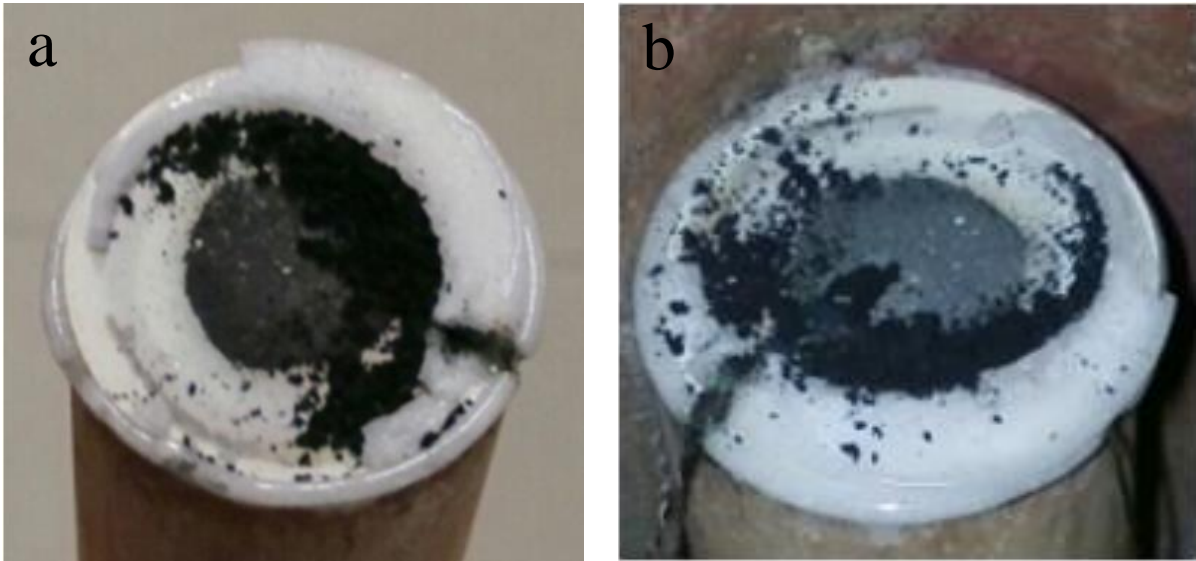
Fig.7.8 Photos of carbon deposition phenomenon on unit cells with different anodes after running 100 h(a): $Ni_{0.5}Cu_{0.5}Ba_{0.05}O_x$-SDC； (b): $Ni_{0.5}Cu_{0.5}Ba_{0.05}O_x$/SDC

Fig. 7.9 shows EDS results of the two cells such anodes operated with dry methane for 10 and 100 h, respectively.

Spectrum a ($Ni_{0.5}Cu_{0.5}Ba_{0.05}O_x$-SDC)

Element	Wt %	At %
C K	8.63	23.66
O K	26.05	53.62
Ni K	10.26	5.76
Cu K	12.71	6.59
Ag L	7.46	2.28
Ba L	1.41	0.34
Ce L	27.25	6.40
Sm L	6.22	1.36
Total	100.00	

60μm

Full Scale 5705 cts Cursor 16.647 (9cts)   KeV

Spectrum b ($Ni_{0.5}Cu_{0.5}Ba_{0.05}O_x$ / SDC)

Element	Wt %	At %
C K	7.92	28.16
O K	12.83	34.27
Ni K	20.35	14.81
Cu K	15.74	10.58
Ba L	2.33	0.73
Ce L	24.57	7.49
Sm L	6.44	1.83
Au M	9.82	2.13
Total	100.00	

40μm

Full Scale 3738 cts Cursor 10.811 (98cts)   KeV

Fig. 7.9 EDS analysis results of different unit cells after long-term stability test:
(a) $Ni_{0.5}Cu_{0.5}Ba_{0.05}O_x$-SDC； (b) $Ni_{0.5}Cu_{0.5}Ba_{0.05}O_x$/SDC

The elements of Ni, Cu, Ba, Sm and Ce with a higher content were examined by EDS in the anode layer for both cells, proving that the as-prepared anodes showed a relatively stable microstructure and

the anode layers were not fell off during the stability test. The C content of the $Ni_{0.5}Cu_{0.5}Ba_{0.05}O_x$-SDC anode, detected by EDS, was 23.66% in anode layer after running only 10 h. However, in the case of $Ni_{0.5}Cu_{0.5}Ba_{0.05}O_x$/SDC, as shown in Fig.7.9 (b), the amount of carbon deposition was only 28.16% after running 100 h. Combining with the voltage drop phenomenon in the long term-stability test, which further proved the porous anode based on three-dimensional SDC electrolyte as scaffold could improve anode microstructure and alleviate carbon deposition to enhance the cell stability in a long period electrochemical reaction for hydrocarbon fuels.

7.4 Conclusion

In this paper, the two single cells with the configuration of $Ni_{0.5}Cu_{0.5}Ba_{0.05}O_x$/SDC | YSZ | LSM-YSZ and $Ni_{0.5}Cu_{0.5}Ba_{0.05}O_x$/SDC were well fabricated, and showed good performance under hydrogen and dry methane at 1073K. Fueled with dry methane, for t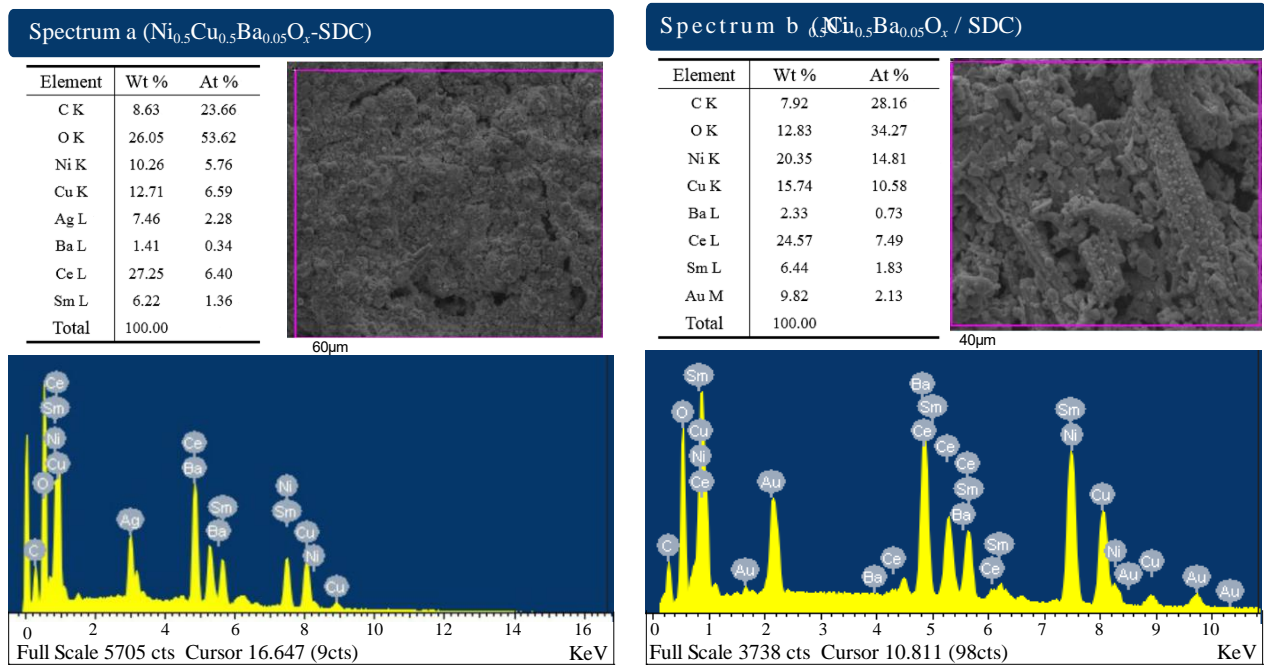he single cell with $Ni_{0.5}Cu_{0.5}Ba_{0.05}O_x$/SDC anode, a maximum power density of 384.54 mW·cm^{-2} was achieved, which was higher than the $Ni_{0.5}Cu_{0.5}Ba_{0.05}O_x$-SDC anode of 324.99 mW·cm^{-2}.

At 1073K, the cells' long-term stability with a constant lower current density of 127.4 mA·cm^{-2} was measured under dry methane. For the cell with $Ni_{0.5}Cu_{0.5}Ba_{0.05}O_x$-SDC anode, operated only 10 h, showed a voltage drop of 5.60% and a severe decreasing trend. However, the voltage of the cell with $Ni_{0.5}Cu_{0.5}Ba_{0.05}O_x$/SDC anode maintained the initial value at the stability test after operation of 100 h, implying the $Ni_{0.5}Cu_{0.5}Ba_{0.05}O_x$/SDC anode had a better stability for dry methane.

SEM morphologies of the tested cell showed that the catalytic metal particles were uniformly coated tubular SDC, leading to increase three phase boundary. The prepared anode presented a steady and porous stereoscopic structure for gas diffusion. The fabrication of anti-carbon catalyst combined with three-dimensional electrode is a potential measure to enhance durability for direct utilization of dry methane as fuel in SOFCs.

Reference

[1] S. Park, J. M. Vohs, R. J. Gorte, Direct oxidation of hydrocarbons in a solid-oxide fuel cell, *Nat.* **404(6775)** (2000) 265-267.

[2] M. D. Gross, J. M. Vohs, R. J. Gorte, Recent progress in SOFC anodes for direct utilization of hydrocarbons, *J. Mater. Chem.* **17(30)** (2007) 3071-3077.

[3] C. Gueret, M. Daroux, F. Billaud, Methane pyrolysis: thermodynamics, *Chem. Eng. Sci.* **52(5)** (1997) 815-827.

[4] M. Mogensen, K. Kammer, Conversion of hydrocarbons in solid oxide fuel cells, *Cheminform.*

33(1) (2003) 321-331.

[5] J. S. Yoon, E. J. Yi, B. H. Choi, M. J. Ji, J. H. Hwang, Methane oxidation behavior over $La_{0.08}Sr_{0.92}Fe_{0.20}Ti_{0.80}O_{3-\delta}$ perovskite oxide for SOFC anode, *Ceram. Int.* **40(1)** (2014) 1525-1529.

[6] M. Asamoto, S. Miyake, K. Sugihara, H. Yahiro, Improvement of Ni/SDC anode by alkaline earth metal oxide addition for direct methane–solid oxide fuel cells, *Electrochem. Commun.* **11(7)** (2009) 1508-1511.

[7] J. H. Jun, T. H. Lim, S. W. Nam, S. A. Hongb, K. J. Yoon, Mechanism of partial oxidation of methane over a nickel-calcium hydroxyapatite catalyst, *Appl. Catal. A-Gen.* **312(8)** (2006) 27-34.

[8] L. Liu, G. Y. Kim, A. C. Hillier, A. Chandraa, Microstructural and electrochemical impedance study of nickel–$Ce_{0.9}Gd_{0.1}O_{1.95}$ anodes for solid oxide fuel cells fabricated by ultrasonic spray pyrolysis, *J. Power Sources* **196(6)** (2011) 3026-3032.

[9] E. Nikolla, J. Schwank, S. Linic. Comparative study of the kinetics of methane steam reforming on supported Ni and Sn/Ni alloy catalysts: The impact of the formation of Ni alloy on chemistry. *J. Catal.* **263(2)** (2009) 220-227.

[10] S. I. Lee, J. M. Vohs, R. J. Gorte, A Study of SOFC Anodes Based on Cu-Ni and Cu-Co Bimetallics in CeO_2 YSZ, *J. Electrochem. Soc.* **151(9)** (2004) A1319-A1323.

[11] C. M. Grgicak, M. PakulskaM, J. S. O'Brien, J. B. Giorgi, Synergistic effects of $Ni_{1-x}Co_x$-YSZ and $Ni_{1-x}Cu_x$-YSZ alloyed cermet SOFC anodes for oxidation of hydrogen and methane fuels containing H_2S, *J. Power Sources.* **183(1)** (2008) 26-33.

[12] H. Kan, H. Lee, Sn-doped Ni/YSZ anode catalysts with enhanced carbon deposition resistancefor an intermediate temperature SOFC, *Appl. Catal. B-Environ.* **97(1)** (2010) 108-114.

[13] A. P. E. York, T. C. Xiao, M. L. H. Green, J. B. Claridge, Methane oxyforming for synthesis gas production, *Catal. Rev.* **49(4)** (2007) 511-560.

[14] A. Rismanchian, J. Mirzababaei, S. S. C. Chuang, Electroless plated Cu–Ni anode catalyst for natural gas solid oxide fuel cells, *Catal. Today* **245** (2015) 79-85.

[15] D. L. Rosa, A. Sin, M. L. Faro, G. Monfortea, V. Antonuccia, A. S. Aricòa, Mitigation of carbon deposits formation in intermediate temperature solid oxide fuel cells fed with dry methane by anode doping with barium, *J. Power Sources* **193(1)** (2009) 160-164.

[16] A. Sin, E. Kopnin, Y. Dubitsky, A. Zaopo, A. S. Aricòb, D. L. Rosa, L. R. Gullob, V. Antonuccib, Performance and life-time behaviour of NiCu–CGO anodes for the direct electro-oxidation of methane in IT-SOFCs, *J. Power Sources* **164(1)** (2007) 300-305.

[17] H. Sumi, T. Yamaguchi, T. Suzuki, H. Shimada, K. Hamamoto, Y. Fujishiro, Effects of anode microstructures on durability of microtubular solid oxide fuel cells during internal steam

reforming of methane, *Electrochem. Commun*. **49** (2014) 34-37.

[18] J. J. Haslam, A. Q. Pham, B. W. Chung, J. F. DiCarlo, R. S. Glass, Effects of the use of pore formers on performance of an anode supported solid oxide fuel cell, *J. Am. Ceram. Soc*. **88(3)** (2005) 513-518.

[19] L. F. Nie, J. C. Liu, Y. J. Zhang, M. L. Liu, Effects of pore formers on microstructure and performance of cathode membranes for solid oxide fuel cells, *J. Power Sources* **196(23)** (2011) 9975-9979.

[20] W. P. Pan, Z. Lü, K. F. Chen, X. Q. Huang, B. Wei , W. Y. Li, Z. H. Wang, W. H. Sua, Novel polymer fibers prepared by electrospinning for use as the pore-former for the anode of solid oxide fuel cell, *Electrochi. Acta*. **55(20)** (2010) 5538-5544.

[21] P. K. Srivastava, T. Quach, Y. Y. Duan, R. Donelson, S. P. Jiang, F. T. Ciacchi, S. Badwal, Electrode supported solid oxide fuel cells: Electrolyte films prepared by DC magnetron sputtering, *Solid State Ionics*. **99(3)** (1997) 311-319.

[22] A. Sarikaya, V. Petrovsky, F. Dogan, Effect of the anode microstructure on the enhanced performance of solid oxide fuel cells, *Int. J. Hydrogen Energy* **37(15)** (2012) 11370-11377.

[23] F. H. Wang, R. S. Guo, Q. T. Wei, Y. Zhou, H. L. Li, S. L. Li, Preparation and properties of Ni/YSZ anode by coating precipitation method, *Mater. Lett*. **58(24)** (2004) 3079-3083.

[24] H. X. You, C. Zhao, B. Qu, G. Q. Guan, A. Abudula, Fabrication of $Ni_{0.5}Cu_{0.5}O_x$ coated YSZ anode by hard template method for solid oxide fuel cells, *J. Alloys Compd*. **669(7)** (2016) 46-54.

[25] M. L. Faro, P. Frontera, P. L. Antonucci, A. S. Aricòa, Ni–Cu based catalysts prepared by two different methods and their catalytic activity toward the ATR of methane, *Chem. Eng. Res. Des*. **93** (2015) 269-277.

[26] X. B. Li, G. Q. Shao, J. M. Luo, J. S. Lu, M. S. Xue, Y. H. Hou, L. P. Deng, Fabrication and characterization of GDC electrolyte/electrode integral SOFC with BaO/Ni-GDC anode, *Mater. Res. Bull*. **50(4)** (2014) 337-340.

Chapter 8

Fabrication of composite anode GDC–SrMoO$_4$–YSZ by hard template method for solid oxide fuel cell

8.1 Introduction

Solid oxide fuel cell (SOFC) as a promising energy device can convert chemical energy into electric power due to its high efficiency, little pollution and fuel flexibility [1-2]. The conventional nickel and yttria-stabilized zirconia (Ni-YSZ) cermet show a good output performance in hydrogen due to Ni's good catalytic activity for fuel oxidation [3]. However, severe deactivation of Ni/YSZ anodes occurs when hydrocarbon fuels applied as fuel in long period operation, due to carbon deposition of the hydrocarbon on the anode surface of Ni catalysts [4-5]. Therefore, to search for Ni-free material with competitive conductivity and electro-catalytic has attracted wide attention.

It is reported that perovskite material such as SrTiO$_3$ [6], Sr$_2$MMoO$_6$ [7], SrMoO$_3$ [8] and La$_{0.75}$Sr$_{0.25}$Cr$_{0.5}$Mn$_{0.5}$O$_3$ (LSCM) [9] showed good coking resistance. More researches are focused on SrMoO$_3$ due to its high conductivity and stability at 1023 K [10]. However, pure SrMoO$_3$ anode had poor power generation performance because of its lower electro-catalytic activity [11]. Generally, it is well known that adding the Ni [12], GDC [13], or SDC [14] into La$_{0.75}$Sr$_{0.25}$TiO$_3$(LST)、La$_{0.75}$Sr$_{0.25}$Cr$_{0.5}$Mn$_{0.5}$O$_3$ (LSCM) can effectively improve its catalytic activity. Therefore, it can introduce Ni, GDC, or SDC into SrMoO$_3$ anode to obtain composite anode. Gross [15] prepared SrMoO$_3$-YSZ anode and used Pd as its catalyst, and the cell show a power density of 148.03 and 169.16 mW·cm^{-2} in H$_2$ and CH$_4$, respectively. Xiao [16] developed and investigated the cell consisting of Gd$_{0.2}$Ce$_{0.8}$O$_{1.9}$ infiltrated SrMoO$_3$-YSZ anode, its power density was reached 160.0 mW·cm^{-2} of in wet methane at 1173 K, suggesting that the introduction of GDC contributed to improve electrical performance.

In this paper, in order to improve the SrMoO$_3$ anode performance for SOFC, SrMoO$_4$ high specific surface area was first prepared by hard template method and then wet impregnation was adopted to fabricate GDC particle coated SrMoO$_4$, which was denoted as GDC-SrMoO$_4$. As such, GDC-SrMoO$_4$ and YSZ were mixed to obtain the ultimate anode material GDC-SrMoO$_4$-YSZ. The single cell with

SrMoO$_4$-YSZ and GDC-SrMoO$_4$-YSZ as anodes were fabricated and performed in hydrogen and dry methane. On basis this, the effect of GDC impregnation and the component of SrMoO$_4$ and YSZ on the cell performance were investigated. It is expected to create a new composite Ni-free anode and obtain good performance.

8.2 Experimental

8.2.1Sample preparation

Anode precursor material SrMoO$_4$ was prepared by hard template method utilizing active carbon fiber felt (ACFF, specific surface area of 870m^2·g^{-1}, porosity 0.86cm^3·g^{-1}) as a template. SrCO$_3$ (Aladdin, 99.95%) and (NH$_4$)$_6$Mo$_7$O$_{24}$·4H$_2$O (Aladdin, 99.9%) in a molar ratio of Sr : Mo=1:1 were weighed and introduced separately into two beakers, A and B. The excessive concentrated nitric acid (HNO$_3$) was added into the beaker A to prepare a solution of Sr(NO$_3$)$_2$, which was then poured into the beaker B. Afterwards, appropriate amount of deionized water was added into the beaker B followed by stirring for preparation of the saturated solution. The proper amount of dried ACFF was added into the as-prepared solution and stirred for 30 min and maintained at the condition for 24 h. Then, the solution was evaporated at 373 K for 12 h. Finally, the dried ACFF was calcined at 1523 K for 2 h, and the SrMoO$_4$ powder was obtained.

GDC was introduced into SrMoO$_4$ by wet impregnation to prepare GDC-SrMoO$_4$. Stoichiometric amounts of Gd(NO$_3$)$_3$ (Aladdin, 99.95%) and Ce(NO$_3$)$_3$ (Aladdin, 99.95%) were weighed and dissolved in deionised water to form the mixed solution. Next, the as-prepared SrMoO$_4$ was weighted and poured into the solution, followed by heating for 24 h at 373 K to complete the impregnation process. Finally, the liquid-solid mixture was calcined at 1173K for 1 h. As such, the composite anode material of GDC-SrMoO$_4$ powder was obtained. The as-prepared SrMoO$_4$ and YSZ (8mol% Y$_2$O$_3$-ZrO$_2$, Tosoh) powders were mixed and ground to obtain the anode material SrMoO$_4$-YSZ. Also, GDC-SrMoO$_4$ and YSZ were used to prepare GDC-SrMoO$_4$-YSZ.

8.2.2 Fabrication of single cells

YSZ electrolyte-supported single cell was prepared as follows. Electrolyte substrate with a thickness of 0.5 mm and a diameter of 20 mm was prepared by pressing YSZ powders (8 mol% Y$_2$O$_3$-ZrO$_2$, Tosoh) with 3 wt% polyvinyl butyral (PVB, relative to YSZ), followed by sintered at 1673 K for 4 h in air. Both anode and cathode were prepared by slurry coating method [24]. The mixture of α-terpineol and ethyl cellulose with a mass ratio of 4:1 was used as binders. As-prepared composite anode material with 40 wt% binder (relative to anode material) was coated on the

electrolyte substrate and sintered at 1523 K for 3h in air. LSM (CAS, China) and YSZ powders in a weighted ratio of 1:1 were mixed with 40 wt% binder (relative to LSM and YSZ) as cathode slurry, which was coated on the other side of electrolyte and sintered at 1373 K for 2 h in air. As such, the single cells with the configuration of GDC-SrMoO$_4$-YSZ | YSZ | LSM and SrMoO$_4$-YSZ | YSZ | LSM were obtained.

8.2.3 Measurement and characterization of single cells

The as-prepared single cells were mounted in a test rig as reported previously [17], where when hydrogen (dry methane) was used as the fuel and oxygen as the oxidant. Pt mesh was used to collect the current and glass ring used to seal the cell. The cell performances were measure from 923 to 1123K in increments of 50K. a CHI660C electrochemical workstation system (CHI604D, Shanghai Chen Hua Instrument Co., Ltd.) with HV–151 potentiostat constant current instrument. The cell was prior to reduce in hydrogen for 2 h at 1173K before test. X-ray diffractometer (SHIMADZU, XD-3A, Japan) with Cu Ka radiation was employed to analyze crystal structure. The morphology and microstructure of the prepared material sample was examined by scanning electron microscopy SEM (JEOL, JSM-5600LV, Japan) before and after the test.

8.3 Results and discussion

8.3.1 Phase and microstructure analysis

Fig. 8.1a shows XRD pattern of the prepared SrMoO$_4$. Compared with the XRD standard SrMoO$_4$ pattern (PDF08-0482), the diffraction peaks are identical, and no unwanted phase is found, proving that the SrMoO$_4$ materials have been produced by hard template method. SrMoO$_4$-YSZ was reduced to SrMoO$_3$-YSZ in hydrogen for 2h at 1173 K. Fig. 8.1b shows the reduced SrMoO$_4$-YSZ pattern. One can see that some characteristic peaks are identical to YSZ pattern (PDF#48-0224) and SrMoO$_4$ phase was still be observed, which indicates that YSZ and SrMoO$_4$ phases co-existed separately and SrMoO$_4$ is difficult to be reduced completely to pure SrMoO$_3$. This result is coincident with the results studied by Smith as reported previously [10, 18-19].

Fig. 8.2 shows the SEM images of SrMoO$_4$ precursor material by hard template method and composite anode material GDC-SrMoO$_4$ by impregnation. As shown in Fig.2a, the as-prepared SrMoO$_4$ still retained the original strips structure of ACF.

For GDC-SrMoO$_4$ shown in Fig. 8.2b and 8.2c, it can be seen that SrMoO$_4$ show tubular shape with a diameter of 5 μm and the hollow structure can be observed in the cross-sectional image. GDC particles are coated on tubular SrMoO$_4$ by wet impregnation, followed by calcined process. The

catalytic GDC particles with size ranging from 50nm to 100nm were uniformly distributed on tubular SrMoO₃ surface, contributing to improve activity of anode material surface and enhance the electrochemical reaction sites for power generation.
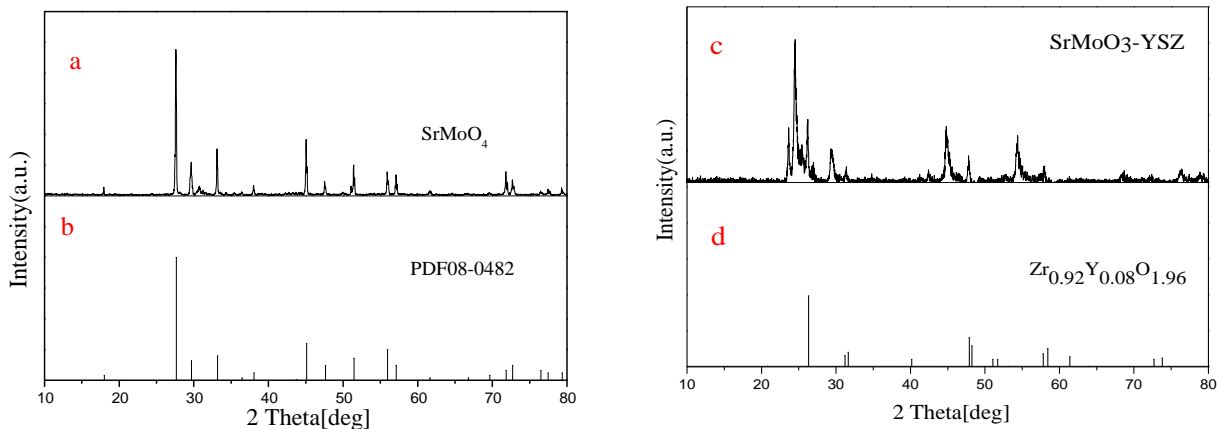

Fig.8.1 XRD patterns of the prepared anode material: (a) SrMoO₄; (b) standard pattern of SrMoO₄; (c) SrMoO₃-YSZ after reduction; (d) YSZ
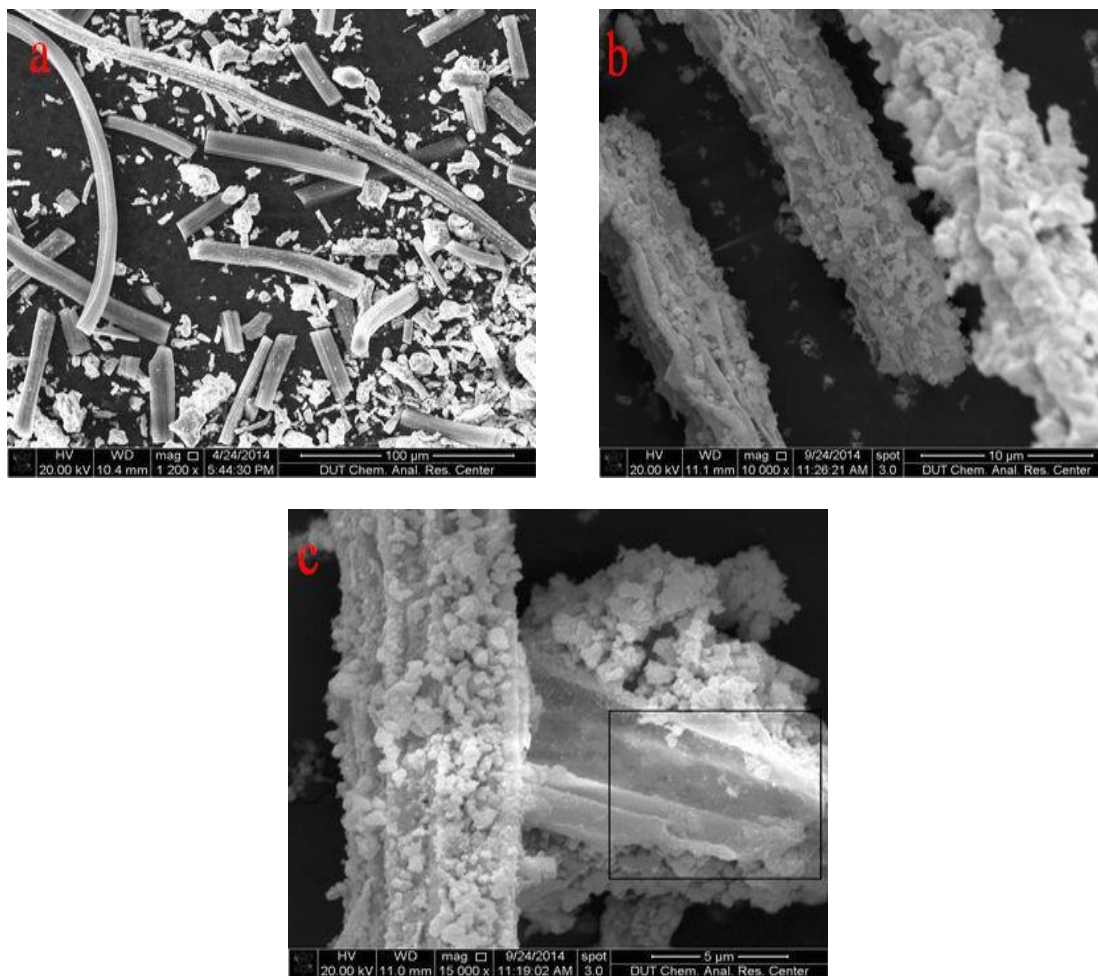
Fig. 8.2 SEM images of the fabricated composite anode material by hard template method: (a) SrMoO₄; (b) GDC-SrMoO₄; (c) GDC-SrMoO₄

111

8.3.2 Cell performance test

Fig. 8.3 shows the typical current - voltage- power density (I-V-P) characteristics curve of the single cell with the configuration of $SrMoO_4$-YSZ | YSZ | LSM-YSZ at various temperatures when hydrogen and methane were used as fuel. In Fig. 8.3(a) the mass ratio of $SrMoO_4$ to YSZ is 3 to 2. In Fig. 8.3(b), 50% GDC was added relative to $SrMoO_4$ mass when the weight ratio of $SrMoO_4$ to YSZ is 3 to 2.
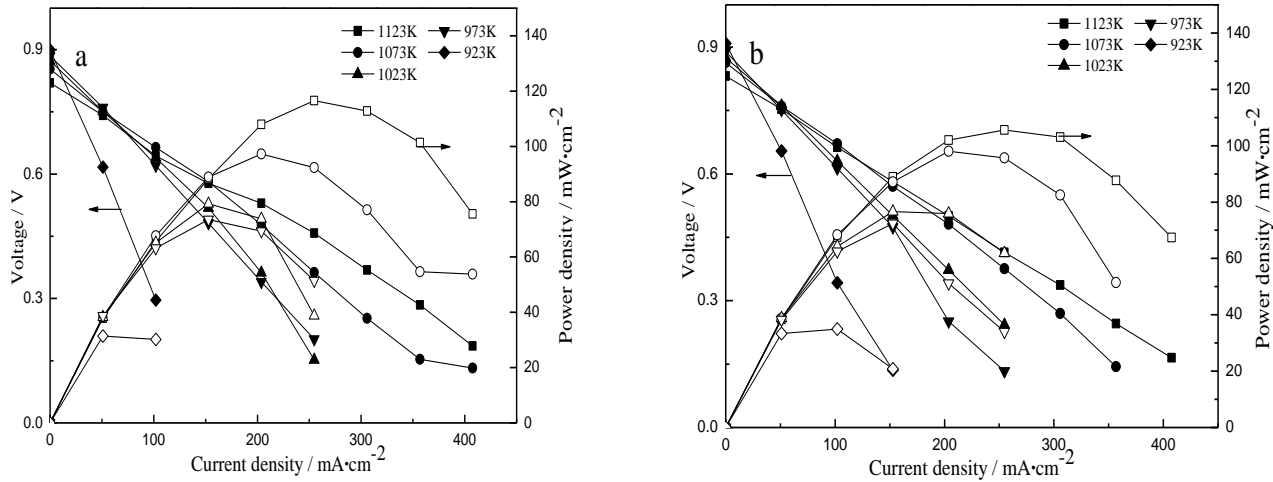
Fig. 8.3 I-V-P curves of single cell with $SrMoO_4$-YSZ as anode: (a)H_2; (b)CH_4

Accordingly, Fig 8.4 shows the typical current - voltage - power density characteristics of the single cell with the configuration of GDC-$SrMoO_4$-YSZ | YSZ | LSM-YSZ at various temperatures when hydrogen and methane were used as fuel. At 1073 K, the maximum power densities of the two cells with $SrMoO_4$-YSZ and GDC-$SrMoO_4$-YSZ as anodes were 97.26 and 184.94mW·cm^{-2}under hydrogen, respectively. Also, their maximum power densities were 98.06 and 190.44mW·cm^{-2}.
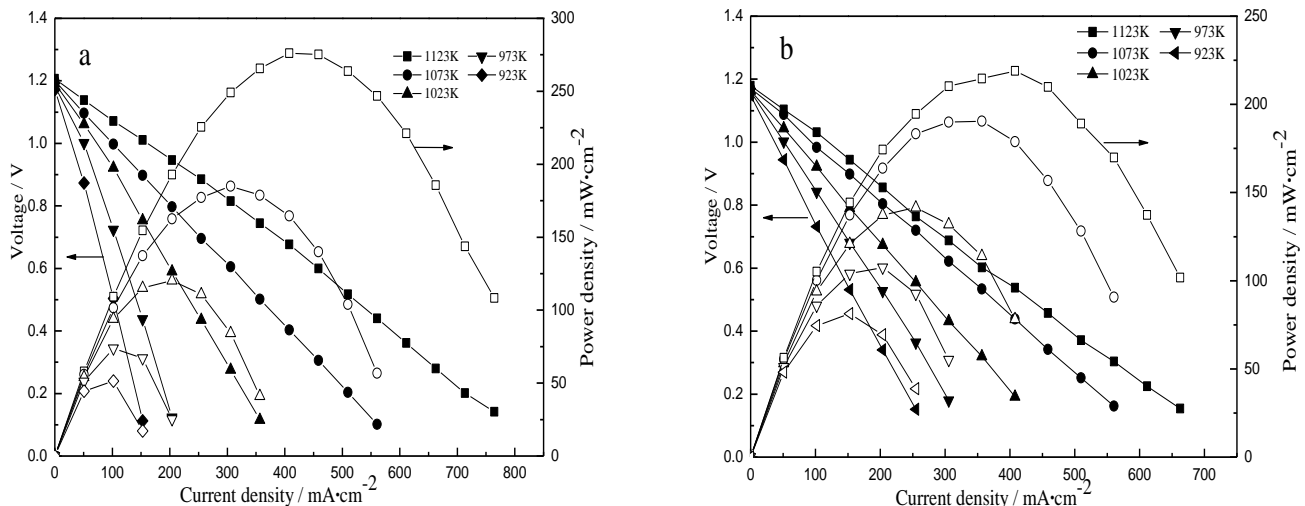
Fig. 8.4 I-V-P curves of single cell with GDC-$SrMoO_4$-YSZ as anode: (a)H_2;(b)CH_4

The measured results indicate that the cell with GDC-SrMoO$_4$-YSZ as anode shows good performance, suggesting that the introduction of catalytic GDC to SrMoO$_4$ can effectively improve cell electrochemical performance. The main reason is that the fine GDC particles spread on the tubular SrMoO$_4$ skeleton can enlarge three phase boundaries. GDC shows the mixed ionic and electronic conductivity can provide new paths for conducted electrons and oxide ions in the anode due to Gd introduction and Ce^{4+} reduction, leading to improve power generation [20].

8.3.3 The influence of addictive YSZ on the GDC-SrMoO$_4$-YSZ anode performance

GDC, SrMoO$_3$ and YSZ exhibit good catalytic activity, electronic conductivity and ionic conductivity, respectively. To obtain better electrical performance, it is necessary to balance the oxygen ionic conductivity and electronic conductivity of anode [21]. Herein, GDC-SrMoO$_4$ was prepared by impregnated 50wt% (relative SrMoO$_4$) GDC to SrMoO$_4$. And the addictive of YSZ in GDC-SrMoO$_4$ using SrMoO$_4$ as a reference was changed to prepare GDC-SrMoO$_4$-YSZ and the effect of mass ratio of SrMoO$_4$ to YSZ on cell performance was investigated. It was expected to obtain the optimal to achieve excellent cell performance.

Fig. 8.5 shows the typical I-V-P curves of the cells consisting of different mass ratio of SrMoO$_4$ to YSZ as anode under hydrogen and dry methane at 1073K.
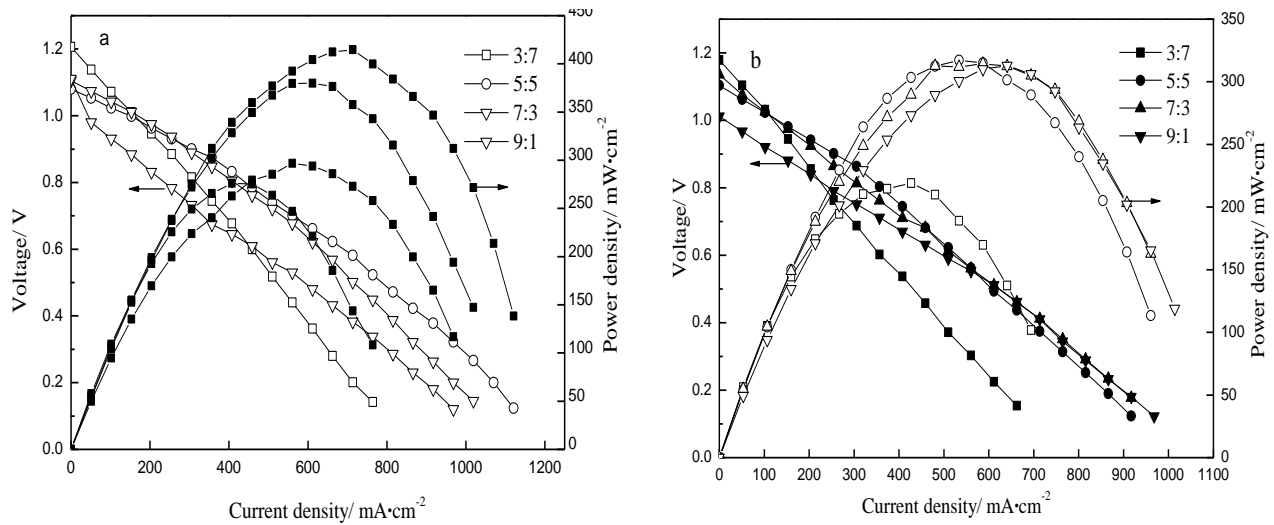
Fig. 8.5 I-V-P curves of single cells with different SrMoO$_4$:YSZ: (a)H$_2$;(b)CH$_4$

It can be seen that the anode composed of different ratio of SrMoO$_4$ to YSZ had an effect on cell output performance in both hydrogen and dry methane. Its power density increased first and then decreased with the SrMoO$_4$ composition increase. Among them, when the mass ratio of SrMoO$_4$ to YSZ was equaled 5:5, the cell exhibited the highest performance and its maximum power densities of 414.61 and 317.15mW·cm^{-2} was achieved in hydrogen and dry methane, respectively. The reason is

113

that lower SrMoO$_4$ composition in anode reduced the electronic conductivity of anode, resulting in limited active reaction sites. However, when the anode contained excessive SrMoO$_4$, the SrMoO$_4$ was easily agglomerated together under high temperature, causing less contact area to combine YSZ to form continuously conductive path, resulting in decreased three phase boundaries [22].

8.3.4 The influence of GDC impregnation on the SrMoO$_4$-YSZ anode performance

In afore-mentioned test, it is reported that the cell with GDC-SrMoO$_4$ as anode shows good performance. Herein, SrMoO$_4$ and YSZ in a mass ratio of 5:5 were used as a reference, and the impregnated GDC content (relative SrMoO$_4$ and YSZ) was investigated to achieve higher cell performance. Fig. 8.6 shows the typical I-V-P curves of the cells with different GDC content impregnated SrMoO$_4$-YSZ as anode under hydrogen and dry methane at 1073 K.

One can see that the impregnated GDC content had an effect on cell output performance in both hydrogen and dry methane. Its power density increased first and then decreased with the impregnated GDC content increase. When the impregnated GDC content was equaled 50wt%, the cell displayed the highest performance and its maximum power density reached 373.54 and 361.01 mW·cm^{-2} in hydrogen and dry methane, respectively. The main reason is that lower impregnated GDC content generated less GDC particles on SrMoO$_4$-YSZ, resulting in the limited catalytic activity and little three phase boundary of anode, causing the lower power generation. When the impregnated GDC content was excessive, the large amount of GDC particles covered on SrMoO$_4$-YSZ scaffolds to hinder fuel gas enter active sites for electrochemical reaction, resulting in the poor cell performance.
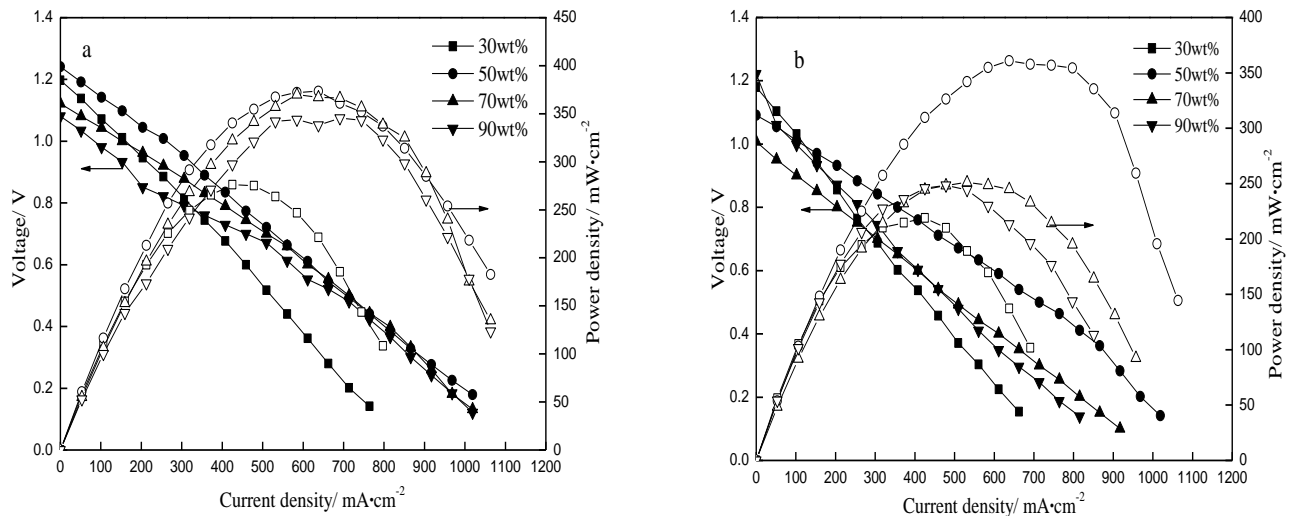

Fig. 8.6 I-V-P curves of single cells with different GDC impregnation: (a)H$_2$;(b)CH$_4$

8.3.5 SEM of tested cell

Fig. 8.7 shows SEM images of the as-prepared single cell with the configuration of GDC-SrMoO$_4$-YSZ | YSZ | LSM-YSZ after test in dry methane.
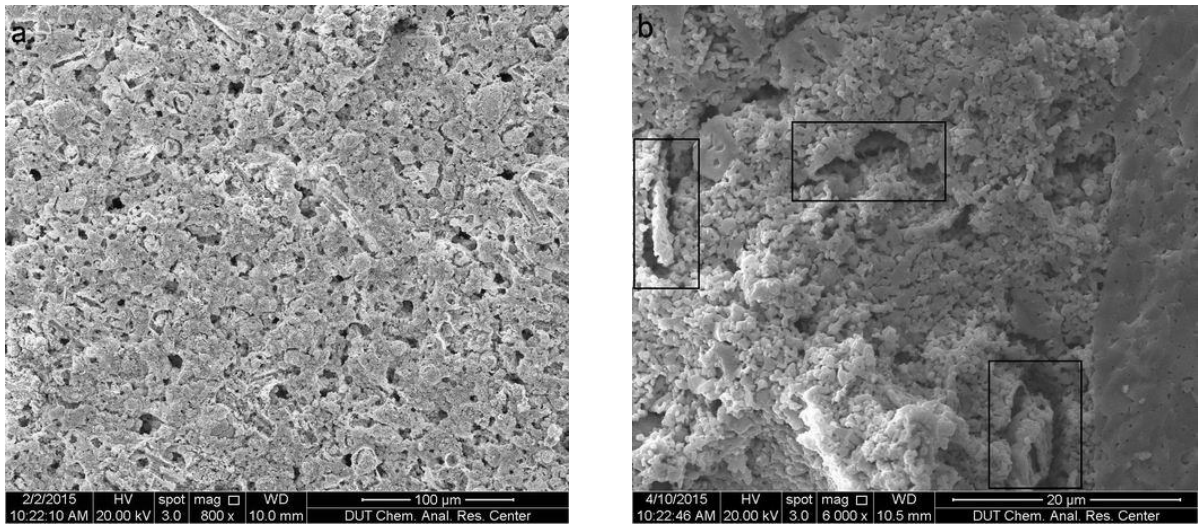
Fig.8.7 SEM images of single cell after test:
(a) anode surface microstructure;(b) cross-sectional microstructure

The component of the GDC-SrMoO$_4$-YSZ was as follows. 50wt% GDC (relative to SrMoO$_4$) was used to impregnate SrMoO$_4$ to prepare GDC-SrMoO$_4$, and the mass ratio of SrMoO$_4$ to YSZ was 5:5. The anode surface in Fig.8.7a shows a typical porous microstructure was formed for rapid diffusion of reactants getting in and the byproducts getting out of the anode reaction areas. Fig.8.7b shows a cross-sectional view of the cell. One can see that the anode layer connected densely with the YSZ electrolyte supporter. The pore pathway structure retained by copied ACF structure was significantly observed. The tubular SrMoO$_4$ coated by GDC particles spread uniformly in the anode to form a porous electrode, leading to generated more TPB sites for improving cell performance.

8.4 Conclusion

In this paper, SrMoO$_4$ material showed a long column shape and hollow structure was prepared by hard template method. Wet impregnation was used to introduce GDC on SrMoO$_4$. The single cells with the configuration of SrMoO$_4$-YSZ | YSZ | LSM-YSZ and GDC-SrMoO$_4$-YSZ | YSZ | LSM-YSZ were fabricated, and their performance were measured, respectively. The results showed that the maximum power density of cell with GDC-SrMoO$_4$-YSZ was reached 190.44mW·cm^{-2}, which is 190% higher than the cell with SrMoO$_4$-YSZ, implying the introduction of GDC can contribute to improve performance. The GDC impregnation and the mass ratio of SrMoO$_4$ to YSZ had effects on cell performance. When the mass ratio of SrMoO$_4$ to YSZ was 5:5 and the GDC impregnation was

50wt% (relative to $SrMoO_4$ and YSZ), GDC-$SrMoO_4$-YSZ showed a maximum power density of 361.01 $mW \cdot cm^{-2}$ under dry methane at 1073 K. For further improvement of the cell performance, optimization of the composition and microstructure of $SrMoO_3$ should be a prerequisite way. The reaction mechanism and stability of CH_4 on these perovskite materials such as $SrMoO_3$ would be further investigated in the future.

Reference

[1] B. C. H. Steele, A. Heinzel, Materials for fuel-cell technologies, *Nat.* **414(6861)** (2001) 345-352.

[2] J. Liu, S. A. Barnett, Operation of anode-supported solid oxide fuel cells on methane and natural gas, *Solid State Ionics* **158(1)** (2003) 11-16.

[3] W. Wang, S. P. Jiang, A. I. Y. Tok, L. H. Luo, GDC-impregnated Ni anodes for direct utilization of methanein solid oxide fuel cells, *J. Power Sources* **159(1)** (2006) 68-72.

[4] M. Santarelli, F. Quesito, V. Novaresio, C. Guerra, A. Lanzini, D. Beretta, Direct reforming of biogas on Ni-based SOFC anodes:Modelling of heterogeneous reactions and validation with experiments, *J. Power Sources* **242** (2013) 405-414.

[5] A. Ovalle, J. C. Ruiz-Morales, J. Canales-Vázquez, D. Marrero-López, J. T. S. Irvine, Mn-substituted titanates as efficient anodes for direct methane SOFCs, *Solid State Ionics* **177(19-25)** (2006) 1997-2003.

[6] M. R. Pillai, I. Kim, D. M. Bierschenk, S. A. Barnett, Fuel-flexible operation of a solid oxide fuel cell with $Sr_{0.8}La_{0.2}TiO_3$ support, *J. Power Sources* **185(2)** (2008) 1086-1093.

[7] K. B. Yoo, B. H. Park, G. M. Choi, Stability and performance of SOFC with $SrTiO_3$-based anode in CH_4 fuel, *Solid State Ionics* **225** (2012) 104-107.

[8] S. P. Jiang, X. J. Chen, S. H. Chan, J. T Kwok, K. A. Khor, $(La_{0.75}Sr_{0.25})(Cr_{0.5}Mn_{0.5})O_3$/YSZ composite anodes for methane oxidation reaction in solid oxide fuel cells, *Solid State Ionics* **177(1-2)** (2006) 149-157.

[9] Y. H. Huang, R. I. Dass, Z. L. Xing, J. B. Goodenough, Double perovskites as anode materials for solid-oxide fuel cells, *Sci.* **312(5771)** (2006) 254-257.

[10] B. H. Smith, M. D. Gross, A highly conductive oxide anode for solid oxide fuel cells, *Electrochem. Solid-State Lett.* **14(1)** (2011) B1-B5.

[11] X. Meng, X. J. Liu, D. Han, H. Wu, J. L. Li, Z. L. Zhan, Symmetrical solid oxide fuel cells with impregnated $SrFe_{0.75}Mo_{0.25}O_{3-\delta}$electrodes, *J. Power Sources* **252** (2014) 58-63.

[12] K. B. Yoo, B. H. Park, G. M. Choi, Stability and performance of SOFC with $SrTiO_3$-based anode in CH_4 fuel, *Solid State Ionics* **225** (2012) 104-107.

[13] H. S. Kim, S. P. Yoon, J. W. Yun, S. A. Song, S.C. Jang, S. W. Nam, Y. G. Shul, $Sr_{0.92}Y_{0.08}TiO_{3-\delta}/Sm_{0.2}Ce_{0.8}O_{2-\delta}$ anode for solid oxide fuel cells running on methane, *Int. J. Hydrogen Energy* **37(21)** (2012) 16130-16139.

[14] K. B. Yoo, G. M. Choi, LST–GDC composite anode on $LaGaO_3$-based solid oxide fuel cell, *Solid State Ionics* **192(1)** (2011) 515-518.

[15] M. D. Gross, J. M. Vohs, Gorte R J, An examination of SOFC anode functional layers based on ceria in YSZ, *J. Electrochem Soc.* **154(7)** (2007) B694-B702.

[16] P. Xiao, X.Ge,. Z. Liu, J. Y. Wang, X. Wang, $Sr_{1-x}Ca_xMoO_3–Gd_{0.2}Ce_{0.8}O_{1.9}$ as the anode in solid oxide fuel cells: Effects of Mo precipitation, *J. Alloys Compd.* **587** (2014) 326-331.

[17] H. X. You, A. Abuliti, X. W. Ding, Y. H. Zhou, Reactions of Low and Middle Concentration Dry Methane over Ni/ YSZ Anode of Solid Oxide Fuel Cell, *J. Power Sources* **165(2)** (2007) 722-727.

[18] P. Xiao, X. M. Ge, L. Zhang, J. M. Lee, J. Y. Wang, X. Wang, H_2 and CH_4 oxidation on $Gd_{0.2}Ce_{0.8}O_{1.9}$ infiltrated $SrMoO_3$–yttria-stabilized zirconia anode for solid oxide fuel cells, *Int. J. Hydrogen Energy* **37(23)** (2012) 18349-18356.

[19] I Baldychev, A. Javadekar, D. J. Buttrey, J. M. Vohs, R. J. Gorte, A study of the redox properties and methanol oxidation rates for molybdenum-based mixed oxides, *Appl. Catal. A: Gen.* **394(1-2)** (2011) 287-293.

[20] R. Martínez-Coronado, J. A. Alonso, M. T. Fernández-Díaz, $SrMo_{0.9}Co_{0.1}O_{2-\delta}$: A potential anode for intermediate-temperature solid-oxide fuel cells (IT-SOFC), *J. Power Sources* **258** (2014) 76-82.

[21] B. Smith, M. D. Gross, SOFC Anodes Prepared by Infiltration of Strontium Molybdate into Porous YSZ,218th ECS Meeting, *Electrochem. Soc.* **12** (2010) 1162-1162.

[22] S. P. Jiang, X. J. Chen, S. H. Chan, J. T. Kwok, K. A. Khor, $(La_{0.75}Sr_{0.25})(Cr_{0.5}Mn_{0.5})O_3/YSZ$ composite anodes for methane oxidation reaction in solid oxide fuel cells, *Solid State Ionics* **177(1)** (2006) 149-157.

Chapter 9

Conclusions and perspectives

9.1 Findings and conclusions

This thesis aims to reveal the reaction mechanism of dry methane's oxidation on the anode and directly use hydrocarbon as the fuels for SOFCs. In this thesis, the reactions on Ni-YSZ anode with different dry methane fluxes were investigated to obtain the mathematical relationship between dry methane flux and operational current. The electrical performance and the abrupt change of the output voltage of Ni-ScSZ anode in low concentrations of dry CH_4 were also studied by a novel method. Also, by modifying microstructure and composition of anode, the high performance anodes with high catalytic activity for direct hydrocarbon utilization and good resistance of carbon formation were developed. In addition, perovskite anode GDC-SrMoO$_4$-YSZ were also fabricated and characterized under methane. Eight chapters are included in this thesis.

In **Chapter 1** and **2**, the brief introduction was displayed on the basic theory, main key component materials, fabrication, measurement, as well as characterization of SOFCs.

In **Chapter 3**, based on Faraday's first law and relationships of the molar ratio between reactions, the influence of methane flux on methane anode reaction was investigated when methane with different flux was fed to the anode chambers. When $v(CH_4) \geq I/(4F)$, dry methane occur following electrochemical reactions when the oxygen anion molar flow continue to increase at anode in sequence.

$CH_4 + O^{2-} \rightarrow CO + 2H_2 + 2e^-$

$CH_4 + 2O^{2-} \rightarrow CO + H_2O + H_2 + 4e^-$

$CH_4 + 3O^{2-} \rightarrow CO + 2H_2O + 6e^-$

$CH_4 + 4O^{2-} \rightarrow CO_2 + 2H_2O + 8e^-$

When $I/(4F) \leq v(CH_4) \leq I/(2F)$, the first two or three reactions occur to dry methane in sequence when the anode phase at the interface oxygen anion molar flow continued to increase. When $v(CH_4) \leq I/(2F)$, only the first reaction in above occurs to dry methane.

118

In **Chapter 4**, the power generation performances of the cell with Ni-ScSZ anodes in different concentrations of dry CH_4 were investigated by detecting the exhaust gas combining with the examination of activation energy. Also, the abrupt changes of the output voltage were studied. When the cell operated with high concentrations of dry CH_4, partial oxidation reactions in anode was occurred and the cell showed a good performance. In low concentrations of dry methane, a series transition process from partial oxidation reaction to a complete oxidation reaction was occurred with the current density increase. However, H_2O was produced in the reaction transition process, resulting in the increased threshold value of $p(H_2O)/p(CH_4)$ at outlet of anode, which caused the anode degradation and indicated the lower cell performance in low concentrations of dry CH_4

In **Chapter 5**, a novel Ni_xCu_{1-x} (x = 0.8, 0.5, 0.2) alloy material without reduction in H_2 was directly prepared as anode by using ACF as template for CH_4-fueled SOFCs. The cell performance power density was increased with the Ni content in Ni_xCu_{1-x} anode increase. Also, fueled in dry CH_4 at a relative current density, no significant degradation was observed for such Ni_xCu_{1-x} anodes after 10 h operation while the conventional NiO anode dropped rapidly after only 2 h, indicating that the Ni-Cu bimetallic material had an effect on mitigating carbon deposition in anode. According to SEM analysis results, the Ni_xCu_{1-x} alloy with a tubular shape showed a relative stable structure after stability test.

In **Chapter 6**, an anode microstructure modification process was demonstrated for methane direct oxidation. A high performance $Ni_{0.5}Cu_{0.5}O_x$-YSZ anode were prepared by hard template method combined with wet impregnation method where tubular YSZ as anode ionic framework and $Ni_{0.5}Cu_{0.5}O_x$ as electronic conductor. YSZ electrolyte-supported single cell with $Ni_{0.5}Cu_{0.5}O_x$-YSZ anode was fabricated for the power generation performance test and the long-term stability test at 1073 K. Due to the effective covering from $Ni_{0.5}Cu_{0.5}O_x$ particles on both internal and external surfaces of tubular YSZ backbone, the active reaction sites in anode were enlarged so that the cell achieved high performance. By comparing the results of the 100 h long-term stability tests under dry CH_4 and wet CH_4 (3% H_2O) respectively, the cell with dry CH_4 showed an obvious voltage drop of 5.27% but the one with wet CH_4 showed the more stable property, suggesting that wet CH_4 had an obvious impact on inhibiting carbon deposition on the anode. SEM and EDS analysis of the tested cell indicated the porous anode structure was quite steady after 100 h operation. Such a three-dimensional microstructure with high specific surface and long channel for fuel transport in the anode was expected to increase TPB and improve its electric properties and carbon deposition resistance.

In **Chapter 7**, to further enhance the anode coking resistance, SDC was adopted to replace YSZ as anode scaffold and $Ni_{0.5}Cu_{0.5}Ba_{0.05}O_x$ was used as the impregnated loading. Also, due to the

consistence of the cathode and electrolyte fabricating process, $Ni_{0.5}Cu_{0.5}Ba_{0.05}O_x$ powder was prepared and then mixed with SDC as a comparison, and the single cell with such contrastive anodes were fabricated to investigate the anode microstructure effect on the cell performance. The cells performance and stability were characterized with dry CH_4 as fuel at 1073 K. The cell with $Ni_{0.5}Cu_{0.5}Ba_{0.05}O_x$/SDC anode showed higher maximum power density than that of $Ni_{0.5}Cu_{0.5}Ba_{0.05}O_x$-SDC anode, the main reason was the catalytic metal particles were uniformly coated tubular SDC as well as a steady and porous stereoscopic structure was formed for gas diffusion, leading to increase TPB, resulting in the higher performance. In stability test, the cell with $Ni_{0.5}Cu_{0.5}Ba_{0.05}O_x$/SDC anode displayed a stable operation compared with that with $Ni_{0.5}Cu_{0.5}Ba_{0.05}O_x$-SDC anode in dry CH_4. Moreover, EDS results demonstrated that carbon deposition on $Ni_{0.5}Cu_{0.5}Ba_{0.05}O_x$/SDC anode after 100 h operation was nearly identical to $Ni_{0.5}Cu_{0.5}Ba_{0.05}O_x$-SDC anode while it operated only 10 h. Therefore, the fabrication of anti-carbon catalyst combined with three-dimensional electrode is potential measure to enhance durability for direct utilization of dry methane as fuel in SOFCs.

In **Chapter 8**, a Ni-free composite anode material of GDC-SrMoO$_4$-YSZ was prepared and investigated for SOFCs. GDC nanoparticles were introduced into SrMoO$_4$ backbone by wet impregnation due to the limited catalytic activity of SrMoO$_4$-YSZ anode. Electrochemical test results showed that the cell performance was greatly improved by the introduction of GDC, both in H_2 and CH_4. The effects of different composition within YSZ and SrMoO$_4$ on the ion and electron conductivity and GDC impregnation on the catalytic activity were further examined to achieve higher cell performance. When the mass ratio of SrMoO$_4$ to YSZ was 5:5 and the GDC impregnation was 50wt% (relative to SrMoO$_4$ and YSZ), the cell showed a maximum power density of 361.01 mW·cm^{-2} when fueled in dry CH_4 at 1073 K. SEM analysis result displayed that SrMoO$_4$ as an anode scaffold was uniformly coated by GDC particles, leading to improve active reaction paths and sites for fuel oxidation.

9.2 Future outlook

Development of new type anode materials or optimization of conventional Ni based anode for SOFCs that operates directly with hydrocarbon fuels is widely expected to be an important technical objective for power generation in the future. Our results show that using Cu modified Ni and fabricating porous anode can effectively increase the operational stability and alleviate carbon deposition in anode for hydrocarbon-fueled SOFCs. For further improvement of the cell performance

and coking resistance, optimization of anode materials should be a prerequisite way, both in the composition and microstructure.

Apart from adding inert metallic copper to prepare Ni-Cu bimetallic anode, Fe, Sn or other metal could be adopted to straightforward modify Ni-based cermet to prepare bimetallic or trimetallic catalysts towards coke formation. Different methods of introducing these metals into the Ni catalyst should be systematically investigated and optimized, and their effects on cell performance and coking resistance also should be examined and compared, it was expected to obtain the simplest ways to fabricate anti-coking anode catalysts that enable cell stable operation using hydrocarbon fuels. This could give possibilities to further optimization of these materials.

Three-dimensional electrode as anode catalyst scaffold is essential to form porous microstructure for fuel gas diffusion in the anode. Except using ACF as template in **Chapter 6** and **7**, adding pore-former with special shape such as cotton-fibers or paper-fibers into raw anode material is also an effective method to upgrade anode microstructure. Compared with irregular and fine pores produced by conventional pore-former, i.e. flour, starch or graphite, cylindrical pores connected with each other are created to form continuous pathways readily with a small amount of fibers. Thus the cell output performance can be improved significantly, especially in anode-supported cells. On basis of this, the fibers are burnt off via high-temperature treatment, and leaves wire-like pores within the anode to form a porous anode substrate, and anti-coking anode catalysts can infiltrate the as-prepared a porous anode substrate via vacuum wet impregnation. After the heat treatment, the catalyst layer coated electrolyte or raw anode are obtained, leading to increase more TPBs. The loading of catalyst can be controlled by repeating the infiltration process and heat treatment. The structural nature of the anode, such as the shape, size and volume fraction of pores are required to be explore and optimize. The optimal preparation technology should be also investigated and identified.

In this thesis, using the anode catalyst particles modified the anode framework is an effective measure to improve TPB length. From viewpoints of theory, an anode micro model based on math such as random packing sphere principle should be constructed to calculate the TPB length in the impregnating anode. The microstructure parameters such as the porosity, particle size and impregnated loading should be designed and evaluated to increase the TPB length, resulting in the improvement of cell performance. Therefore, the ideal quantitative relation between TPB and performance can be created and demonstrated as a reference for experiment.

To examine the gas transport properties in the porous anode, an anode geometric micro model should be established and simulated by computational fluid dynamics (CFD) or Comsol, which can be used as a reference for experiment.

Electrochemical and thermal performance stability with GDC-SrMoO$_4$-YSZ composite anode are crucially important properties that have not been investigated in **Chapter 8** during this thesis. Also, A and B sites in SrMoO$_3$ can be partially or fully substituted to obtain the composite material with better electrical conductivity and ionic conductivity. This could give possibilities to further optimization of these materials.

Additionally, new type anode materials, i.e. perovskite or ceria-based anode materials, should be further explored to enhance cell performance and suppress carbon formation. It would be great of interest in energy cost if these materials are to be applied within the SOFC technology.

List of publications

List of publications and presentations

1. <u>**Hongxin You**</u>, Cong Zhao, Bin Qu, Guoqing Guan, Abuliti Abudula. Fabrication of $Ni_{0.5}Cu_{0.5}Ox$ coated YSZ anode by hard template method for solid oxide fuel cells. *Journal of Alloys & Compounds*, 2016 (669) 46-54.

2. <u>**Hongxin You**</u>, Cong Zhao, Yajun Guan, Guoqing Guan, Abuliti Abudula. Fabrication of Composite Anode GDC–$SrMoO_4$–YSZ by Hard Template Method for Solid Oxide Fuel Cell. *Journal of the Chinese Ceramic Society* 2016 (44) 919-924.

3. <u>**Hongxin You**</u>, Cong Zhao, Bin Qu, Runjie Liu, Guoqing Guan, Lijun Xu, Abuliti Abudula. Fabrication of $Ni_{0.5}Cu_{0.5}Ba_{0.05}O_x$ coated SDC stereoscopic anode by hard template method for solid oxide fuel cells. *Journal of Fuel Chemistry and Technology* 2016 (44) 1272-1280

4. <u>**Hongxin You**</u>, Bin Qu, Guoqing Guan, Abudula Abuliti. Influence of dry methane reactions on the cell output characteristics of solid oxide fuel cells. *American Journal of Analytical Chemistry*, 2015 (6) 253-262.

5. <u>**Hongxin You**</u>, Hongjie Gao, Runjie Liu, Gang Chen, Abuliti Abudula, Xinwei Ding. The Effect of Dry Methane Flux on the Methane Reactions in Solid Oxide Fuel Cell at Ni-YSZ Anode. *Journal of Chemical Engineering of Chinese Universities*. 2014 (28) 1004-1009.

6. <u>**Hongxin You**</u>, Cong Zhao, Lijun Xu, Guoqing Guan, Abuliti Abudula. Thermal analysis of 1Kw PEMFC-CHP system for residential applications. *Chinese Journal of Power Sources* (Accepted).

Patent

1 <u>**You Hongxin**</u>, Cao Lei, Qu Bin, Liu Runjie, Preparation method of Ni-Cu coated electrolyte material ZL 201310262984.6, application date on Jun. 27, 2013, authorization date on Jun. 10, 2015.

2 <u>**You Hongxin**</u>, Xu Junwei, Preparation method of porous fuel cell anode material NiCu/C, ZL 201110260959.5, application date on Sept. 5, 2011, authorization date on Nov. 6, 2013.

List of papers presented in conferences

International conferences

1. **<u>Hongxin You</u>**, Cong Zhao, Can Li, Bin Qu, Guoqing Guan, Abuliti Abudula. Cotton-fibers Used as Pore Former for the Anode with High Porosity and Long Cylindrical Pores of Solid Oxide Fuel Cells. *3rd International Conference on Advanced Materials, Structures and Mechanical Engineering (ICAMSME 2016)* (Incheon, Korea) 20-22 May 2016.

2. **<u>Hongxin You</u>**, Cong Zhao, Bin Qu, Yajun Guan, Junwei Xu, Guoqing Guan, Abuliti Abudula. Ni-Cu alloy anode material prepared with hard template method. *Proceeding of the 3rd annual 2015 international conference on material science and environmental engineering (ICMSEE2015)* (Wuhan, Hubei, China) 5-6 June 2015.

3. **<u>Hongxin You</u>**, Yajun Guan, Bin Qu, Shuang Zhang, Guoqing Guan, Abuliti Abudula. Research on SOFC of composite anode material $SrMoO_3$-YSZ impregnated with $Gd_{0.2}Ce_{0.8}O_{1.9}$ by hard template method. *2014 2nd international conference on future material engineering and industry application (ICFMEIA 2014)* (Hong Kong, China) 10-11 December 2014.

4. **<u>Hongxin You</u>**, Bin Qu, Lei Cao. Comparison of $Ni_{0.8}Cu_{0.2}O_x$ anode material prepared with sol-gel method and $Ni_{0.8}$-$Cu_{0.2}$-coated YSZ composite anode material prepared with polyol Method. *2013 International Conference on Materials Science, Machinery and Energy Engineering, (MSMEE 2013)* (Hong Kong, China) 24-25 December 2013

Domestic conferences

1. **<u>Hongxin You</u>**, Guoqing Guan, Abuliti Abudula. Oxidation behavior of dry methane at nickel-scandia-stabilized zirconia anodes in solid oxide fuel cells. *23rd The Japan Institute of Energy*. (Fukuoka, Japan) 19-20 July 2014.

.

Reference Results

1 **<u>Hongxin You</u>**, Hongjie Gao, Runjie Liu, Gang Chen, A. Abuliti, Xinwei Ding, The Effect of Dry Methane Flux on the Methane Reactions in Solid Oxide Fuel Cell at Ni-YSZ Anode, *Journal of Chemical Engineering of Chinese Universities*, **28(5)** (2014) 1004-1009.

2 **<u>Hongxin You</u>**, Hongjie Gao, Gang Chen, A. Abuliti, The conversion among reactions at Ni-based anodes in solid oxide fuel cells with low concentrations of dry methane, *Journal of Power Sources*, **196(5)** (2011) 2779-2784.

3 **<u>Hongxin You</u>**, Hongjie Gao, Gang Chen, A. Abuliti, Xinwei Ding, Effects of dry methane concentration on the methane reactions at Ni-YSZ anode in solid oxide fuel cell, *Journal of Fuel Chemistry and Technology*, **41(3)** (2013) 374-379.

4 **<u>Hongxin You</u>**, Ruirui Liu, Runjie Liu, A. Abuliti, Review of anode catalyst development of direct methane SOFC, *Chinese Journal of Power Sources*, **35(4)** (2011) 455-457

5 **<u>Hongxin You</u>**, Gaodong Gao, Liang Zhou, A. Abuliti, Power generating perform ances of ethanol on the SOFC with Ni-ZnO-ZrO$_2$ –YSZ anode, *Journal of Fuel Chemistry and Technology*, **38(1)** (2010) 116-120.

6 **<u>Hongxin You</u>**, Gang. Chen, Ruirui Liu, Yihui. Zhou, A. Abuliti, Xinwei. Ding, Preparation and electrochemical properties of NiO–CGO anode support solid oxide fuel cell with ScSZ/CGO composite electrolyte, *Journal of the Chinese Ceramic Society*, **37(8)** (2009) 1306-1310.

7 **<u>Hongxin You</u>**, A. Abuliti, Xinwei Ding, Yihui Zhou, Reactions of low and middle concentration dry methane over Ni/YSZ anode of solid oxide fuel cell, *Journal of Power Sources*, **165(2)** (2007) 722-727.

8 **<u>Hongxin You</u>**, Gang. Chen, Xinwei. Ding, Lixin Wang, A. Abuliti, Preventing carbon deposition of Cu-Ce-Zr-O/YSZ anodes operating with methane in solid oxide fuel cells, *Chemical Industry and Engineering Progress*, **27(12)** (2008) 1986-1990.

9 **<u>Hongxin You</u>**, Xinwei Ding, Guodong Gao, A. Abuliti, Effect of operation conditions on reaction over anode in SOFC, *Chemical Industry and Engineering Progress*, **27(10)** (2008) 1624-1636.

10 **<u>Hongxin You</u>**, Guodong Gao, Xinwei. Ding, A. Abuliti, Reaction conditions and rules of methane in anode of SOFC, *Battery Bimonthly*, **38(5)** 2008 278-280.

Acknowledgements

I would like to express my deep gratitude to my supervisor Prof. Dr. Abuliti Abudula for offering me a precious opportunity to conduct my PhD thesis in his laboratory, providing the research conditions in Hirosaki University and Dalian University of Technology, preciseness discussion and his kind encouragements during my PhD program.

I would like to thank Prof. Dr. Guoqing Guan, North Japan Research Institute for Sustainable Energy (NJRISE), Hirosaki University, for important comments and valuable advices.

I would like to thank Dr. Tao Yu, Hirosaki University, for important help and valuable advices.

I would like to thank Cong Zhao, Gang Chen, Can Li, Bing Qu, Yajun Guan, Junwei Xu, Hongjie Gao, and Zhiyu Wen, the graduate students at Dalian University of Technology, which supported me throughout my study in the PhD program.

I am also indebted to all colleagues at our institute for making it a great place to continue work in Hirosaki University. Especially I want to thank Zhang Peng, Yufei Ma and Ji Cao for helping me to handle with relevant procedures in Hirosaki University.

Special thanks go to my colleague at Dalian University of Technology. Especially I want to thank Xinwei Ding, Mingshu Bi, Runjie Liu, Yihui Zhou Xiaojuan Wang and Yuqiang Dai. In particular, I would like to thank Prof. Xinwei Ding for his patience guiding me to analyzing the methane reactions from thermodynamic and kinetic, and I have benefited from Prof. Xinwei Ding.

Thanks to me brother and sisters for them financial help.

Finally I appreciate the understanding, patience and love of my wife Lixia Ye, and to my beloved daughter Fangyuan You for encouraging me to overcome the effects of the sequelae of cerebral infarction.

Hongxin You
September 18th, 2016

Curriculum Vitae

Hongxin You

Born January 3rd, 1963

Dalian, Liaoning, China

Citizen of China

Research Interest:

SOFC, methane anode reaction on SOFC, anode material of SOFC, SOFC performance testing system.

Education and Research Experience:

4.2017-3.2014	Ph.D. in Energy Engineering at the Hirosaki University, Aomori, Japan
4.2017-10.1998	Assoc. Prof., College of Chemical Machinery, Chemical Environment and Life Science Division, Dalian University of Technology, China.
10.1998-9.1989	Lecturer, Department of Chemical Engineering and Machinery, Dalian University of Technology, China.
9.1989-7.1987	Teaching assistant, Department of Chemical Engineering and Machinery, Dalian University of Technology, China.
6.1987-9.1984	M. E., Department of Chemical Engineering and Machinery, Dalian University of Technology, China.
7.1984-9.1980	B.S.E., Department of Chemical Engineering and Machinery, Dalian University of Technology, China.